



# Exploring bipolar electrochemistry for the modification of unusual conducting substrates

Iuliia Malytska

## ► To cite this version:

Iuliia Malytska. Exploring bipolar electrochemistry for the modification of unusual conducting substrates. Theoretical and/or physical chemistry. Université de Bordeaux, 2018. English. NNT : 2018BORD0135 . tel-02283554

**HAL Id: tel-02283554**

**<https://theses.hal.science/tel-02283554>**

Submitted on 11 Sep 2019

**HAL** is a multi-disciplinary open access archive for the deposit and dissemination of scientific research documents, whether they are published or not. The documents may come from teaching and research institutions in France or abroad, or from public or private research centers.

L'archive ouverte pluridisciplinaire **HAL**, est destinée au dépôt et à la diffusion de documents scientifiques de niveau recherche, publiés ou non, émanant des établissements d'enseignement et de recherche français ou étrangers, des laboratoires publics ou privés.

THÈSE PRÉSENTÉE  
POUR OBTENIR LE GRADE DE  
**DOCTEUR DE**  
**L'UNIVERSITÉ DE BORDEAUX**

ÉCOLE DOCTORALE DES SCIENCES CHIMIQUES  
SPÉCIALITÉ : Chimie-Physique

Par Iuliia Malytska

**Exploring bipolar electrochemistry for the modification of  
unusual conducting substrates**

Sous la direction de : Prof. Alexander KUHN  
Co-directeur : Dr. Laurent BOUFFIER

Soutenue le 10.09.2018

Membres du jury :

M. Inagi, Shinsuke  
Mme. Hellwig, Petra  
Mme. Lecomte, Sophie  
M. Schuhmann, Wolfgang  
M. Gooding, Justin  
M. Kuhn, Alexander  
M. Bouffier Laurent

Professeur, Tokyo Institute of Technology, Japan  
Professeur, Université de Strasbourg, France  
Directeur de recherche, CNRS, Bordeaux, France  
Professeur, Ruhr-Universität Bochum, Germany  
Professeur, UNSW Sydney, Australia  
Professeur, INP Bordeaux, France  
Chargé de Recherche, CNRS, France

Rapporteur  
Rapporteur  
Présidente  
Examineur  
Examineur  
Directeur de thèse  
Co-directeur de thèse

## **Modification de substrats conducteurs originaux par électrochimie bipolaire**

### **Résumé**

L'électrochimie bipolaire est un phénomène basé sur la polarisation d'un objet conducteur soumis à un champ électrique. Contrairement à l'électrochimie conventionnelle, c'est la chute de potentiel en solution imposée par les deux électrodes sources qui permet de réaliser les réactions électrochimiques. Lorsqu'un objet conducteur est immergé dans une solution électrolytique et soumis à un champ électrique, il est polarisé et se comporte comme une électrode bipolaire. La différence de potentiel entre l'électrolyte et l'électrode bipolaire est la force motrice pour les réactions de réduction et d'oxydation promues aux deux extrémités de l'électrode bipolaire. L'oxydation se produira à l'une des extrémités, combinée simultanément avec la réduction à l'autre extrémité.

L'électrochimie bipolaire est une technique d'adressage sans fil qui permet de générer une réactivité électrochimique asymétrique à la surface d'un objet conducteur. Au cours de la dernière décennie, l'électrochimie bipolaire a trouvé de nombreuses applications telles que la synthèse de micro- et nanoparticules asymétriques, l'électrodéposition, la détection, la propulsion de micro-objets, etc. L'avantage de cette technique repose sur le mode d'adressage sans fil qui peut être utilisé pour modifier des matériaux fragiles sans contact ou encore pour modifier simultanément un ensemble de particules en même temps.

Dans la présente thèse, l'électrochimie bipolaire a été appliquée à différents matériaux semi-conducteurs et systèmes biologiques. De plus, les nouvelles propriétés générées sur ces nouveaux substrats ont été étudiées en utilisant diverses techniques de caractérisation.

L'électrodéposition bipolaire est un outil de choix pour la génération d'objets asymétriques. En utilisant cette approche, un dépôt de métal a été réalisé sur substrats organiques de type complexes de transfert de charge. Ces nouveaux matériaux hybrides métal/organique se sont révélés de bons candidats pour la génération asymétrique de photo-voltage sous illumination.

Un matériau semi-conducteur inorganique, tel que les dichalcogénures de métaux de transition a également été utilisé comme substrat pour l'électrochimie bipolaire. Différents dépôts de métaux ont été réalisés sur les macro-particules de  $\text{MoSe}_2$ . Les dichalcogénures de métaux de transition sont également connus pour leur activité électrocatalytique, notamment pour la réaction d'évolution de l'hydrogène. La production d'hydrogène sans fil sur des cristaux de  $\text{MoSe}_2$  a également été réalisée par électrochimie bipolaire. De plus, l'électrochimie bipolaire peut être utilisée avec une suspension de microparticules de  $\text{MoSe}_2$  pour réaliser une électrolyse quantitative d'une solution contenant une espèce chimique oxydable.

Enfin, l'électrochimie bipolaire pourrait également être utilisée pour étudier indirectement la conductivité de molécules biologiques telles que l'ADN. L'objectif principal était de développer une méthode en électrochimie bipolaire pour la modification asymétrique de l'ADN par des nanoparticules métalliques. Tout d'abord, des expériences ont été réalisées en utilisant l'électrodéposition bipolaire à l'aide d'une électrophorèse capillaire (CABED) suivie d'une imagerie par TEM. Des résultats positifs ont été obtenus mais avec une faible reproductibilité.

La seconde approche consiste à étirer des molécules d'ADN sur une surface isolante par peignage et à visualiser cette fois-ci les dépôts par microscopie AFM.

**Mots clés :**

Électrochimie bipolaire ; Électrodéposition ; Particules asymétriques ; Complexes à transfert de charge organiques ; Diséleniure de molybdène ; Conductivité de l'ADN.

---

## **Exploring bipolar electrochemistry for the modification of unusual conducting substrates**

### **Abstract**

Bipolar electrochemistry is a phenomenon based on the polarization of conductive objects in an electric field. In contrast to conventional electrochemistry, the drop of potential in the electrolyte solution triggers the involved redox reactions. When a conductive object is positioned in an electric field present in a solution between two feeder electrodes, it is polarized and becomes a bipolar electrode. The potential difference between the electrolyte and the bipolar electrode is the driving force for reduction/oxidation reactions at the two extremities of the bipolar electrode; oxidation will occur at one end, combined simultaneously with reduction at the other end.

Bipolar electrochemistry is a concept that allows generating an asymmetric reactivity at the surface of a conductive object. During the last decade, bipolar electrochemistry found many applications such as the synthesis of asymmetric micro- and nano-particles, electrodeposition, sensing, propulsion of microobjects, electroanalysis etc. The advantage of this technique is its wireless character, which allows the modification of delicate materials and also to electrochemically address many objects simultaneously.

In the present thesis, the approach was applied to different semiconducting materials and biological systems. In addition, properties of substrates of different nature have been studied using bipolar electrochemistry.

In this way, it was possible to create metal deposits on organic charge transfer salts in a site-specific way. The resulting hybrid metal/organic particles were tested for the asymmetric generation of photovoltage under illumination.

Inorganic transition metal dichalcogenides were also used as a substrate for bipolar electrochemistry. Deposition of different metals on MoSe<sub>2</sub> macroparticles was performed. Transition metal dichalcogenides are known for their catalytic activity with respect to hydrogen evolution reaction. Therefore, wireless hydrogen production on MoSe<sub>2</sub> crystals and microparticles could be demonstrated by using bipolar electrochemistry. In the latter case it is possible to envision their use for electrochemical decontamination of solutions in the bulk.

Finally, bipolar electrochemistry has also been used for studying the conductivity of biological molecules (DNA). The primary goal was to develop a new approach for the asymmetric modification of DNA by metal nanoparticles. Experiments were performed by using either Capillary Assisted Bipolar Electrodeposition (CABED) with the DNA molecules present in the bulk, or by immobilizing DNA as stretched entities on model surfaces for subsequent modification. Encouraging first results could be evidenced by TEM or AFM measurements.

### **Keywords:**

Bipolar electrochemistry; Electrodeposition; Asymmetric particles; Organic charge transfer salts; Molybdenum diselenide; DNA conductivity.

---

**Unité de recherche**

Institut des Sciences Moléculaires (ISM), UMR CNRS 5255, Université de Bordeaux

Groupe Nanosystèmes Analytiques (NSysA)

Site ENSCBP, Bordeaux INP

16, avenue Pey Berland,

33607 Pessac FRANCE

## Acknowledgments

I would like to express my sincere thanks to my both supervisors Pr. Alexander Kuhn and Dr. Laurent Bouffier for their continuous guidance, scientific support and assistance during these three years. I am particularly grateful for the encouragement given to me during all the time, for optimism and for all scientific and personal advices.

I also would like to thank the jury members Pr. Petra Hellwig, Pr. Shinsuke Inagi, Pr. Wolfgang Schuhmann, Pr. Justin Gooding, and Dr. Sophie Lecomte for accepting the request to evaluate this work.

I gratefully acknowledge the University of Bochum and in particular Pr. Schuhmann as well as the ERC grant Electra for providing me the financial support.

I thank the Placamat platform, University of Bordeaux, especially Marion Gayot, François Weill for TEM characterization of DNA samples.

I'm indebted to Marjorie Drac and Dr. Etienne Schwob from IGMM, University of Montpellier for all silanization and DNA combing experiments that they did for us.

Acknowledgement go also to Dr. Marcin Kielar, Pr. Wantz Guillaume from IMS group, University of Bordeaux for their help to establish the experiments of photovoltage measurements.

I thank all members of the NSysA group for the friendly atmosphere and nice working environment. I very much appreciate the help and support from all of you. Aline Simon-lalande, Cécile Allilaire thank you for help in all administrative questions; Patrick Garrigue, Dr. Bertrand Goudeau, Véronique Lapeyre thanks a lot for technical support; Pr. Valérie Ravaine, Dr. Stéphane Arbault, Dr. Adeline Perro-marre, Pr. Neso Sojic, Dr. Dodzi Zigah, Dr. Stéphane Reculosa thank you for scientific discussions during seminars and help.

I am also grateful to all student members of NSysA that I have met, for their friendship and great atmosphere: Dr Alexandar Karajic, Dr. Milica Sentic, Dr. Anne de Poulpiquet, Dr. Vasilica Lates, Beatriz Diez Buitrago, Alessandra Zanut, Gibran Hernandez Moreno, Eugenio Gianessi, Dr. Li Haidong, Magdalena Murawska, Dr. Thittaya Yutthalekham, Dr. Oranit Phuakkong, Supakit Tiewchareon, Dr. Churalat Wattanakit, Dr. Hélène Labbie, Maria, Laura Adam, Alice Dauphin, Paul Chassagne, Camille Colin, Mathieu Coudert, Marie-Charlotte Tatry, Sunpet Assavapanumat, Malinee Niamlaem, Dr. Bhavana Gupta, Dr. Lin Zhang, Dr. Gerardo Salinas, Dr. Pauline Lefrancois, Dr. Priyanka Dutta, Silvia Voci, Dr. Elena Villani. Fatima Ezzahra Errami, Sharvina Shanmugathasan, Paul Galanopoulo, Thomas Delahaye, Mariana Campos Afonso. It is a great pleasure to be the part of this friendly group!

Finally, I would like to thank my parents and family for their love and support over the years. Special thanks to my brother Volodymyr for being accessible at any moment, for his help, support and for scientific explanations and advises. I am very grateful to my husband Taras for the enormous support, patience and for being with me at any moment even over a long distance.

Thank you very much!

Iuliia Malytska

## Table of contents

<b>Symbols .....</b>	<b>3</b>
<b>Abbreviations.....</b>	<b>4</b>
<b>Preface.....</b>	<b>6</b>
<b>Chapter I. Introduction to bipolar electrochemistry .....</b>	<b>7</b>
1.1. Introduction to bipolar electrochemistry and main objectives of the thesis.....	7
1.2. Principle of bipolar electrochemistry and its difference with conventional electrochemistry .....	8
1.3. Applications of bipolar electrochemistry .....	12
1.3.1. Analytical applications of BPE. Electrochemical detection .....	12
1.3.2. Asymmetric modification of micro and nanoparticles .....	16
1.3.3. Semiconducting materials as a substrate for bipolar electrochemistry.....	22
1.3.4. Asymmetric swimmers generated with bipolar electrochemistry .....	23
1.4. Goal of the thesis.....	27
<b>References .....</b>	<b>28</b>
<b>Chapter II. Bipolar electrochemistry with semiconducting materials.....</b>	<b>31</b>
2.1. Introduction to organic charge-transfer salts.....	31
2.1.1. Crystal structure.....	32
2.1.2. Electrical properties.....	33
2.2. Asymmetrical Janus particles: synthesis and their applications.....	33
2.2.1. BPE gradient formation.....	36
2.2.2. Indirect bipolar electrodeposition.....	37
2.3. Bipolar electrochemistry with organic crystals for metal deposition.....	38
2.3.1. Experimental details .....	39
2.3.2. Results and discussion.....	40
2.3.3. Metal-organic hybrid materials .....	49
2.3.4. Electrical characterization (asymmetric photovoltage generation) .....	49
2.3.5. Conclusions .....	51
2.4. Introduction to transition metal dichalcogenides .....	52
2.4.1. Crystal structure.....	52
2.5. Bipolar electrochemistry with macroscale MoSe <sub>2</sub> crystals .....	53
2.5.1. Asymmetric modification by different metals with BPE .....	53
2.5.2. Wireless hydrogen production on a single crystal.....	56
2.5.3. Bipolar electrochemical decontamination with macro-particles of MoSe <sub>2</sub> .....	58
2.5.4. Bulk bipolar electrochemical decontamination with micro-particles of MoSe <sub>2</sub> .....	62
2.5.5. Conclusions .....	66
<b>References .....</b>	<b>67</b>
<b>Chapter III. Bipolar electrochemistry with biological material .....</b>	<b>70</b>
3.1. DNA charge transport and studies of DNA conductivity .....	70
3.1.1. Introduction to DNA structure.....	70



3.1.2. DNA charge transport.....	71
3.1.3. Mechanism of charge transport .....	74
3.2. Bipolar electrochemistry for the asymmetrical modification of DNA by metal particles	75
3.2.1. Instrument description .....	76
3.2.2. CABED for asymmetrical metal deposition on DNA .....	78
3.2.3. Deposition of DNA molecules on the surface for BPE .....	83
3.2.3.1. Preparation of the surface for combing DNA and AFM characterization .....	83
3.2.3.1.1. <i>Silanization of mica with APTES</i> .....	84
3.2.3.1.2. <i>Silanization of mica with 7-octenyltrichlorosilane</i> .....	87
3.2.3.2. Design of new set-up for BPE experiments on mica .....	89
3.3. Wireless DNA hybridization detection with BPE .....	91
3.3.1. Introduction .....	91
3.3.2. Experimental part .....	92
3.3.2.1 <i>Preparation of CB/Au Janus particles with BPE</i> .....	92
3.3.2.2. <i>DNA probe immobilization and target hybridization on CB/Au particles</i> .....	93
3.3.2.3. <i>BPE experiments for sensing DNA hybridization event</i> .....	94
<b>References .....</b>	<b>96</b>
 <b>Chapter IV. Conclusions and perspectives .....</b>	 <b>98</b>
4.1. Conclusions .....	98
4.2. Perspectives .....	99

## Symbols

Symbol	Meaning	Units
$V$	polarization potential at the solution/substrate interface	V
$\Delta V_e$	potential difference between the two poles of the bipolar electrode and the solution	V
$\Delta V_{min}$	minimum potential value to trigger electrochemical reactions at bipolar electrode	V
$d$	distance between the feeder electrodes	cm
$d$	diameter of sphere	cm
$E^\circ$	standard potential for the redox couple	V
$E_a$	anode potential	V
$E_{appl}$	applied potential between the feeder electrodes	V
$E_c$	cathode potential	V
$l_e$	length of a bipolar electrode	cm, mm, $\mu\text{m}$
$\text{pK}_a$	acid dissociation constant	none
$r$	radius of sphere	cm
$S$	surface area of a sphere	$\text{mm}^2$ , $\text{nm}^2$
$\varepsilon$	applied electric field	$\text{V cm}^{-1}$
$\eta_{an}$	anodic overpotential	V
$\eta_{cat}$	cathodic overpotential	V
$\lambda$	wavelength	nm
$\pi$	mathematical constant	none

## Abbreviations

Abbreviation	Meaning
A	acceptor
Abs	absorbance
AFM	atomic force microscopy
APTES	3-aminopropyl-triethoxy-silane
AR	Amplex Red
BE	bipolar electrode
BMIM	1-butyl-3-methylimidazolium
bp	base pair
BPE	bipolar electrochemistry
CABED	capillary-assisted bipolar electrodeposition
CB	carbon bead
CE	capillary electrophoresis
CMT	carbon microtubes
CNT	carbon nanotubes
CT	charge transfer
CV	cyclic voltamperometry
D	donor
DIPEA	N,N-Diisopropylethylamine
DMSO	dimethylsulfoxide
DNA	deoxyribonucleic acid
dsDNA	double-stranded DNA
ECL	electrogenerated chemiluminescence
EDP	electrophoretic deposition paint
EDX	energy dispersive X-ray spectroscopy
EOF	electroosmotic flow
EPF	electrophoretic flow
ET	electron transfer
HER	hydrogen evolution reaction
H <sub>2</sub> Q	hydroquinone
HRP	horseradish peroxidase
IBED	indirect bipolar electrodeposition
ITO	indium-tin oxide
MB	Methylene Blue
MOFs	metal-organic frameworks
MWCNT	multi-walled carbon nanotube
NAD <sup>+</sup>	nicotinamide adenine dinucleotide
NHE	normal hydrogen electrode
NP	nanoparticle
OCTS	7-octenyltrichlorosilane
PEG	poly(ethylene glycol)
Ppy	polypyrrole
Q	Benzoquinone
RF	Resorufin
SAM	self-assembled monolayer
SEM	scanning electron microscopy
SPR	surface plasmon resonance
ssDNA	single-stranded DNA
TEM	transmission electron microscopy

TFSI	bis(trifluoromethylsulfonyl)imide
TMAOH	tetramethylammonium hydroxide
TMB	tetramethylbenzidine
TMDCs	transition metal dichalcogenides
TMTSF	tetramethyltetraselenafulvalene
TMTTF	tetramethyltetrathiafulvalene
TPrA	tripropylamine
TTF	tetrathiafulvalene
ZIF	zeolitic imidazolate framework

---

## Preface

The concept of bipolar electrochemistry is well known now as a method allowing to promote asymmetric reactivity on conducting objects. Another specificity of this method it is wireless action that makes it quite unique. Bipolar electrochemistry applications vary from surface patterning to sensing devices.

The aim of the present thesis was to study the utility of bipolar electrochemistry for the modification of unusual objects of different nature including biological systems. In chapter 1 a brief introduction to traditional electrochemistry and bipolar electrochemistry is presented. It also reviews recent applications of bipolar electrochemistry in different fields such as analytical detection, synthesis of asymmetric particles and micromotor generation. The following chapters describe the different experimental systems and the obtained results.

The formation of deposits of different nature can lead to new properties of materials. Thus, bipolar electrochemistry is studied in chapter two with respect to the modification of organic and inorganic crystals.

Bipolar electrochemistry can also be employed for the partial transformation of more “exotic” materials such as biological systems as we demonstrate in chapter three. First, DNA conductivity and charge transport are briefly discussed. Then, bipolar electrochemical metal deposition on DNA is explored in order to investigate its electrical properties. Different approaches are developed for optimizing the experimental conditions and the characterization of the samples. Finally, bipolar electrochemistry is used for sensing DNA hybridization with a straight forward optical read-out.

Chapter four contains the conclusion and possible future application of bipolar electrochemistry in nanoscience and microswimmer development.

## Chapter I. Introduction to bipolar electrochemistry

### 1.1. Introduction to bipolar electrochemistry and main objectives of the thesis

The phenomenon of bipolar electrochemistry (BPE) was first exploited about four decades ago<sup>1</sup>, however, nowadays has been reinvestigated for a broad range of applications in the areas of analytical chemistry<sup>2,3</sup>, surface patterning<sup>4-6</sup>, material science<sup>7-13</sup>, electronic devices<sup>14</sup>, and also macro- or microswimmer development<sup>15-17</sup>. As illustrated on the histogram below, (Fig. 1.1) the number of research papers in this field has increased exponentially in the last fifteen years, showing that BPE is a highly competitive and promising research area. The aim of this manuscript is to present the progress made in the frame of the present thesis in some specific areas of BPE and to outline some future possibilities.

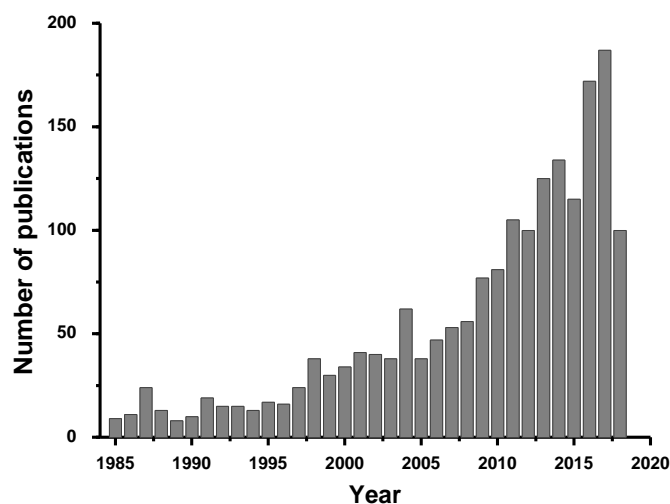


Fig. 1.1. Histogram showing the number of publications related to Bipolar Electrochemistry listed on July 2018. Adapted from SciFinder website (<https://scifinder.cas.org>).

Contrary to conventional electrochemical systems, in bipolar electrochemistry oxidation and reduction reactions can be driven simultaneously on the two poles of one electrode, therefore called bipolar electrode (BE). An important feature of this method is the absence of any direct electrical connection between the bipolar electrode and the power source. Also, this technique allows carrying out various redox reactions that can be used for surface modification and for the synthesis of asymmetric particles. The wireless mode allows performing the same process on large quantities of particles that are simultaneously addressed. In addition, the absence of any necessary immobilization on electrodes facilitates operation with small micro- or even nano particles.

Therefore, bipolar electrochemistry has been identified as a simple and low-cost technique for surface modification of substrates of different sizes made out of either metal, semiconductor<sup>18,19</sup> or carbon materials<sup>20</sup>. The use of materials exhibiting a high electrical conductivity is always favored in order to promote faradaic processes on such bipolar electrodes. However, the

chemical nature of the bipolar electrode has not yet been varied too much. That's why the main objective of this work was to study bipolar electrochemical processes on new types of materials such as special types of semiconductors (including organic-based) and bioorganic substrates. Such materials, to date, were not described as bipolar electrodes. We believe that their asymmetric modification can readily open a wide range of applications in nanoscience.

## 1.2. Principle of bipolar electrochemistry and its difference with conventional electrochemistry

Electrochemistry is a fundamental research area that studies the interplay between electrical energy and chemical energy. Electrochemistry can be found in a large number of industrial and research applications such as electrolysis, corrosion control, electrosynthesis, fuel and solar cells, electrochemical energy storage devices as for example batteries and supercapacitors, sensors for detection of various substances *etc.*

In the beginning let's consider a classic electrochemical cell and compare such a setup with a bipolar electrochemical configuration.

In a traditional electrochemical configuration, the cell usually consists of three independent electrodes: working, counter and reference electrodes, respectively. The reaction of interest takes place at the working electrode (WE). To ensure that the potential value of the WE is fully controlled, it is measured against the reference electrode (RE)<sup>21</sup> (Fig. 1.2). This electrode is designed such that the potential difference at its interface remains constant during the experiment. In order to keep this potential difference constant, no significant current must go through the RE because it promotes charge redistribution at the electrode-surface interface and as a result changes the potential difference. Therefore, the current resulting from reactions at the WE flows through a third electrode called counter electrode (CE)

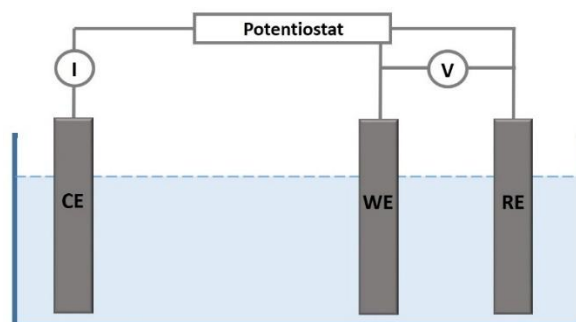


Fig. 1.2. Scheme of an electrochemical cell consisting of three electrodes: a working electrode (WE), a counter electrode (CE) and a reference electrode (RE). A power supply is used to drive the reaction in the desired direction while the ampermeter and voltmeter allow measuring the current and potential that can be related to the extent of reaction.

Electrochemical reactions occur as the result of charge transfer across the electrode-solution interface<sup>21</sup>. The driving force for the electron transfer is the difference between the potential of the electrode and the solution. This value is controlled by changing the potential applied to the WE with the help of a power supply.

For example, when the applied potential at the working electrode is tuned to a more negative value than the formal potential of an electroactive molecule dissolved in the solution, electrons may be transferred from the electrode to the species in solution and this results in an electrochemical reduction. This flow of electrons from the electrode to the solution results in a reduction current that can be measured and related to the amount of species reduced. On the contrary, when the potential of the working electrode is adjusted to more positive values, then electrons are transferred from the electroactive species of the solution towards the electrode resulting in an oxidation reaction. Hence, the oxidation current is related to the amount of oxidized species. (Fig. 1.3)

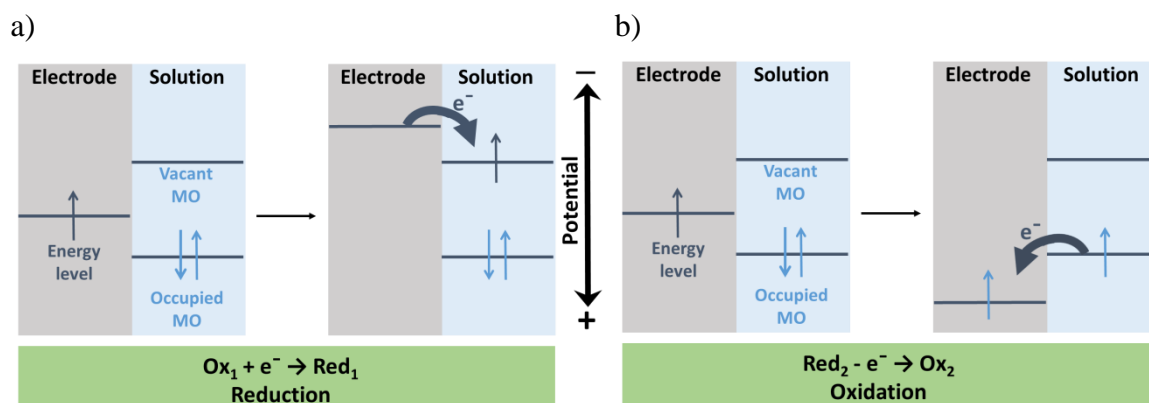


Fig. 1.3. Reduction (a) and oxidation (b) reaction involving solution species Ox and Red respectively as a result of changes in the electrode potential.

Thereby, in convectional electrochemistry the driving force of the redox reactions is directly controlled by the potential of the working electrode.

The concept of BPE is based on the phenomenon of interfacial polarization of conductive objects in an electric field. Such a polarization creates different electrochemical conditions at the two opposite sides of an object and can lead to electrochemical reactions (simultaneous oxidation and reduction) on each extremity. This conductive substrate is therefore called a bipolar electrode since it exhibits two opposite polarities at the same time.

In contrast to electrodes in conventional electrochemistry, the bipolar electrodes are not connected through a wire to the power source. So its potential cannot be controlled directly.

The typical experimental configuration of a bipolar electrochemical cell is shown in Figure 4. The cell consists of two feeder electrodes (a feeder cathode and feeder anode, respectively) connected to a power supply and immersed in an electrolyte. When a given voltage,  $E_{appl}$ , is applied between both driving electrodes, the potential is varying linearly across the solution. At the same time, the conductive object placed inside the solution remains equipotential. It means that its potential is constant everywhere on his surface. That's why there is an interfacial potential difference between the potential in solution and the object. Its value varies laterally along the bipolar electrode surface. These interfacial potential differences on the BE surface are split into cathodic and anodic overpotentials that represent the driving force of bipolar electrochemistry. The principle of electron transfer occurring between the bipolar electrode and the solution is the same as in conventional electrochemistry (Fig. 1.3). On the areas of the



electrode where the potential of the species in solution is more negative (energy of electrons higher), electrons are transferred from the solution species to the BE, causing the oxidation reaction on this side (Fig. 1.4b). On the other side, the potential of the BE is more negative, so electrons moves from the electrode to the solution, leading to a reduction reaction.

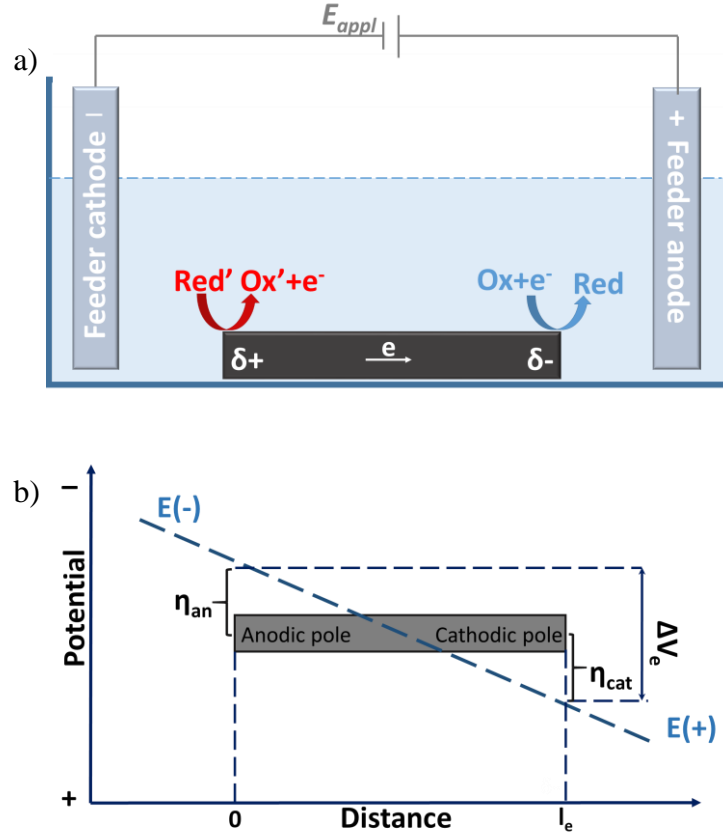


Fig. 1.4. Illustration of (a) the principle of BPE and (b) the interfacial potential polarization between the solution and the BE that generates cathodic and anodic overpotentials and promotes redox reactions at the two opposite sites.

Nevertheless, a sufficient electric field is needed to drive redox reactions at the two poles of a BE. In the BPE setup, two feeder electrodes are spaced by a distance  $d$  and the potential difference applied between them is

$$E_{appl} = E_a - E_c, \quad (\text{Eq. 1.1})$$

where  $E_a$  and  $E_c$  are the potentials of the feeder anode and the cathode respectively. The electric field in the solution is determined by the formula

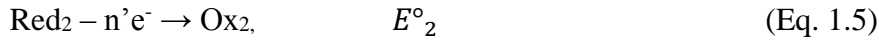
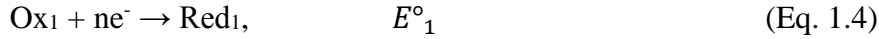
$$\varepsilon = \frac{E_a - E_c}{d} = \frac{E_{appl}}{d} \quad (\text{Eq. 1.2})$$

When a bipolar electrode is placed in such a field, the fraction of electric field which drops over this object depends on its length,  $l_e$  according to:

$$\Delta V_e = \varepsilon \times l_e = \frac{E_{appl}}{d} \times l_e \quad (\text{Eq. 1.3})$$

where  $\Delta V_e$  represents the potential difference between the two poles of the bipolar electrode and the solution, in other words – the overpotentials allowing to drive the two faradaic reactions occurring simultaneously:  $\Delta V_e = \eta_{an} - \eta_{cat}$

The electroactive species in solution can undergoes the following reactions:



Where  $n$  and  $n'$  indicate the number of electrons involved in each half-reaction with  $E^\circ_1$  and  $E^\circ_2$  being the standard potential for the redox couples  $\text{Red}_1/\text{Ox}_1$  and  $\text{Red}_2/\text{Ox}_2$ , respectively. For two redox reactions to occur simultaneously at the opposite sides of the bipolar electrode,  $\Delta V_{\min}$  must be at least equal to the difference between the formal potentials of the two redox couples involved:

$$\Delta V_{\min} = E^\circ_1 - E^\circ_2 \quad (\text{Eq. 1.6})$$

If the applied electric field induces a sufficient polarization over the size of a conductive object ( $\Delta V_e > \Delta V_{\min}$ ), then the electrochemical reactions (Eq. 1.4) and (Eq. 1.5) can occur at both ends of the conductive object. It is necessary that the reactions occur simultaneously at both poles of the conductive substrate to maintain electroneutrality. In another words, the electrons generated at the anodic pole due to an oxidation reaction must be consumed in a reduction process at the cathode.

$\Delta V_{\min}$  is a constant value for two coupled half-reactions (eq. 1.6) and can be considered as the polarization potential threshold value that should be overcome before the conductive substrate can behave as a bipolar electrode, promoting oxidation/reduction reactions. Another important parameter is the length of the bipolar electrode. As can be deduced from the Eq. 3, the applied potential needed to drive faradaic processes depends inversely on the BE length:

$$E_{\text{appl}} = \frac{\Delta V_e}{l_e} \times d \quad (\text{Eq. 1.7})$$

When the dimensions (parallel to the electric field lines) of a bipolar electrode are smaller, a higher applied potential difference between the feeder electrodes is needed to drive a desired reaction.

BPE experiments can be performed in two configurations: open (Fig. 1.5a) and closed (Fig. 1.5b).

In closed bipolar electrochemistry the substrate forms a physical barrier between both compartments where the feeder electrodes are immersed and divides the electrolyte into two separate areas<sup>22</sup>. In this case the electrochemical current passes exclusively through the bipolar electrode and can be directly measured due to the absence of an ionic current path and can give information about the rates of the faradaic processes<sup>22</sup>. In addition, the potential across the substrate is strictly proportional to the potential applied across the feeder electrodes<sup>23</sup>, because there is no other current pathway. The main advantage of this configuration is that electrochemical reactions occur on the substrate already at a relatively low electric field strength.

In contrast, in open bipolar electrochemistry, the conductive substrate is immersed in the electrolyte and the overall current is divided into two fractions: one fraction of the current is flowing through the conducting object, and another fraction – through the solution via the migration of charged species. Therefore, in this configuration, it is important to work with low ionic strength solutions in order to favor a current flow through the conducting object. A too high ionic strength leads to a large ionic current through the solution, preventing the current to pass through the bipolar substrate.

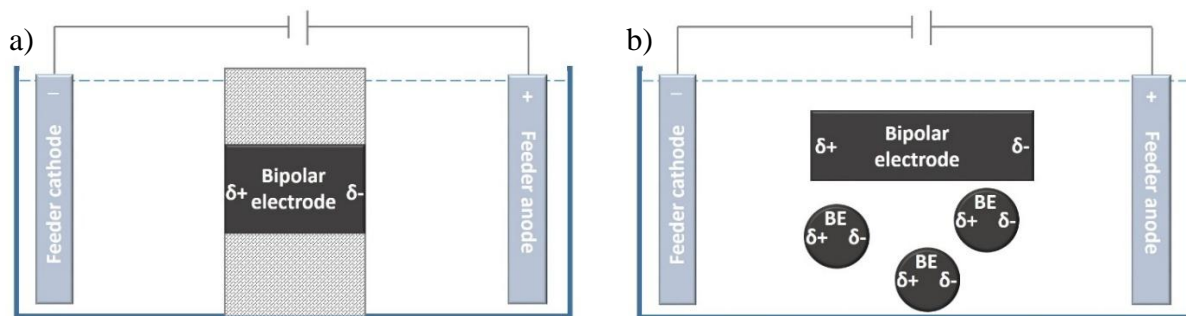


Fig. 1.5. Scheme of a conductive substrate placed between two feeder electrodes in an electrolyte solution in the (a) closed bipolar configuration, and (b) open bipolar electrochemical cell.

### 1.3. Applications of bipolar electrochemistry

While the basic concepts associated with BPE have been known for several decades, nowadays this method has been reinvestigated and received considerable attention due to the possible miniaturization of bipolar electrodes. The use of micro- or even nanometer scale objects opened various applications in many fields such as analytical chemistry<sup>2,3</sup>, surface patterning<sup>4-6</sup>, material science<sup>7-13</sup>, electronic devices<sup>14</sup>, and macro- or microswimmer development<sup>15-17</sup>.

#### 1.3.1. Analytical applications of BPE. Electrochemical detection

Starting from the first undergraduate lectures, conventional electrochemistry is known as a valuable analytical tool for different applications. BPE readily complements this domain having several key advantages for analytical purposes, especially for sensing and screening. As was mentioned before, there is no need of connection (i.e. wiring) between a bipolar electrode and the power source and therefore a lot of electrodes can be controlled simultaneously with a single power supply. Also, BPE allows to perform detection at electrodes of micro- or even nanoscale dimensions opening access to a very local measurement in a specific environment or to enhance the analytical response due to the large electroactive surface area developed by thousands of electrodes in parallel.

The principle of BPE sensing and screening devices is based on the coupling of electrochemical reactions at opposite sides of a BE. Since the same amount of current is passing through the two poles of the BE, it can be used to perform a given reaction at one pole (sensing reaction) and to transduce it to an analytical signal at the other pole (reporting reaction). If for example the sensing reaction is an electrochemical reduction, then the concomitant oxidative reaction will take place at the anodic pole of the BE<sup>24</sup>. Due to charge neutrality, the amount of oxidized species at the anodic pole must correspond to the number of electrons involved at the cathodic pole of BE. Usually, a reporting reaction generates an easily observable signal such as electrochemiluminescence (ECL)<sup>25-29</sup>, fluorescence<sup>30</sup> or anodic dissolution of metal films<sup>3,31,32</sup> which are typically used as reporting reactions.

A first basic sensing platform based on bipolar electrochemistry was developed by Crook's group<sup>3,31</sup>. They used a gold electrode partially covered with a thin silver layer on the reporting side and the cathodic electrochemical reaction triggers the dissolution of the silver layer at the

anodic pole (Fig. 1.6). Once again, as the reduction and oxidation reactions are correlated, the rate of one is identical to the rate of the other. As a consequence, the sensing reaction triggers a proportional amount of Ag dissolution. As a proof of principle, the sensing of *p*-benzoquinone in solution was studied<sup>31</sup>. During application of an electric field, *p*-benzoquinone is reduced at the cathodic poles of BEs, which enables the oxidation of Ag at the anodic poles. The dissolution of the Ag layer starts more efficiently at the very end of the BEs (i.e. extremity of the anodic poles) and proceeds towards the center. Fig 6b shows such a dissolution after 290 s of experiment with a shorter length of Ag coating on the BEs (the dark regions of the electrodes correspond to the parts where Ag electro-dissolution took place). Furthermore, by using a split BPE configuration, the charge passing through the BE can be measured externally and a linear relationship between charge and remaining Ag film length was established.

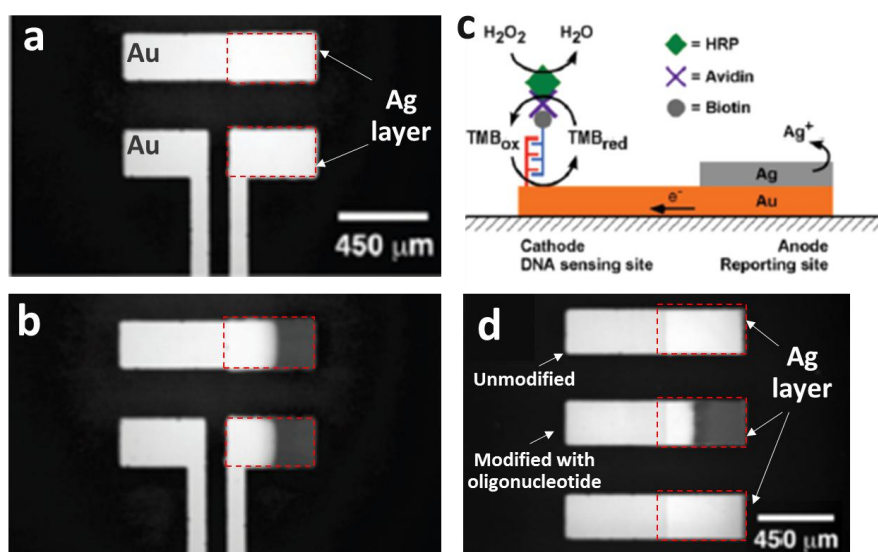


Fig. 1.6. BPE sensing based on dissolution of a metal film. (a, b) Optical micrographs of Ag-coated continuous (top) and split (bottom) BPE configurations (a) before and (b) after application of the electric field for 290 s in a solution of *p*-benzoquinone. (c) Scheme of the DNA sensing platform. (d) Optical micrograph of oligonucleotide modified (middle) or thiol-protected (top and bottom) electrodes after application of the electric field. Adapted from ref.<sup>31</sup>

Based on an extension of this proof-of-principle demonstration, more complex sensing systems were developed for DNA detection<sup>31</sup> with a typical strategy presented in Fig. 1.6c. The cathodic pole of a gold BE was modified with an oligonucleotide and the anodic pole with a silver layer. The target complementary biotin-modified oligonucleotide was connected with an avidin-functionalized horseradish peroxidase (HRP). Hybridization of the complementary DNA strand labeled with HRP catalyzes the  $\text{H}_2\text{O}_2$  conversion and activates the oxidation of tetramethylbenzidine (TMB). When applying a sufficiently high electric field across the BE, oxidized TMB is reduced at cathodic pole, and this triggers the simultaneous oxidation (electro-dissolution) of Ag metal present at the anodic pole, probing the hybridization step (Fig. 1.6d).

This technique was also reported for screening electrocatalysts for molecular oxygen reduction reaction<sup>3,32</sup>. The setup was comprised of an indium-tin oxide (ITO) bipolar electrode, containing different electrocatalysts of interest deposited at the cathodic pole and parallel silver

microbands at the anodic one (Fig. 1.7 a, b). Two different catalysts were studied consisting of Pt and Au dendrimer-encapsulated nanoparticles and compared to an unmodified ITO surface. After exposure for a certain time to the electric field, the different catalytic efficiencies are visually observable and can be easily determined by counting the remaining number of silver microbands (Fig. 1.7e).

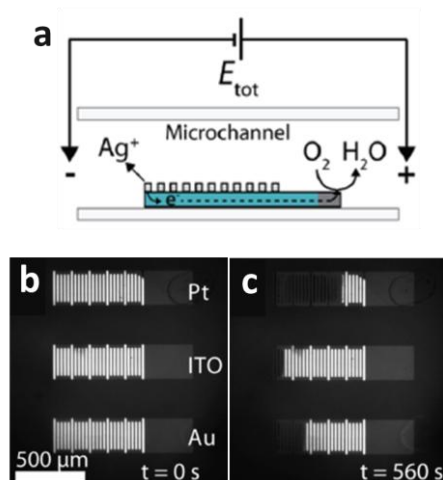


Fig. 1.7. (a) Scheme of the sensing platform used for screening oxygen reduction electrocatalysts. (b, c) Optical micrographs showing a set of three BEs that have different electrocatalysts at their cathodic poles (b) before and (c) after application of the electric field. Adapted from ref.<sup>3</sup>

The combination of BPE with a reporting ECL process can be an even more sensitive tool. Crooks' group<sup>26,27,33,34</sup> exemplified the detection of a large variety of compounds by using such a technique. They used an initial set-up consisting of three Au electrodes that were positioned inside a microfluidic device. An electric field was applied via a power supply by two Pt wires that were placed in reservoirs at both ends of the microfluidic channel. In the reported examples, the reduction of an analyte at the cathodic pole of the Au electrode is transduced by the emission of light due to the simultaneous oxidation of  $[\text{Ru}(\text{bpy})_3]^{2+}$  luminophore and the ECL co-reactant, tri-*n*-propylamine (TPrA), at the anodic pole. First, using microfluidics-based sensing systems, the authors reported the detection of benzyl viologen<sup>35</sup>, ferrocyanide<sup>33,34</sup> and dopamine<sup>34</sup>. Afterwards, this technique was used for the detection of DNA<sup>26,27</sup>. It was also shown, that anodic and cathodic reactions are coupled electrically and the ECL intensity at the anode is directly related to the rate of the cathodic reaction<sup>35</sup>.

The typical device for DNA detection is presented in Fig 1.8a. The gold plates modified with thiol-functionalized DNA probes were used as BEs (Fig. 1.8b). These plates were incubated in a solution containing the target DNA functionalized with Pt nanoparticles. Then, the cell was filled with a solution containing  $[\text{Ru}(\text{bpy})_3]^{2+}$  and under application of electric field, a red light emission was observed at the anodic pole signaling the DNA hybridization (Fig. 1.8c). The ECL observed at the anodic pole corresponds to  $[\text{Ru}(\text{bpy})_3]^{2+}$  oxidation and occurs together with oxygen reduction catalyzed by Pt nanoparticles at the cathodic pole. Therefore, when a target Pt-NPs modified DNA is present in a given solution, the emission of light is observed (Fig. 1.8c top) while in its absence, no light was emitted (Fig. 1.8c bottom).

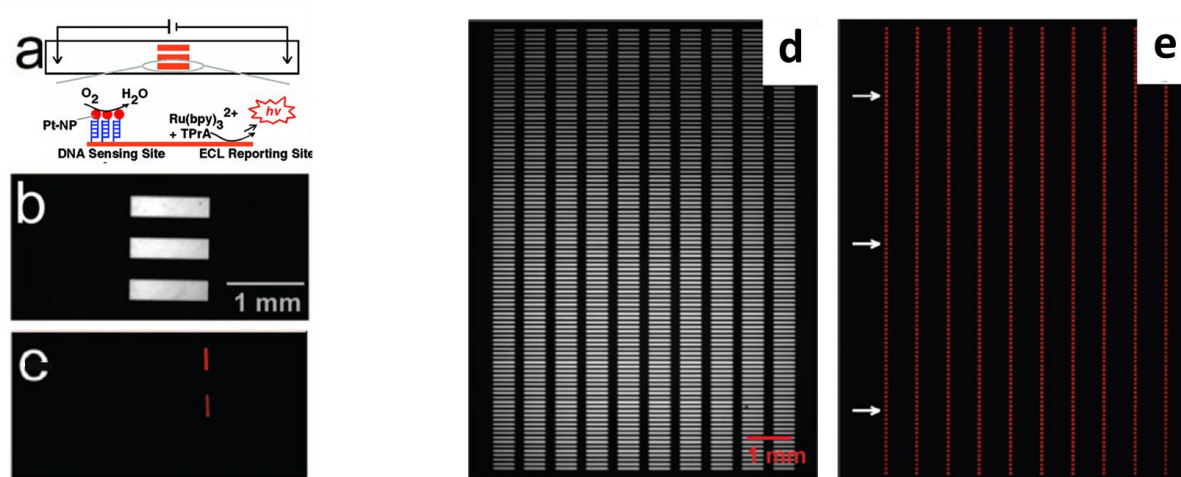


Fig. 1.8. BPE sensing based on ECL signal. (a) Schematic illustration of the microdevice. (b, d) Optical micrograph of the bipolar electrodes used. (c, e) The ECL signal as result of complementary DNA hybridization (two top electrodes are exposed to the labeled target; bottom electrode – no target DNA in solution). Adapted from ref.<sup>26,27</sup>

The same principle was adapted for arrays of up to 1000 individual bipolar electrodes<sup>26</sup> (Fig. 1.8d, e). It was shown that the ECL signal could be generated simultaneously at the cathodic poles of all microelectrodes due to oxygen reduction reaction at the anodic poles, leading to a high density sensing array.

Finally some redox active species in solution were also indirectly detected by fluorescence<sup>30</sup>. Since upon application of a potential, pH gradients are generated near the vicinity of the bipolar electrode edges, a fluorescent pH sensitive reporter can be used to quantify reactions on the BE. There are two advantages with this approach. First, it is possible to detect species which are either oxidized or reduced at the BE. Second, immobilization of chemical species at the BE is not anymore required. The authors have chosen fluorescein as a pH-sensitive dye having a higher quantum yield when fully deprotonated (i.e. dianionic form). Thereby its fluorescence is higher under more basic conditions and this property was used as an indicator of electrochemical reactions at the bipolar electrode. The detection of 1,4-naphthoquinone or dopamine was shown in this work. In the first case, the reduction of 1,4-naphthoquinone to benzoquinone takes place at the cathodic side of the bipolar electrode where protons are also consumed. In another case, dopamine oxidation takes place at the anodic pole of the bipolar electrode, which is coupled with proton reduction reaction at the cathodic pole. In both cases, the consumption of  $H^+$  increases locally the pH, which leads to an enhancement of the fluorescence of fluorescein (Fig. 1.9).



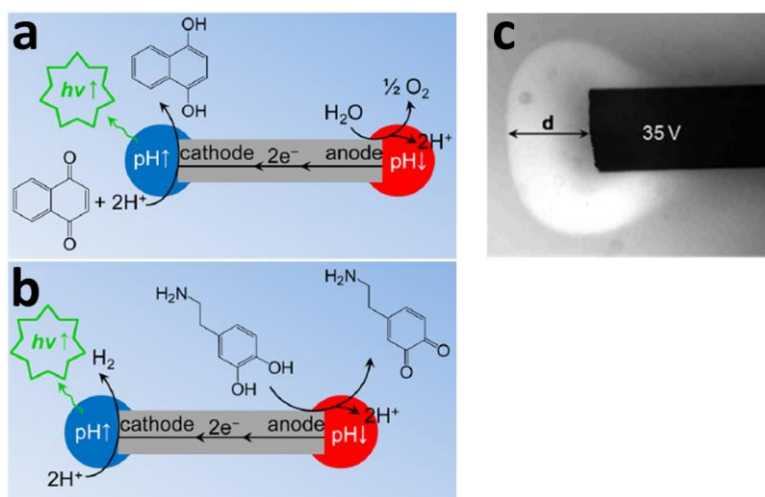


Fig. 1.9. Scheme of detection of (a) 1,4-naphthoquinone and (b) dopamine by localized pH-triggered fluorescence enhancement. (c) Fluorescence microscope image for the detection of 1,4-naphthoquinone at the cathodic side of bipolar electrode in the presence of the fluorescein. Adapted from ref.<sup>30</sup>

### 1.3.2. Asymmetric modification of micro and nanoparticles

For the first time bipolar electrochemistry has been reported in fluidized bed reactors where conducting particles are dispersed and act as individual electrodes<sup>36</sup>.

A fluidized electrode consists of a bed of conducting particles supported by a distributor through which the electrolyte flows<sup>36–39</sup>. Because of the large electrode area per unit volume, development efforts were focused on the application of fluidized electrodes in organic synthesis,<sup>37,39</sup> as fuel cell<sup>38,40</sup> and electrochemical battery electrodes<sup>41</sup>.

As an example, the work of Backhurst' group can be cited. They have demonstrated the successful cathodic reduction of *m*-nitrobenzene sulfonic acid to the corresponding metanilic acid (*m*-aminobenzene sulfonic acid) in aqueous sulphuric acid. It was reported that the performance of fluidized bed electrode is highly dependent on the degree of fluidization<sup>39</sup>.

Fluidized bed electrochemical reactors have also been used for degradation of organic pollutants as demonstrated in a work of Zhou and Wu<sup>42</sup>. The authors reported the oxidation of *p*-nitrophenol using fluidized bed electrodes with high efficiency.

A new era of BPE started at the end of 90's revealing novel attractive features for various applications in fields ranging from analytical chemistry to materials science<sup>24,43</sup>. New electrochemical cells and new micro-objects started to be used for BPE. Bradley's group was the first to demonstrate contactless deposition of metal or polymer on micrometer sized conducting particles or carbon nanowires<sup>7,9,14,44,45</sup>.

They have also adapted the concepts of bipolar electrochemistry to the formation of Cu wires between two particles<sup>14</sup>. The method is based on the concomitant electrodisolution and electrodeposition between two components in one direction under the influence of an electric field.<sup>14</sup> This method is known as Spatially Coupled Bipolar Electrochemistry (SCBE) and is used to connect discrete metal substrates. Under the applied electrical field, copper ions are

produced by the oxidation of copper on one face of the copper bead (i.e. anodic pole). The concentration of copper ions between the two beads continues to increase until it becomes sufficient for the reduction of copper ions at the cathodic pole on the opposite bead. Dendrite growth is initiated by the reduction of copper ions that have been generated by the electrodisolution of copper. Growth of the dendrites continues until it contacts the neighbouring copper bead (Fig. 1.10). This initial work demonstrated that it was possible to make a contact between isolated micrometer-sized structures using only an electrical field and without any chemical additives. This technique opens new approaches in microelectronic engineering and can serve as an alternative to photolithography methods for making electrical contacts.

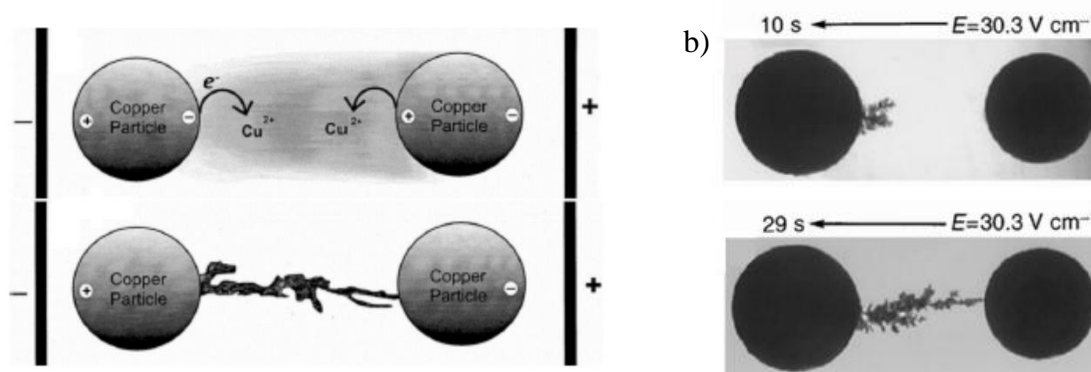


Fig. 1.10. (a) Schematic illustration of wire formation between two metal particles under bipolar conditions. (b) Wire formation after application of an electric field of  $30.3 \text{ V cm}^{-1}$  during 10 s and 29 s, respectively. Adapted from ref.<sup>14</sup>

In 1999, a bipolar electrochemical experiment was first used to trigger electrodeposition of a palladium catalyst on micrometer-sized graphite particles<sup>44</sup> (Fig. 1.11). In this work, graphite particles were sandwiched between cellulose paper to avoid any movement during the modification. The space between two flat graphite electrodes was filled with a  $\text{PdCl}_2$  solution in a mixture of toluene/acetonitrile (1:1) and an electric field was applied. The electric field triggers electrodeposition of palladium by reduction of  $\text{Pd}^{2+}$  on the cathodically polarized region of each particle, and this reaction is combined with the oxidation of the solvent at the anodic side. After washing the paper, catalytically active graphite particles were obtained.

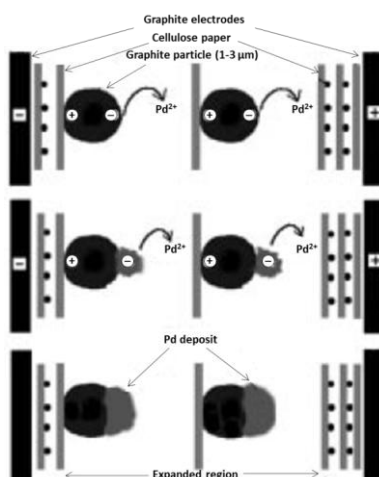


Fig. 1.11. Schematic illustration of the preparation of catalyst by bipolar electrodeposition. Adapted from ref.<sup>44</sup>



Bipolar electrodeposition has been effectively used in the same way to deposit Pd onto carbon nanotubes (CNTs) and carbon nanofibers (CNFs)<sup>8</sup>. At the same time the deposition of polypyrrole on carbon nanopipes (CNPs)<sup>9</sup> was also reported. Such material was shown to be interesting due to the possibility to guide water inside a nanopipe. Bradley's group also obtained bifunctional carbon particles modified with Pd and Au at the two opposite sides<sup>44</sup>. To deposit sequentially these two different metals, the carbon particles were first immersed in a solution of PdCl<sub>2</sub> in toluene/acetonitrile (1:1) solvent and the electric field was applied. Then the solution of palladium was replaced by AuBr<sub>3</sub> and the same electric field was applied with reversing the polarity to allow the second electroreduction to occur at the opposite side of the particles.

After these initial works, several groups focused their attention on electrodeposition by using bipolar electrochemistry. In the last fifteen years this technique was used to deposit different materials such as metals<sup>10,11,20</sup> or conducting polymers<sup>46–48</sup> to create a large variety of asymmetric particles.

Bipolar electrochemistry progressively became a straightforward method to produce asymmetric particles. Such objects consisting of two (or more) components of different nature and/or exhibiting different chemical properties<sup>49</sup> are known in the literature as *Janus* particles<sup>50</sup>. In contrast to other methods, BPE does not need any physical connection of the particles with a 2D-template or with a power source, thus allowing the bulk synthesis of various multicomponent micro- and nanoparticles in solution. This is indeed very suitable for industrial large-scale production and various applications.

Bradley's group performed the primary work for the development of bipolar electrodeposition technology. Then, BPE was expanded and adapted to the modification of objects featuring different shapes such as anisotropic carbon beads and carbon tubes<sup>20</sup>.

Recently, our group developed a method to modify glassy carbon beads with different metals in the bulk<sup>20</sup>. To avoid the rotation of these particles during the electrodeposition step, the viscosity of the reaction medium was increased by addition of a jellifying agent. Using appropriate experimental conditions, carbon beads were modified by deposition of gold and silver<sup>20</sup>.

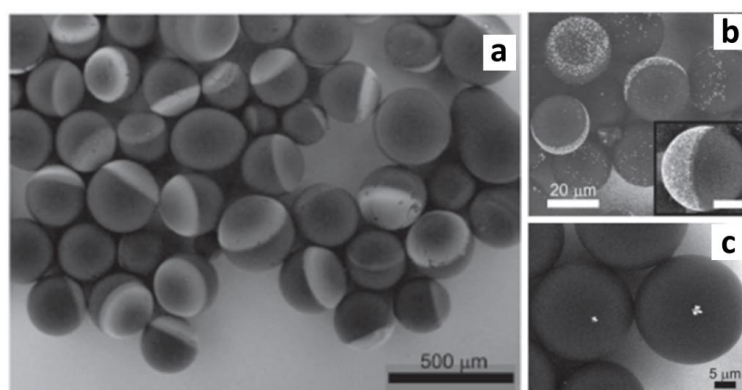


Fig. 1.12. Electron microscope images of glassy carbon beads modified with (a, b) gold and (c) silver. Adapted from ref.<sup>20</sup>

Due to the polydispersity of the carbon particles their intrinsic polarization is size-dependent in the same electric field and therefore the deposit size is varying from an almost hemispherical metal coating to a single point deposit (Fig. 1.12a). It was even shown that by controlling the electric field strength, it is possible to obtain a silver cluster focused at a single spot of the beads (Fig. 1.12c).

Carbon beads were also asymmetrically modified with an organic layer by bipolar electrografting<sup>46</sup>. In this case, functional aryl diazonium molecules were grafted on one end of a glassy carbon bead by electrochemical reduction. To visualize the grafted organic layers, the microparticles were further treated with negatively-charged gold nanoparticles, interacting with pending ammonium groups, or with amino-fluorescein when possessing carboxylic acid groups. In the first case the grafted layer was characterized by scanning electron microscopy (SEM) (Fig. 1.13a) while in the second case a fluorescence microscope was used to observe the beads labeled with the fluorophore (Fig. 1.13b).

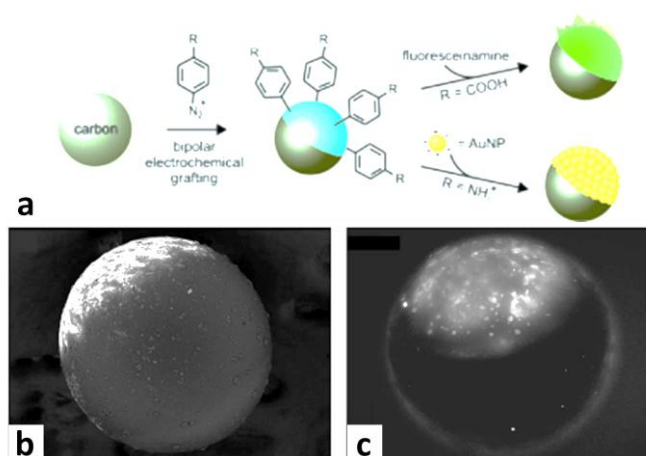


Fig. 1.13. (a) Schematic illustration of the modification of carbon beads with aryl diazonium compounds followed by detection either with nanoparticles or with a fluorophore. (b) SEM image of a glassy carbon bead modified by an amino-functionalized organic layer and post-treated with negatively charged gold nanoparticles. (c) Fluorescent micrograph of a glassy carbon bead modified by a carboxylic acid organic layer and post-treated with fluoresceinamine. Adapted from ref.<sup>46</sup>

Kong and coworkers reported the site-selective electrodeposition of the organic conducting polymer polypyrrole (PPy) on spherical carbon beads<sup>47</sup>. They also introduced the use of an ionic liquid such as 1-butyl-3-methylimidazolium bis(trifluoromethylsulfonyl)imide ([BMIM][TFSI]) as a reaction medium. Compared to a usual organic solvent ( $\text{CH}_3\text{CN}$ ), the PPy layers obtained in an ionic liquid had smaller surface roughness and better mechanical stability (Fig. 1.14).

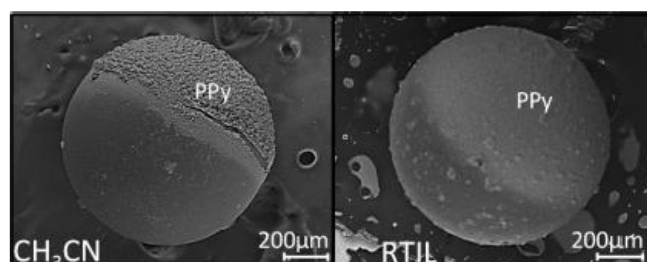


Fig. 1.14. Glassy carbon beads modified with PPy by BPE in (a) acetonitrile with  $\text{TBA}[\text{PF}_6]$  as supporting electrolyte and (b) in [BMIM][TFSI] ionic liquid medium. Adapted from ref.<sup>47</sup>

Since not all materials can be directly deposited from electroactive precursors, indirect bipolar electrochemistry was proposed as an alternative method to produce asymmetric particles from redox-inactive species<sup>51</sup>. This approach consists in creating suitable conditions to promote secondary reactions induced by electrochemical processes. As an example, when an electric field is applied across an aqueous solution, each bipolar electrode has an acidic and a basic side. Water reduction at the cathodic side of BE leads to local formation of OH<sup>-</sup> ions (i.e. H<sup>+</sup> consumption) and therefore a pH increase while water oxidation into oxygen causes the concomitant production of H<sup>+</sup> and a pH decrease<sup>52</sup>. This local change in pH can be easily observed *in-situ* by adding a pH indicator<sup>52</sup>. Such a pH change in the vicinity of the polarized object can be used to indirectly deposit organic layers such as electrophoretic deposition paints or inorganic layers<sup>51</sup>. As an example, SiO<sub>2</sub> can be produced by polycondensation of the hydrolyzed tetraethylorthosilicate precursor (Si(OCH<sub>3</sub>)<sub>4</sub>), which is catalyzed by hydroxyl ions. When the bipolar electrode is polarized, the local OH<sup>-</sup> concentration rises at the cathodic pole leading to selective SiO<sub>2</sub> deposition<sup>51</sup> (Fig. 1.15a). In addition, the morphology of the deposit can vary depending on the nature of the silica precursor used. For example, silane with fewer alkoxide groups will have less chemical functions for polycondensation, and therefore lead to more flexible and smoother layers. Titanium oxide deposits can be obtained at the anodic pole of bipolar electrodes by a sol-gel procedure starting from a colloidal solution of titanium(IV) isopropoxide and tetramethylammonium hydroxide (TMAOH)<sup>51,53</sup> (Fig. 1.15b). Similar experiments have also been carried out to deposit electrophoretic paint<sup>51</sup> (Fig. 1.15c). The anodic electrophoretic deposition paints are negatively charged due to the presence of carboxyl groups. Under polarization of the carbon beads in solution, a local change of pH promotes the neutralization of these carboxyl groups at the anodic pole of the bipolar electrode.

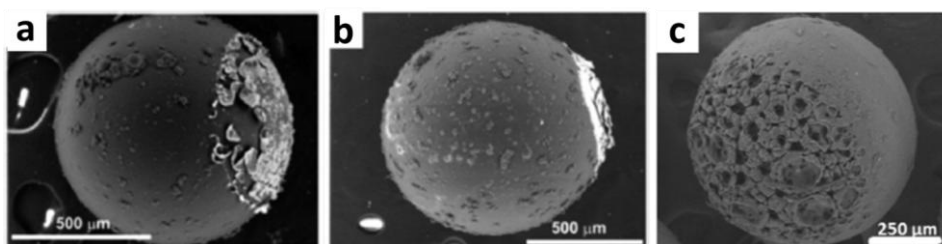


Fig. 1.15. SEM images of glassy carbon beads modified by indirect bipolar electrochemistry with (a) silica, (b) titanate and (c) cathodic electrophoretic deposition paint, respectively. Adapted from ref.<sup>51</sup>

As a result, the polymer chains precipitate due to a decrease in solubility and get deposited at the surface. In the same way, carbon beads can be modified with cathodic electrophoretic deposition paint. Due to the porosity of such deposits (Fig. 1.15c), this type of materials can be used as an immobilization matrix for different species like dyes or nanoparticles.

The concept of bipolar electrochemistry was also adapted to the modification of anisotropic carbon tubes<sup>10,11,13,54</sup>. This method is based on a capillary electrophoresis (CE) technique and called capillary assisted bipolar electrodeposition (CABED). The CE equipment provides several important advantages for bipolar electrodeposition on suspensions of particles. Most

importantly, this technology allows applying high values of electric field, which is the essential parameter for the polarization of small (nano)objects. Furthermore, the presence of liquid flux, generated by electroosmotic flow (EOF) within the capillary allows the movement of particles from the starting point (injection) to the final point (collection) and therefore many particles can be modified at the same time during their passage through the capillary. In addition, anisotropic particles are readily aligned by the electric field and keep the same orientation during modification, so they do not need to be immobilized.

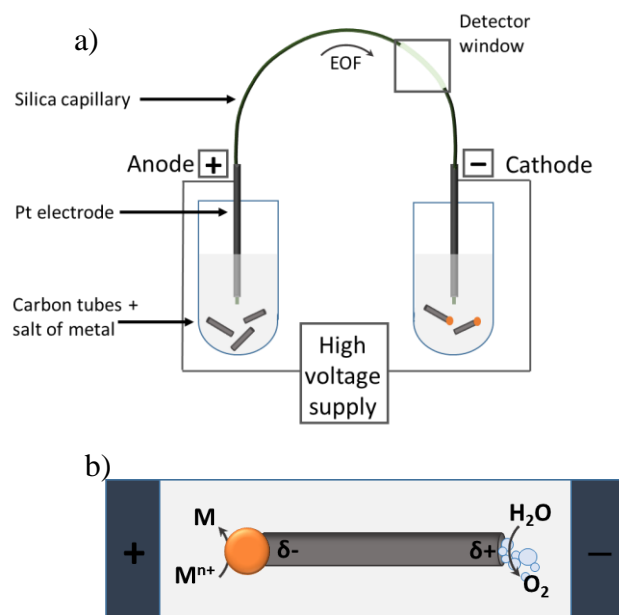


Fig. 1.16. (a) Schematic illustration of the set up for capillary-assisted bipolar electrodeposition (CABED). (b) Schematic illustration of a tubular bipolar object in the capillary during CABED process.

By using this setup, the selective modification of carbon microtubes was performed<sup>13</sup>. Various clusters of different metals such as gold, nickel<sup>11</sup>, copper<sup>13</sup> were successfully obtained at the extremity of these tubes (Fig. 1.17a-c). The schematic illustration of the set-up used is presented in Figure 1.16. Both ends of the silica capillary are placed inside two compartments with two feeder electrodes connected to the power source. Then the suspension of carbon tubes to be modified together with the electrodeposible component (usually a metal salt) is injected at anodic compartment. When the electric field is applied, an EOF is generated inside the capillary and transports the carbon tubes and metals cations from the anodic compartment to the cathodic one. During the passage through the capillary, the reduction of metal salt to metal cluster takes place at the cathodically polarized side of the tubes and this reaction is combined with water oxidation at the anodically polarized side (Fig. 1.16b). Finally, asymmetrically modified objects can be obtained and collected at the outlet compartment (Fig. 1.16a).

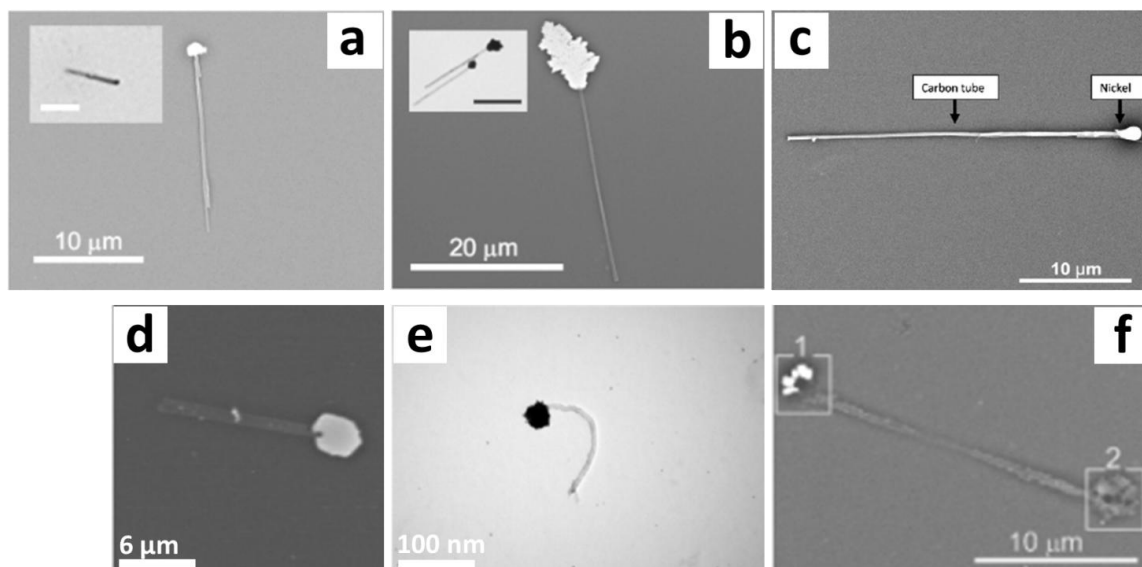


Fig. 1.17. SEM pictures of CMTs modified at one extremity with (a) gold, (b) copper, (c) nickel, (d) silver, (e) TEM image of a MWCNT modified with gold, (f) SEM image of a dumbbell-like CMT modified with copper at one end and PPy at another. Adapted from ref.<sup>10,11,13</sup>

The same method was used to modify smaller objects such as multi-walled carbon nanotubes (MWCNTs) with gold (Fig. 1.17e)<sup>10</sup>. Metal clusters were detected by TEM imaging and their nature was confirmed with EDX spectroscopy. The CABED technology was also used to obtain dumbbell-like carbon microtubes modified either symmetrically by copper on both sides or with copper at one end and PPy at the other end<sup>13</sup> (Fig. 1.17f). To achieve this double-side modification, pulsed potential was used allowing the reorientation of the tubes between the deposition steps.

### 1.3.3. Semiconducting materials as a substrate for bipolar electrochemistry

The examples described above show that BPE is quite versatile and is a simple technique to perform redox reactions at two extremities of a conducting object. However, the majority of these experiments were performed on bipolar electrodes made out of either metallic or carbon materials that exhibit a high electrical conductivity. In a BPE cell, the object should be more conductive than the surrounding media, in order to favor the bipolar current flowing through it. In the case of a highly conducting media, a majority of the current passes through the solution as ionic current, thus limiting drastically the electrochemical reactivity on the bipolar electrode. This explains why metallic substrates are among the best to be used for BPE. Nevertheless for some applications it would be interesting to extend the concept of BPE also to less good conductors such as semiconductors. Only few works describe semiconducting materials as a possible substrate for BPE<sup>18,19</sup>. Ongaro *et al.* proposed for the first time a special procedure for the site-specific deposition of metal on TiO<sub>2</sub> nanofibers<sup>19</sup>. They exposed nanofibers to an electric field simultaneously with UV light irradiation. This coupling allows the generation of excited electron-hole pairs and drives them to the opposite extremities of the fibers where they can react with redox species in solution (Fig. 1.22a). When TiO<sub>2</sub> nanofibers were dispersed in

chloroauric acid solution and exposed to UV light without electric field, random gold deposits were formed all over the nanofibers' surfaces. Meanwhile, under an applied electric field, electrons created by UV light absorption were directed to the positively polarized side of the fibers leading to gold reduction on it. In this way, the deposit was localized on a single extremity only but not alongside the entire surface. (Fig. 1.22a).

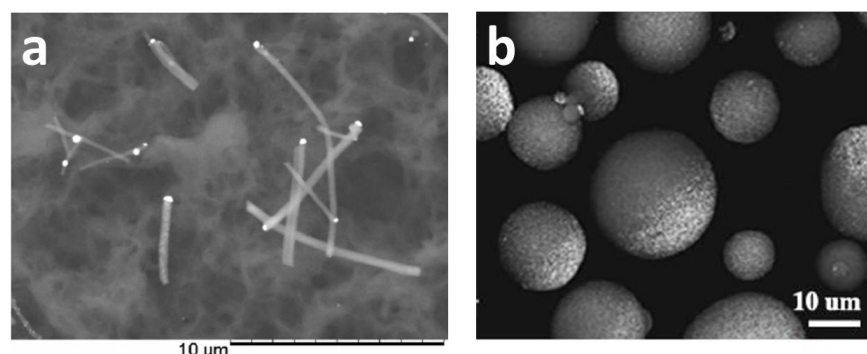


Fig. 1.22. SEM images of (a)  $\text{TiO}_2$  nanofibers and (c)  $\text{TiO}_2$  microparticles generated by UV irradiation under the simultaneous application of an electric field. Adapted from ref.<sup>18,19</sup>

Isotropic  $\text{TiO}_2$  semiconducting particles were also successfully modified by light-induced bipolar electrochemistry with either gold or platinum<sup>18</sup>. The authors used the same principle as in the previous work for metal deposition with the difference that isotropic particles must be immobilized to prevent their rotation during the experiment. Under simultaneous application of both electric field and UV irradiation, electrons and holes are separated, which breaks the symmetry of these semiconducting particles and promotes the modification selectively at one side. The gold or platinum deposits were observed at the anodic side of macro- or microscale  $\text{TiO}_2$  particles. This observation is somehow surprising as it is an opposite polarity compared to bipolar electrochemistry on conducting objects. However, this can be explained based on electric field-induced charge separation occurring inside the semiconductor particle. In addition, such a combination of electric field with UV light promotes electrodeposition at much lower potentials than the theoretical values needed for conventional bipolar electrodeposition. In this case, light provides the chemical energy and the electric field favors separation of electrons and holes in space, pulling them to the opposite extremities of the particles.

These initial works show that BPE can be potentially applied not only to well-conducting materials but also to semiconducting objects. BPE allows to break the symmetry of particles by modifying them selectively at one extremity and in a wireless way. Such metal/semiconductor hybrid materials are interesting for potential applications in photocatalysis, photovoltaics, environmental decontamination or energy conversion.

#### 1.3.4. Asymmetric swimmers generated with bipolar electrochemistry

Nanotechnology in its primary sense involves manipulating matter at the nanoscale. One example are roving micro- and nano-objects, capable to carry out a desired lateral or rotational motion.

Among other approaches, BPE is a versatile technique that has been used for motion generation. This goal can be achieved in two ways. The motion of particles can be induced either directly due to chemical reactions in solution close to the surface of a bipolar electrode<sup>16,43,55–58</sup> or indirectly by the synthesis of functionalized particles with a deposit that can drive motion as a function of a given external stimulus<sup>11,12,59,60</sup>.

As discussed above, during a BPE experiment, reduction and oxidation reactions take place simultaneously at the opposite ends of conducting particles. This principle was used to move particles either by the decomposition of solvent near the ends of a conducting particle<sup>16,58</sup> or by dissolution of a metallic object at its anodic side and re-deposition of dissolved metal cations at the opposite side<sup>15</sup>.

The group of Mallouk demonstrated that bimetallic Pt/Au nanorods can be propelled in  $\text{H}_2\text{O}_2$  solution by its simultaneous oxidation at the Pt moiety and reduction at the Au end<sup>58</sup>. Due to charge balance, protons created at the Pt side move from the anodic end to the cathodic end of the rod. The movement of protons would occur primarily in the electrical double layer of the metal-solution interface, resulting in an EOF of water from Pt to Au and a movement of the rod in the opposite direction (Fig. 1.18).

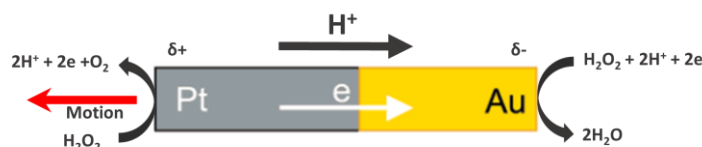


Fig. 1.18. Bipolar electrochemical decomposition of  $\text{H}_2\text{O}_2$  at a bimetallic Pt/Au nanorod. Adapted from ref.<sup>58</sup>

Another example of motion was based on a deposition/dissolution mechanism<sup>15</sup>. In this work, a Zn dendrite was placed in a capillary filled with an aqueous  $\text{ZnSO}_4$  solution. When electric field is applied, the Zn dendrite acts as BE, its anodic pole starts to dissolve due to metal oxidation, while deposition takes place due to reduction from  $\text{Zn}^{2+}$  in solution at its cathodic pole. This results in the apparent locomotion of the dendrite (Fig. 1.19). The change in morphology observed during the movement proves that the transport of these dendrites is due to a dynamic self-regeneration mechanism.

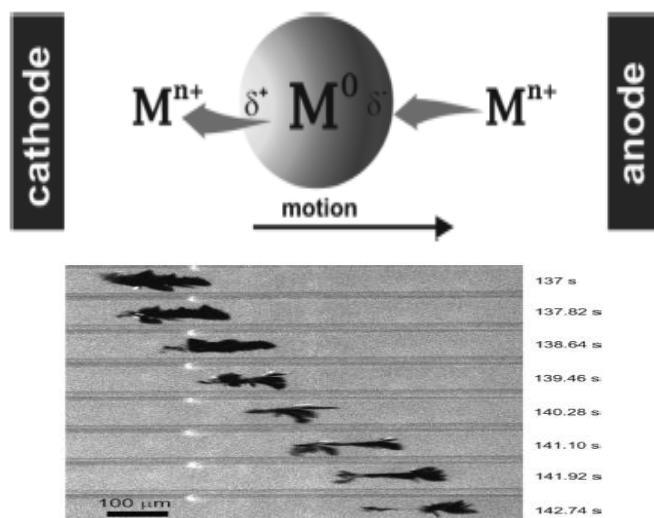


Fig. 1.19. (a) Bipolar self-regeneration principle and (b) Optical micrographs of a zinc dendrite in a glass capillary filled with a zinc sulfate solution under the influence of an external electric field. Adapted from ref.<sup>15</sup>



Another mechanism for micro-object propulsion is based on asymmetric bubble production in the presence of an electric field<sup>16</sup>. In this experiment due to simultaneous oxidation and reduction of water, oxygen and hydrogen bubbles are produced at opposite poles of a spherical BE. Since the amount of H<sub>2</sub> produced at the cathodic pole of the BE is twice larger than O<sub>2</sub> produced at the anodic pole, the resulting force pushes the bead towards the feeder cathode (Fig. 1.20a, b, c). For enhancing the propulsion speed, one bubble-producing reaction can be eventually quenched. This was achieved by addition of a sacrificial molecule (hydroquinone) which is easier to oxidize than water (Fig. 1.20d, e, f).

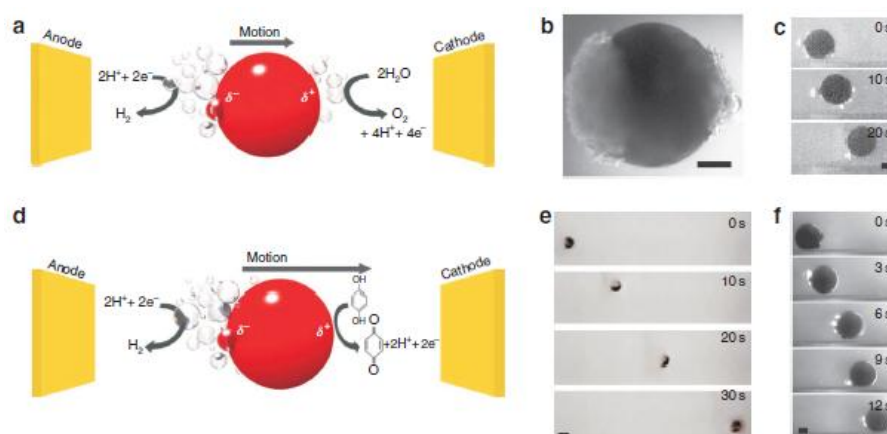


Fig. 1.20. Motion generation by BPE. (a) Scheme of water splitting by BPE. (b) Optical micrograph of a stainless steel 1 mm spherical particle exposed to an electric field. The left part of the bead is the cathodic pole where H<sub>2</sub> bubbles are produced whereas the right part is the anodic pole where O<sub>2</sub> bubbles are produced. Scale bar, 250 μm. (c) Translational motion generated with a 285-μm glassy carbon sphere in the presence of an electric field. Scale bar, 100 μm. d–f) Quenching of O<sub>2</sub> bubble production. (d) Scheme of proton reduction and HQ oxidation. (e) Translational motion generated on a 1-mm stainless steel bead exposed to an electric field. Scale bar, 1 mm. (f) Translational motion generated with a 275-μm glassy carbon sphere. Scale bar, 100 μm. Adapted from ref.<sup>16</sup>

In addition, the same principle was used to generate motion in the vertical plane<sup>48</sup>. In this work a GC bead was positioned inside a capillary of about the same inner diameter and bubbles generated underneath due to water reduction lift up the bead. Water oxidation at the anodic side of the bead was also replaced by electrogenerated chemiluminescence (ECL) in order to prepare light-emitting beads<sup>56</sup>. In this experiment [Ru(bpy)<sub>3</sub>]<sup>2+</sup> and tri-*n*-propylamine (TPrA) were oxidized on the anodic side of the particle to produce ECL while water was reduced on the cathodic side to produce hydrogen bubbles. As a result, the bead simultaneously lifts upward and emits red light (Fig. 1.21). Levitation of the particle in a glass capillary was monitored by taking optical images at different times (Fig. 1.21c). The inset shows the position of ECL inside the capillary as a function of time.



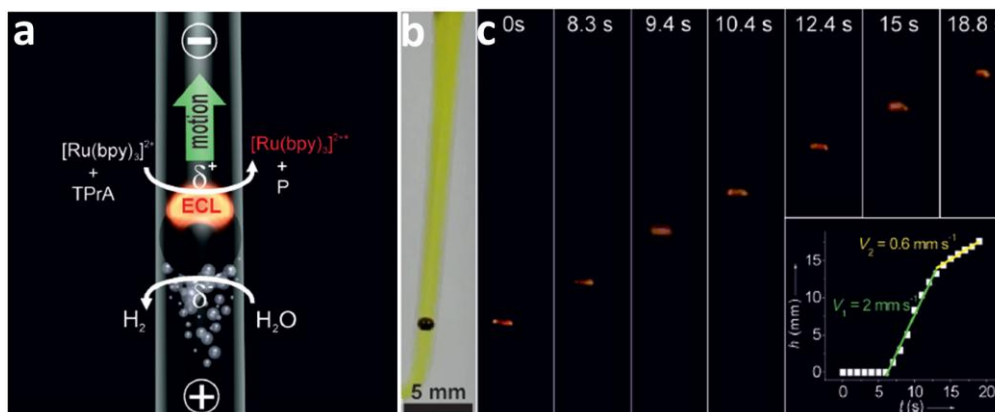


Fig. 1.21. (a) Light-emitting electrochemical swimmer. Simultaneous reduction of  $\text{H}_2\text{O}$  at the cathodic pole (bottom of the bead) and oxidation of ECL reagents at the anodic pole (top of the bead) induces both motion and light emission from the bead in a glass capillary. (b) Image of the bead placed in a vertical capillary taken under white light. (c) Series of optical images in the dark showing a GC bead emitting ECL at different times during its motion. The inset shows the change in height of the bead as a function of time. Adapted from ref.<sup>56</sup>

This system driven by BPE was adapted to monitor glucose content in solution<sup>55</sup>. Glucose dehydrogenase oxidizes glucose with conversion of  $\text{NAD}^+$  to NADH. The latter acts as co-reactant for  $[\text{Ru}(\text{bpy})_3]^{2+}$  to generate ECL. This contribution demonstrates that such ECL swimmers can be used in bioanalytical applications.

A similar work was reported with a blue light emitting swimmer driven by bipolar electrochemistry when changing the nature of the luminophore<sup>61</sup>. In that case, the mechanism is different, because the motion was generated by hydrogen peroxide oxidation to form oxygen bubbles at the anodic pole of the particle. The presence of  $\text{H}_2\text{O}_2$  reactant is necessary to enhance the light emission intensity originating from the luminol dye at the same pole. Therefore, the oxidation of luminol and  $\text{H}_2\text{O}_2$  occurs at the same pole of the bipolar electrode, which is moving towards the feeder anode in such a configuration.

In these two last cases, ECL provides a direct visualization of the BPE motion and can also serve as a sensing tool in analytical chemistry.

BPE can also be used to indirectly induce motion<sup>11,12,59</sup>. Since BPE allows to synthesize asymmetric micro- or nanoobjects, the nature of the deposit can be tuned to trigger motion.

For example, carbon microtubes modified at one extremity with a ferromagnetic Ni particle can be moved by using an external magnetic field<sup>11</sup>. In another case, carbon tubes with a Pt cluster can be used for generating either linear or rotational motion<sup>12</sup>. Since Pt has catalytic properties for  $\text{H}_2\text{O}_2$  decomposition, the resulting  $\text{O}_2$  bubbles drive the propulsion of these tubes in a linear way. When the Pt cluster is not centered with respect to the tube axis, it promotes the rotation of the tubes<sup>12</sup>.

Asymmetry is a crucial parameter for the generation of controlled motion, therefore since BPE is an easy technique to induce asymmetry, it is a very competitive method for generating micro- and nanomotors.

#### 1.4. Goal of the thesis

Despite the unique advantages and possibilities of BPE, to date only a limited number of materials were explored as bipolar electrodes. The aim of this thesis work consists in broadening the scope of BPE by investigating new and more exotic materials. In particular, organic conducting crystals, organic macromolecules and inorganic semiconducting materials were chosen for this study. In the first part, the successful modification of fully organic conducting crystals will be described. In the second part, we demonstrate that inorganic semiconducting dichalcogenides ( $\text{MoSe}_2$ ) can be used as bipolar substrates for the preparation of hybrid materials and also for analytical purposes.

In addition, we studied the possibility to use bipolar electrode as an analytical platform for different purposes such as detection of DNA hybridization or the development of sensing devices based on an original readout strategy. This will be described in the third chapter.

In the last part of this thesis, we are going to explore the possibility to use bipolar electrochemistry as a valuable tool for studying the intrinsic conductivity of a given object. Indeed, in some cases, fundamental studies of material conductivity are quite complicated. For nanoobjects it is usually difficult or even impossible to establish direct electric contact with an electronic measuring instrument. Meanwhile, the simple asymmetric bipolar metal electrodeposition from a salt solution can tell whether the substrate is conductive or not. The formation of metal deposits can serve as a confirmation of an electron transfer process from one end of the studied substrate to the other, and consequently prove electronic conductivity. In this work, we investigate the possibility to use bipolar electrochemistry as a tool for studying the conductivity of DNA molecules.

## References

- (1) Fleischmann, M.; Goodridge, F.; J. H. King, C. Bipolar fluidized bed electrodes. US4124453A, November 7, 1978.
- (2) Mavr , F.; Anand, R. K.; Laws, D. R.; Chow, K.-F.; Chang, B.-Y.; Crooks, J. A.; Crooks, R. M. *Anal. Chem.* **2010**, 82 (21), 8766–8774.
- (3) Fosdick, S. E.; Crooks, R. M. *J. Am. Chem. Soc.* **2012**, 134 (2), 863–866.
- (4) Ulrich, C.; Andersson, O.; Nyholm, L.; Bj refors, F. *Angew. Chem. Int. Ed.* **2008**, 47 (16), 3034–3036.
- (5) Ramakrishnan, S.; Shannon, C. *Langmuir* **2010**, 26 (7), 4602–4606.
- (6) Ishiguro, Y.; Inagi, S.; Fuchigami, T. *Langmuir* **2011**, 27 (11), 7158–7162.
- (7) Bradley, J.-C.; Babu, S.; Mittal, A.; Ndungu, P.; Carroll, B.; Samuel, B. J. *Electrochem. Soc.* **2001**, 148 (9), C647.
- (8) Bradley, J.; Babu, S.; Ndungu, P. *Fullerenes, Nanotub. Carbon Nanostructures* **2005**, 13 (3), 227–237.
- (9) Babu, S.; Ndungu, P.; Bradley, J.-C.; Rossi, M. P.; Gogotsi, Y. *Microfluid. Nanofluidics* **2005**, 1 (3), 284–288.
- (10) Warakulwit, C.; Nguyen, T.; Garrigue, P.; Limtrakul, J.; Kuhn, A. *Nano Lett.* **2008**, 8 (2), 500–504.
- (11) Loget, G.; Larcade, G.; Lapeyre, V.; Garrigue, P.; Warakulwit, C.; Limtrakul, J.; Delville, M.-H. H.; Ravaine, V.; Kuhn, a. *Electrochim. Acta* **2010**, 55 (27), 8116–8120.
- (12) Fattah, Z.; Loget, G.; Lapeyre, V.; Garrigue, P.; Warakulwit, C.; Limtrakul, J.; Bouffier, L.; Kuhn, a. *Electrochim. Acta* **2011**, 56 (28), 10562–10566.
- (13) Loget, G.; Lapeyre, V.; Garrigue, P.; Warakulwit, C.; Limtrakul, J.; Delville, M.-H.; Kuhn, A. *Chem. Mater.* **2011**, 23 (10), 2595–2599.
- (14) Bradley, J.-C.; Chen, H.-M.; Crawford, J.; Eckert, J.; Ernazarova, K.; Kurzeja, T.; Lin, M.; McGee, M.; Nadler, W.; Stephens, S. G. *Nature* **1997**, 389 (6648), 268–271.
- (15) Loget, G.; Kuhn, A. *J. Am. Chem. Soc.* **2010**, 132 (45), 15918–15919.
- (16) Loget, G.; Kuhn, A. *Nat. Commun.* **2011**, 2, 535.
- (17) Loget, G.; Kuhn, A.; Garrigue, P.; Warakulwit, C.; Limtrakul, J.; Delville, M.-H.; Kuhn, A.; Merko i, A.; Wang, J.; Lauga, E.; Wang, J. *Lab Chip* **2012**, 12 (11), 1967.
- (18) Tiewcharoen, S.; Warakulwit, C.; Lapeyre, V.; Garrigue, P.; Fourier, L.; Elissalde, C.; Buff re, S.; Legros, P.; Gayot, M.; Limtrakul, J.; Kuhn, A. *Angew. Chem. Int. Ed.* **2017**, 56 (38), 11431–11435.
- (19) Ongaro, M.; Roche, J.; Kuhn, A.; Ugo, P. *ChemElectroChem* **2014**, 1 (12), 2048–2051.
- (20) Loget, G.; Roche, J.; Kuhn, A. *Adv. Mater.* **2012**, 24 (37), 5111–5116.
- (21) Bard, A. J.; Faulkner, L. R. *Electrochemical methods : fundamentals and applications*; Wiley, 2001.
- (22) Cox, J. T.; Guerrette, J. P.; Zhang, B. *Anal. Chem.* **2012**, 84 (20), 8797–8804.
- (23) Guerrette, J. P.; Oja, S. M.; Zhang, B. *Anal. Chem.* **2012**, 84 (3), 1609–1616.

- (24) Fosdick, S. E.; Knust, K. N.; Scida, K.; Crooks, R. M. *Angew. Chem. Int. Ed.* **2013**, 52 (40), 10438–10456.
- (25) Chang, B.-Y.; Chow, K.-F.; Crooks, J. A.; Mavr , F.; Crooks, R. M. *Analyst* **2012**, 137 (12), 2827–2833.
- (26) Chow, K.-F.; Mavr , F.; Crooks, J. A.; Chang, B.-Y.; Crooks, R. M. *J. Am. Chem. Soc.* **2009**, 131 (24), 8364–8365.
- (27) Chow, K.-F.; Mavr , F.; Crooks, R. M. *J. Am. Chem. Soc.* **2008**, 130 (24), 7544–7545.
- (28) Mavr , F.; Chow, K.-F.; Sheridan, E.; Chang, B.-Y.; Crooks, J. A.; Crooks, R. M. *Anal. Chem.* **2009**, 81 (15), 6218–6225.
- (29) Lin, X.; Zheng, L.; Gao, G.; Chi, Y.; Chen, G. *Anal. Chem.* **2012**, 84 (18), 7700–7707.
- (30) Bouffier, L.; Doneux, T.; Goudeau, B.; Kuhn, A. *Anal. Chem.* **2014**, 86 (8), 3708–3711.
- (31) Chow, K.-F.; Chang, B.-Y.; Zaccheo, B. A.; Mavr , F.; Crooks, R. M. *J. Am. Chem. Soc.* **2010**, 132 (27), 9228–9229.
- (32) Fosdick, S. E.; Berglund, S. P.; Mullins, C. B.; Crooks, R. M. *Anal. Chem.* **2013**, 85 (4), 2493–2499.
- (33) Zhan, W.; Alvarez, J.; Crooks, R. M. *Anal. Chem.* **2003**, 75 (2), 313–318.
- (34) Zhan, W.; Alvarez, J.; Sun, L.; Crooks, R. M. *Anal. Chem.* **2003**, 75 (6), 1233–1238.
- (35) Zhan, W.; Alvarez, J.; Crooks, R. M. *J. Am. Chem. Soc.* **2002**, 124 (44), 13265–13270.
- (36) Fleischmann, M.; Ghoroghchian, J.; Rolison, D.; Pons, S. *J. Phys. Chem.* **1986**, 90 (23), 6392–6400.
- (37) Goodridge, F.; King, C. J. H.; Wright, A. R. *Electrochim. Acta* **1977**, 22 (10), 1087–1091.
- (38) Hiddleston, J. N.; Douglas, A. F. *Nature* **1968**, 218 (5141), 601–602.
- (39) Backhurst, J. R.; Coulson, J. M.; Goodridge, F.; Plimley, R. E.; Fleischmann, M. *J. Electrochem. Soc.* **1969**, 116 (11), 1600.
- (40) Berent, T.; Fells, I.; Mason, R. *Nature* **1969**, 223 (5210), 1054–1055.
- (41) Backhurst, J. R.; Goodridge, E.; Plimley, R. E.; Fleischmann, M. *Nature* **1969**, 221 (5175), 55–57.
- (42) Zhou, M.; Wu, Z.; Ma, X.; Cong, Y.; Ye, Q.; Wang, D. *Sep. Purif. Technol.* **2004**, 34 (1–3), 81–88.
- (43) Loget, G.; Zigah, D.; Bouffier, L.; Sojic, N.; Kuhn, A. *Acc. Chem. Res.* **2013**, 46 (11), 2513–2523.
- (44) Bradley, J.-C.; Ma, Z. *Angew. Chem. Int. Ed.* **1999**, 38 (11), 1663–1666.
- (45) Bradley, J.-C.; Crawford, J.; McGee, M.; Stephens, S. G. *J. Electrochem. Soc.* **1998**, 145 (3), L45.
- (46) Kumsapaya, C.; Baka , M.-F.; Loget, G.; Goudeau, B.; Warakulwit, C.; Limtrakul, J.; Kuhn, A.; Zigah, D. *Chem. - A Eur. J.* **2013**, 19 (5), 1577–1580.
- (47) Kong, S.; Fontaine, O.; Roche, J.; Bouffier, L.; Kuhn, A.; Zigah, D. *Langmuir* **2014**, 30 (11), 2973–2976.

- (48) Koefoed, L.; Shimizu, K.; Pedersen, S. U.; Daasbjerg, K.; Kuhn, A.; Zigah, D. *RSC Adv.* **2016**, 6 (5), 3882–3887.
- (49) Pawar, A. B.; Kretzschmar, I. *Macromol. Rapid Commun.* **2010**, 31 (2), 150–168.
- (50) Du, J.; O'Reilly, R. K. *Chem. Soc. Rev.* **2011**, 40 (5), 2402.
- (51) Loget, G.; Roche, J.; Gianessi, E.; Bouffier, L.; Kuhn, A. *J. Am. Chem. Soc.* **2012**, 134 (49), 20033–20036.
- (52) Arora, A.; Eijkel, J. C. T.; Morf, W. E.; Manz, A. *Anal. Chem.* **2001**, 73 (14), 3282–3288.
- (53) Natarajan, C. *J. Electrochem. Soc.* **1996**, 143 (5), 1547.
- (54) Fattah, Z.; Garrigue, P.; Goudeau, B.; Lapeyre, V.; Kuhn, A.; Bouffier, L. *Electrophoresis* **2013**, 34 (14), 1985–1990.
- (55) Sentic, M.; Arbault, S.; Goudeau, B.; Manojlovic, D.; Kuhn, A.; Bouffier, L.; Sojic, N.; Sojic, N.; Kan, C.; Wang, J. *Chem. Commun.* **2014**, 50 (71), 10202–10205.
- (56) Sentic, M.; Loget, G.; Manojlovic, D.; Kuhn, A.; Sojic, N. *Angew. Chem. Int. Ed.* **2012**, 51 (45), 11284–11288.
- (57) Jiang, J.-Z.; Guo, M.-H.; Yao, F.-Z.; Li, J.; Sun, J.-J.; Limtrakul, J.; Bouffier, L.; Kuhn, A.; Kuhn, A.; Wang, J. *RSC Adv.* **2017**, 7 (11), 6297–6302.
- (58) Wang, Y.; Hernandez, R. M.; Bartlett, D. J.; Bingham, J. M.; Kline, T. R.; Sen, A.; Mallouk, T. E. *Langmuir* **2006**, 22 (25), 10451–10456.
- (59) Bouffier, L.; Ravaine, V.; Sojic, N.; Kuhn, A. *Curr. Opin. Colloid Interface Sci.* **2016**, 21, 57–64.
- (60) Fattah, Z. A.; Bouffier, L.; Kuhn, A. *Appl. Mater. Today* **2017**, 9, 259–265.
- (61) Bouffier, L.; Zigah, D.; Adam, C.; Sentic, M.; Fattah, Z.; Manojlovic, D.; Kuhn, A.; Sojic, N. *ChemElectroChem* **2014**, 1 (1), 95–98.

## Chapter II. Bipolar electrochemistry with semiconducting materials

### 2.1. Introduction to organic charge-transfer salts

Organic conductors are materials that consist of organic molecules or polymers containing carbon together with hydrogen, oxygen, and often sulfur.

In principle, organic conductors can be divided into two main groups: conducting polymers and organic charge-transfer salts. In the first case, the conjugated  $\pi$  electron system is responsible for conductivity. The second group are donor/acceptor complexes. For our studies, we selected organic conductors from the latter representatives because they are known to exhibit good conductivity, low production cost and offer also the opportunity to fine-tune their physical properties by slight variations of the chemical components involved in their structure. Also, contrary to conducting polymers they are easily available in microcrystalline form.

Such materials are formed from a donor part, which has low ionization energy, and an acceptor part with a high electron affinity. Thus, an electron transfer between those molecules can easily take place.

Organic charge-transfer salts, after their discovery, attracted enormous attention due to low-dimensionality of their structure. These compounds constructed from planar organic molecules, have anisotropic structures that lead to anisotropic physical properties. For example, the electrical conductivity is high along one direction, while it is much smaller along the perpendicular direction. In addition, the electronic properties of organic conductors can be tuned by changes in the molecular structure as well as by external parameters (pressure, temperature). Consequently, organic charge transfer salts can exhibit a variety of features and the resulting properties can be adjusted over a wide range.

Most of the charge transfer salts consist of donor acceptor (D-A) complexes. They form D<sub>2</sub>A complexes, where each of the two donor molecules donates one electron to the acceptor.

The donor molecules are the building blocks of the organic conductors. They are organized in linear columns of parallel sheets of flat organic molecules (Fig. 2.1) that are arranged in segregated stacks of cations and anions, respectively. Due to such a structure, molecular orbitals are overlapping between the parallel sheets of organic molecules, which causes delocalization of the charge carriers between the molecules and an enhanced conductivity along the direction of the molecular overlapping. Due to this structure, electron transfer capability and therefore electrical conduction becomes anisotropic, i.e. the electrical conductivity along one direction is much higher than that in the other directions. Furthermore, the orbital overlap of the organic molecules defines the properties and due to this anisotropy even the dimensionality of the systems.

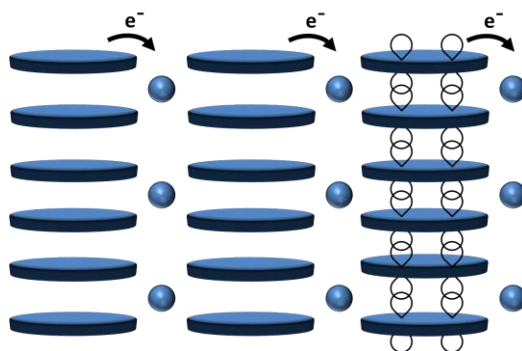


Fig. 2.1. Schematic representation of charge transfer in organic charge-transfer salts. The planar donor molecules (cations) are packed in stacks alternating with chains of acceptor molecules (anions) shown as balls. The intermolecular overlap of  $\pi$ -orbitals between the donor molecules is shown in the right stack, as an example.

Such compounds are so called one-dimensional conductors (1-D), because their conductivity is significant only in one direction. The molecular arrangement of these materials determines the final shape of the crystal. Indeed, these crystals grow to form sticks, where the long direction is parallel to the highest conductive direction.

Such organic charge-transfer salts was first synthesized in the 1970's by J. M. Fabre<sup>1</sup>. The general formula of such molecules is  $(\text{TMTTF})_2\text{X}$ , where X is an inorganic monovalent anion like  $\text{PF}_6^-$ ,  $\text{AsF}_6^-$ ,  $\text{ReO}_4^-$ ,  $\text{BF}_4^-$ ,  $\text{SbF}_6^-$ , etc. Fabre salts  $(\text{TMTTF})_2\text{X}$  contain sulfur atoms in the structure whereas the Bechgaard salts  $(\text{TMTSF})_2\text{X}$  are analogs that include selenium instead of sulfur as shown in Fig. 2.2a.<sup>2</sup>

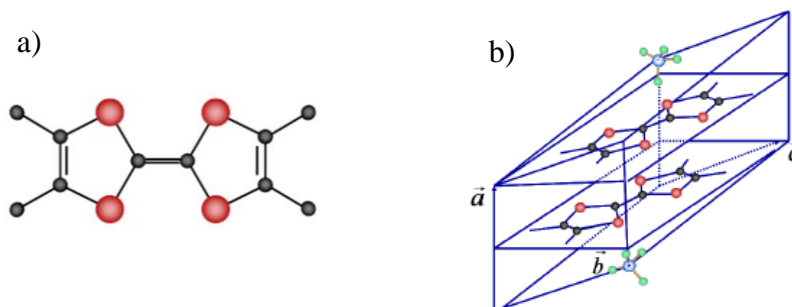


Fig. 2.2. (a) Chemical structure of tetramethyltetrathiafulvalene (TMTTF) or tetramethyltetraselenafulvalene (TMTSF) molecules, where S or Se shown as red balls, carbon - black balls. (b) The unit cell of  $(\text{TMTYF})_2\text{X}$ . Adapted from ref.<sup>3</sup>

### 2.1.1. Crystal structure

For Fabre- and Bechgaard salts, the stoichiometric ratio of cations to anions in the crystal is 2:1, resulting in a general formula of  $(\text{TMTYF})_2\text{X}$ , where Y= S or Se and X being an inorganic anion<sup>4</sup>. In some cases a stoichiometric ratio of 1:1 is also observed for example in tetrathiafulvalene-chloranil TTF-CA, or in tetrathiafulvalene 7,7,8,8 tetracyanoquinodimethane TTF-TCNQ, when acceptor parts are organic molecules. The unit cell is composed of two TMTYF molecules and one inorganic anion X (Fig. 2.2b).

Within the crystal, the organic molecules form layers which are separated by other layers made from inorganic anions, as shown in Fig. 2.3. The electrons are transferred from the organic layer to the inorganic counter-anions.

In the (*a*)-direction, Bechgaard and Fabre salts are arranged in a zig-zag configuration of TMTYF molecules (Fig. 2.2b, 2.3a). The layers of organic stacks are alternating with layers of anions in the (*c*)-direction. Along the (*b*)-direction, the donor stacks are shifted from each other (Fig. 2.2b, 2.3b).

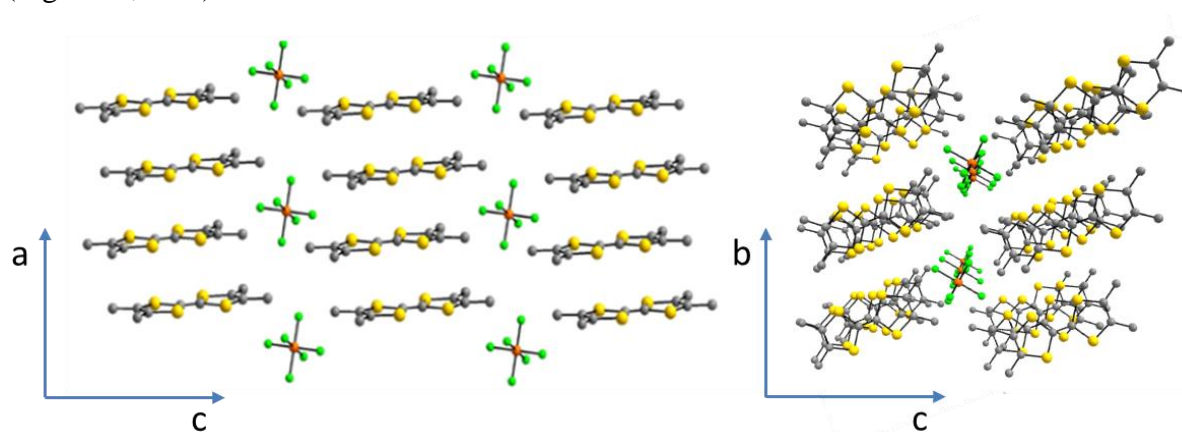


Fig. 2.3. Illustration of the molecular arrangement of the one-dimensional organic conductor  $(\text{TMTYF})_2\text{PF}_6$  crystals, with Y being S or Se, in the (*a*)-(*c*) plane (left), in the (*b*)-(*c*) plane (right). Grey balls – C, yellow balls – S or Se, red – P, green – O. The organic molecules (gray, yellow color) form layers, which are separated from each other by the anions (bright green and red color) along the long molecular axis. Adapted from ref.<sup>5</sup>

### 2.1.2. Electrical properties

The segregated stack structure is responsible for anisotropic electrical conductivity. Since the initial discovery, numerous analogues of fulvalenes have been prepared and studied with a special focus on the measurement of their conductivity under different experimental conditions. The Fabre and Bechgaard salts have a rather large value of electric conductivity at room temperature ( $\sigma = 20 \text{ S m}^{-1}$  for  $(\text{TMTTF})_2\text{PF}_6$  and  $\sigma = 100 \text{ S m}^{-1}$  for  $(\text{TMTSF})_2\text{PF}_6$ ) which can reach metal conductivity. Several tetramethyltetraethia(selena)fulvalene salts possess also superconducting properties at low temperatures.<sup>6</sup>

## 2.2. Asymmetrical Janus particles: synthesis and their applications

Janus particles are typically characterized by two different sides that exhibit different nature, chemical properties or polarity. The name originates from the Roman God Janus, who is presented with two faces.



In Figure 2.4, some of the most common architectures of Janus particles are gathered with various geometries such as spheres, rods and discs.<sup>7</sup> The two parts for rods and discs can be defined either along the vertical or horizontal axes.

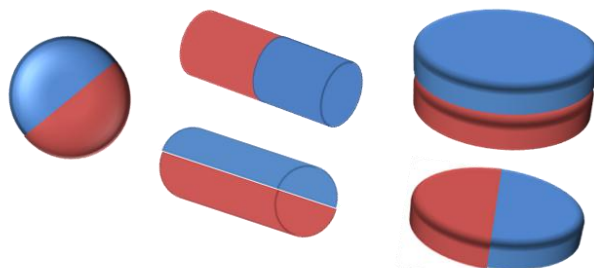


Fig. 2.4. Schematic illustration of Janus particles with different shapes.

There are several methods available for the production of Janus particles<sup>7–11</sup>. One of the historical ways to obtain Janus particles is the so-called masking/unmasking techniques.<sup>8</sup> Another method is based on the generation of directional fluxes or fields of deposable materials that decorate particles in an anisotropic way. In this case, the particles are immobilized on the surface of a substrate, and only the exposed face of the particle is therefore modified. This route advantageously allows to avoid sequential masking and unmasking steps. However, as a drawback, the method has generally low yields, as it requires a monolayer of spheres, and also the quality of the coating is very size-dependent, becoming critical when decreasing the particles size.

Microcontact printing is another approach, where particles are functionalized via transfer of chemical compounds from a stamp to the substrate. Often Janus particles can be obtained by interfacial contact with a reactive medium. In this case, only areas exposed to the reactive medium undergo a proper functionalization.

In addition, microfluidic methods can also be used. This involves the use of liquid flows of different chemical composition in independent inlet capillaries which merge to generate droplets and form bi- or multi- phasic particles. With this method, it is possible to control both the shape and functionality of the resulting particles.

However, the limitation of all these techniques is the necessity to proceed through several preparation steps and also the rather small yields that do not allow to scale up the production to an industrial level. Quite recently, the successful production of Janus particles by bipolar electrochemistry was demonstrated.<sup>12,13</sup> This technique does not require any immobilization of the particles to be modified, thus a bulk production of asymmetric particles is easier and can be achieved in a wireless way. The concept of bipolar electrochemistry to create new asymmetric objects was used in this thesis.

Janus particles are the focus of major ongoing research activities because this class of asymmetric materials exhibits unprecedented anisotropic properties with many possible applications, especially for electronics, advanced spectroscopy and optics.

Janus particles can be easily fabricated with bipolar electrochemistry. As mentioned in the first chapter, the intrinsic advantage of this method is the absence of any physical connection between the power source and the bipolar objects. The bipolar electrochemical approach can be

applied to any sufficiently conducting object in order to achieve an electrochemically induced break of symmetry. The symmetry breaking enabled by bipolar electrodeposition facilitates the efficient synthesis of dissymmetric objects. Therefore, layers of different chemical composition, electrodeposited on the ends of bipolar electrodes can be used to create various Janus particles with different shape, size and/or composition.

As described in the previous chapter, bipolar electrochemistry is an unconventional approach compared to a classic electrochemical setup. Electric field applied to electrolyte solution causing polarization potential between the solution and the conductive object and promoting oxidation and reduction reactions at the opposite poles of the bipolar object (Fig. 2.5).

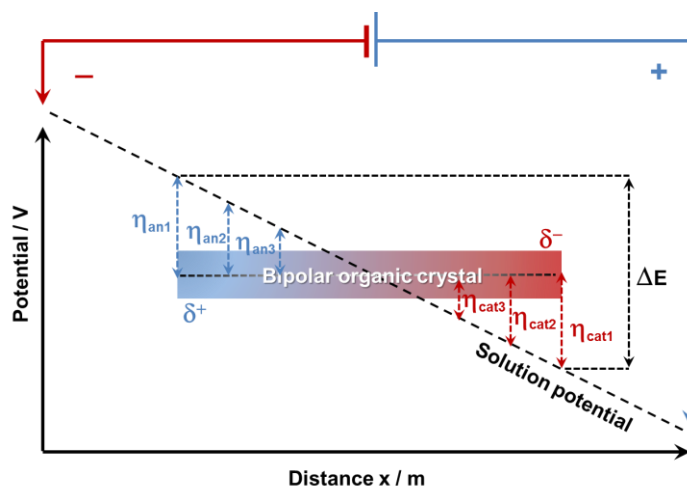


Fig. 2.5. Schematic illustration of the principle of bipolar electrochemistry based on the polarization potential established alongside a conducting object immersed in an electrolyte and exposed to an electric field. In the present case, the bipolar electrode is an organic single crystal. adapted from ref.<sup>14</sup>

So far, BPE has proven to be very versatile for site-selective wireless electrodeposition by tuning the nature of the chemical species involved in the bipolar reactions occurring at the extremities of a conducting object. For instance, the reduction of a metal precursor to form the corresponding metal,<sup>15,16</sup> the electrooxidation of a monomer to form a polymer layer,<sup>17</sup> the electrografting of an organic layer,<sup>18</sup> pH-induced local precipitation,<sup>19</sup> and the deposition of various inorganic structures were reported.<sup>19–21</sup> However, all these experiments were performed on BEs made out of either metal or carbon allotropes, thus ensuring a high electrical conductivity.<sup>22,23</sup> This has the advantage that BPE is favored when the BE is more conductive than the surrounding media, due to the competition between the Faradaic current flowing through the bipolar electrode and the ionic current occurring across the surrounding electrolyte.

In the open configuration, the conductive object is immersed inside an electrolyte in between two feeder electrodes. The driving force for electrochemical reactions on the BE is the potential difference established at the interface between the substrate and the solution. Assuming that the solution potential in the bipolar set-up drops linearly across the substrate, the rate of redox reactions is highest at the edges of the bipolar electrode and decreases towards its center. Therefore, by controlling the applied potential, a gradient in surface functionalization of the BE is possible by adsorption or desorption of specific molecules.<sup>24</sup>

### 2.2.1. BPE gradient formation

For example, *Ulrich et al.* reported the use of bipolar electrochemistry to pattern electrode surfaces. Their work shows the presence of a potential gradient along the surface of a bipolar electrode.<sup>24</sup> In this work, a gold BE was placed in a bipolar electrochemical cell containing a mixture of  $[\text{Fe}(\text{CN})_6]^{4-}$  and  $[\text{Fe}(\text{CN})_6]^{3-}$ . During application of an electric field across the solution,  $[\text{Fe}(\text{CN})_6]^{4-}$  was oxidized to  $[\text{Fe}(\text{CN})_6]^{3-}$  at the anodic pole of the electrode.

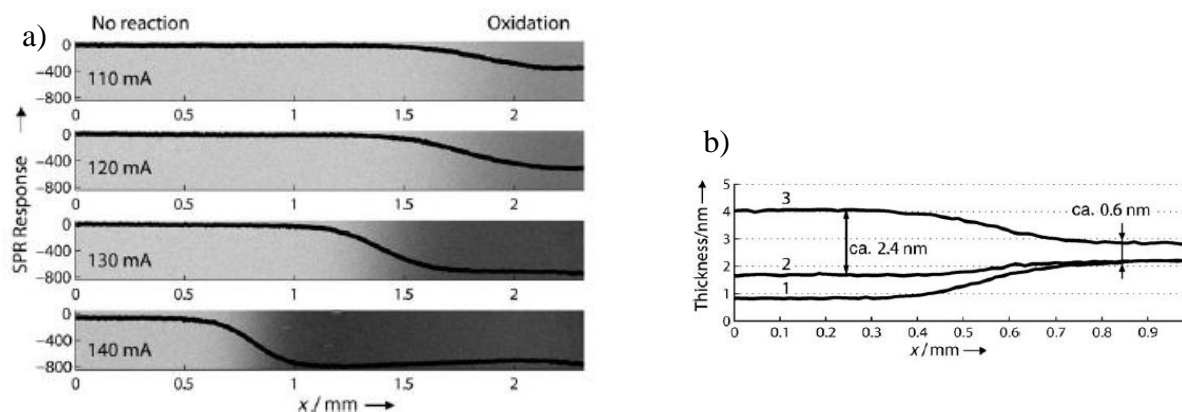


Fig. 2.6. (a) Intensity change of the surface plasmon resonance (SPR) signal due to the change in the refractive index when  $[\text{Fe}(\text{CN})_6]^{4-}$  is oxidized to  $[\text{Fe}(\text{CN})_6]^{3-}$  at the anodic side of a bipolar electrode for different total currents. (b) Line profiles collected by ellipsometry corresponding to the thickness of a gradient: line 1 - after the desorption of mPEG during BPE, line 2 - after the backfilling with another aPEG, which has a terminated carboxylic group, and line 3 - a formed protein gradient after the incubation with lysozyme. Adapted from ref.<sup>24</sup>

This reaction results in changes in refractive index of these redox species close to the surface of the bipolar electrode and therefore can be monitored along its length by Surface Plasmon Resonance (SPR) as shown in Figure 2.6. This measurement reflects the characteristics of the electric-field-induced potential gradient. The various plots indicate how the position and width of the gradient changes as a function of applied current.

In the same work, using BPE, the authors created molecular gradients on the surface. They used a gold surface covered with a thiol-based self-assembled monolayer (SAM) of  $\text{HS-C}_2\text{H}_4\text{-(O-C}_2\text{H}_4)_6\text{-OCH}_3$  (mPEG) as the BE and ellipsometry to characterize the thickness of the corresponding gradients. During the application of the electric field the thiol species were electrochemically desorbed from the cathodic part of the bipolar gold electrode (Fig. 2.6b, line 1). Then, the obtained surface was incubated with a second thiol  $\text{HS-C}_2\text{H}_4\text{-(O-C}_2\text{H}_4)_8\text{-COOH}$  (aPEG), which has terminal carboxy groups (Fig. 2.6b, line 2). Subsequently, the carboxy groups on the surface were activated and used as binding sites to target a protein (lysozyme). Indeed, an increase in thickness after protein functionalization was observed (Fig. 2.6b, line 3). This method is a suitable way to obtain molecular gradients only on one side of an object and such SAMs could be used for protein-immobilization procedures.

*Shannon's group*<sup>25</sup> reported the deposition of Cd, CdS, and S gradients on a gold wire. The substrate was immersed in a solution containing  $\text{S}_2\text{O}_3^{2-}$  and  $\text{Cd}^{2+}$  and a sufficient electric field was applied to drive the electrodeposition. Since the standard redox potential of each compound is different, the deposition involves one or several precursors at different positions on the wire.

The reduction of  $\text{Cd}^{2+}$  into Cd started at the edge of the cathodic pole, followed by CdS and S deposits, shifted towards the middle of the bipolar electrode. The evolution of the chemical composition of the electrodeposit was further confirmed by using Auger electron spectroscopy (AES) and confocal Raman microscopy.

*Tisserant et al.*<sup>26</sup> prepared metal composition gradients of copper or nickel on cylindrical carbon fibers. The aspect ratio of the fiber is well-adapted to enable a discrimination of the deposition morphology by using scanning electronic microscopy. The authors studied and discussed the screening in morphology and roughness depending on the position alongside the BE by comparison to conventional electrodeposition.

### 2.2.2. Indirect bipolar electrodeposition

Besides surface modification by direct electrodeposition reactions on the bipolar electrode, indirect bipolar electrodeposition (IBED) was also reported. For example, IBED was applied to site-selective *in situ* synthesis of metal-organic frameworks (MOFs) on metallic wires and particles. By using the IBED technique, reactive metal ions are generated at the surface of a metallic substrate by oxidation and further react with ligand species that are dissolved in the solution to form coordination-based network structures<sup>20</sup>. Figure 8a and b shows the mechanism for the site-selective modification of a zinc wire by a Zeolitic Imidazolate Framework (ZIF-8),  $[\text{Zn}(\text{2-MeIm})_2]$  (2-MeIm=2-methylimidazole). In this example, a Zn wire was used both as a metal source and a substrate for the deposition process.

In the same way, the formation of copper-based MOFs was exemplified with HKUST-1,  $[\text{Cu}_3(\text{BTC})_2(\text{H}_2\text{O})_3]$  (BTC=1,3,5-benzenetricarboxylate). A copper metal bead served as BE as well as source of  $\text{Cu}^{2+}$  ions for the *in situ* MOF synthesis. When the potential is applied, selective oxidation of the copper bead occurs, which promotes the production of  $\text{Cu}^{2+}$  ions

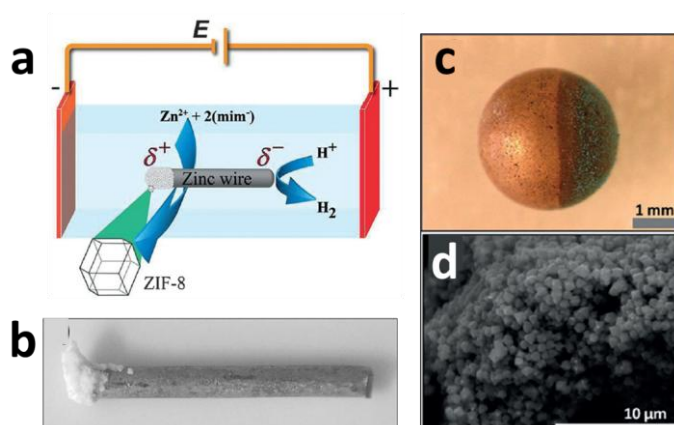


Fig. 2.7. a) Scheme and b) image of side-selective modification of a zinc wire with ZIF-8 on the anodically polarized side triggered by IBED. c) Copper bead modified with HKUST-1 at 20 V in the presence of 1,3,5-benzenetricarboxylic acid and (d) corresponding SEM image showing the structuration of the deposit. Adapted from ref.<sup>20</sup>

localized on one hemisphere, resulting in the formation of MOF selectively in this area (Fig. 2.7c, d). Therefore, this technique can be also applied to generate such micro- and nanoobjects with a variety of other materials.

The investigation of low dimensional frameworks is currently in the focus of strong research activities. Many interesting properties are exclusive of the reduced dimensionality of those structures and are not observed in three dimensional systems. The interest in these materials is related to their high anisotropy, i.e., the electrical conductivity is high along one or two directions, while it is smaller by several orders of magnitude along perpendicular direction(s).

Among other possible methods, bipolar electrochemistry proposes a valuable and attractive technique for the modification of “two-dimensional” particles. As it was shown above, it is a single-step method which is a key-advantage compared to multi-steps approaches. Also, it can achieve high yields of modified objects for a diversity of possible applications thanks to the possibility to employ a variety of conducting metal-based particles in combination with a range of electroactive precursors for functionalization. Meanwhile, up to now, only few examples are known regarding the application of bipolar electrochemical methods with other substrates than glassy carbon or metal, such as semiconducting TiO<sub>2</sub> nanofibers<sup>27</sup> or TiO<sub>2</sub> microbeads<sup>28</sup>. One of the objectives of this thesis work is to extend the field of application of BPE to new objects. Obviously, using an organic material as BE necessitates an intrinsic high conductivity. Among other organic conducting materials, charge-transfer salts are well-known and seem to be very promising candidates.

### **2.3. Bipolar electrochemistry with organic crystals for metal deposition**

In order to extend the range of applications of Janus particles prepared by BPE, we report in this chapter the use of organic single crystals as bipolar electrodes. We selected Fabre and Bechgaard salts, which are well-known organic conductor structures based on tetramethylnitratetrafulvalene (TMTTF) and tetramethylnitratetra-selenafulvalene (TMTSF) as donors (Fig. 2.8) and hexafluorophosphate as counterion<sup>2</sup>. These materials have been identified as possible bipolar electrode candidates because they exhibit a suitable conductivity and have also interesting potential applications in organic electronics or photocatalysis.

Such organic crystals are fragile with respect to mechanical stress and can therefore be irreversibly damaged during conventional electrodeposition experiments. Here, the key advantage of BPE is indeed the possibility to modify such crystals without any electronic or mechanical contact thanks to the wireless addressing capability.

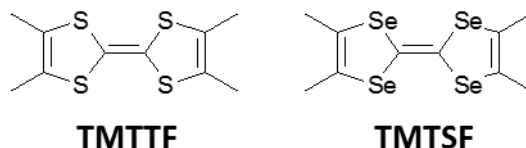


Fig. 2.8. Chemical structures of Tetramethyltetrathiafulvalene (TMTTF) and Tetramethyltetraselenafulvalene (TMTSF).

In our study, we have investigated the behavior of hexafluorophosphate salts of tetrathia- and tetraselenafulvalene under bipolar electrochemical conditions.

As mentioned before, BPE is a straightforward and contactless method for producing asymmetric particles or more generally for the creation of chemical gradients of various nature. However, BPE experiments are well-adapted mostly for well-conducting materials acting as bipolar electrodes made out of metal, graphite or glassy carbon materials. In fact, varying the chemical nature of the bipolar electrode itself has not been widely investigated so far.

The aim of this chapter was therefore to adapt the concept of bipolar electrodeposition to others materials especially to semiconducting objects and to develop a proper methodology for the creation of original metal/organic Janus objects.

Such hybrid materials nowadays have a great interest, because they can potentially be exploited for a number of applications, such as photocatalysis,<sup>29</sup> assembly of particles,<sup>30,31</sup> and photovoltaics<sup>32</sup> which cannot be addressed by simple semiconductor particles.

This is generally related to the fact that they can combine physical and chemical properties related to the metal moiety and the semiconductor component or even display unique properties not seen in each of the precursor.<sup>33</sup> Such hybrid structures combine different material components into a single entity and provide a way of modifying and tuning the resulting properties of these particles.

Therefore, in this section, the fabrication of Janus metal/organic particles by BPE is reported. In particular, this technique was used to deposit copper on needle-like macroscopic organic charge transfer crystals such as hexafluorophosphate of tetramethyltetrathiafulvalene ((TMTTF)<sub>2</sub>PF<sub>6</sub>) or tetramethyltetraselenafulvalene ((TMTSF)<sub>2</sub>PF<sub>6</sub>).

### 2.3.1. Experimental details

**Materials.** (TMTTF)<sub>2</sub>PF<sub>6</sub> and (TMTSF)<sub>2</sub>PF<sub>6</sub> crystals used in this study were prepared by electrocrystallization. All aqueous solutions were prepared with Milli-Q grade water (Millipore, resistivity 18.2 MΩ cm at 25 °C). Copper sulfate (CuSO<sub>4</sub>, anhydrous, 98% purity) was purchased from Alfa Aesar. Silver sulfate (Ag<sub>2</sub>SO<sub>4</sub>, puriss., ≥99.5%), hydroquinone (HOC<sub>6</sub>H<sub>4</sub>OH, abbreviated H<sub>2</sub>Q, 99.5% minimal purity) was purchased from Sigma-Aldrich. Dichloromethane (CH<sub>2</sub>Cl<sub>2</sub>, chromasolv, ≥99.8%), acetonitrile (CH<sub>3</sub>CN, analytical grade) and tetrabutylammonium hexafluorophosphate (Bu<sub>4</sub>NPF<sub>6</sub>, for electrochemical analysis, ≥99.0%) were purchased from Sigma-Aldrich. Tetramethyltetraselenafulvalene (TMTSF, 97%) and Tetrathiaafulvalene (TTF, 99%) was purchased from Acros Organics.

*Equipment.* Bipolar electrodeposition experiments were performed in a homemade cell comprising two plastic cuvettes connected by a glass capillary. The studied organic crystals were positioned inside the capillary prior to BPE experiments. The feeder electrodes are gold plates (10 × 25 mm) purchased from ACM (78640 Villiers, France). The typical distance between both feeder electrodes is ~5 cm, and they are connected to an external power supply (Keithley 6517 electrometer).

*Microscopy.* Organic crystals were characterized by using an optical stereomicroscope (Leica MSV266) and a scanning electron microscope (Hitachi, TM-1000).

*Conventional Electrochemistry.* Cyclic voltammetry (CV) experiments were carried out in an electrochemical cell comprising a gold working electrode ( $\phi = 2.0$  mm), a platinum mesh counter electrode, and a silver wire pseudo-reference connected to a potentiostat (Autolab, PGSTAT12). The working electrode was carefully polished with alumina and rinsed before each experiment. Since the tested organic molecules are not well-soluble in water, CVs were recorded in organic solvents at room temperature. A 1 mM TMTTF solution was prepared in acetonitrile (CH<sub>3</sub>CN) whereas a 1 mM TMTSF solution is obtained in dichloromethane (CH<sub>2</sub>Cl<sub>2</sub>). Each solution contained 0.1 M Bu<sub>4</sub>NPF<sub>6</sub> as supporting electrolyte. CVs were measured at different scan rates ranging from 0.01 to 1.00 V s<sup>-1</sup>.

*Electrical Measurements.* Photovoltage measurements were performed with two carbon Scotch tape electrodes (SPI Supplies, 8 mm width) with ~1 mm spacing and connected to a high-precision voltmeter (Keithley 2001 multimeter). A LabVIEW script (version 9.0) was written and used to record the photovoltage signal. Organic crystals were carefully positioned between both electrodes prior to measurements. A commercial red laser beam ( $\lambda = 635$  nm) was used for the illumination of the extremities of these crystals.

### 2.3.2. Results and discussion

(TMTTF)<sub>2</sub>PF<sub>6</sub> and (TMTSF)<sub>2</sub>PF<sub>6</sub> were prepared using a classic electrocrystallization method by collaborators from the University of Angers, France.<sup>34</sup> The average length of these crystals was in the range of 1–3 mm and a typical diameter up to ~200  $\mu$ m.<sup>10</sup> The conductivity at room temperature of these Fabre and Bechgaard crystals is sufficiently high<sup>1,2,35,36</sup> (20 S cm<sup>-1</sup> for (TMTTF)<sub>2</sub>PF<sub>6</sub> and 500 S cm<sup>-1</sup> for (TMTSF)<sub>2</sub>PF<sub>6</sub>, respectively), exhibiting almost a metallic behavior. These conductivity values are higher than the typical ionic conductivity of supporting electrolyte, therefore they are excellent candidates to undergo bipolar electrochemistry.

To demonstrate the possibility of using such organic crystals as bipolar electrodes, the site selective electrodeposition of different metals was tested. As described in the previous chapter, BPE has already been used for the deposition of many metals such as gold, silver, copper and nickel on carbon materials.<sup>18,22,37,38</sup>

The bipolar electrochemical cell was assembled from two plastic compartments, connected by a capillary (inner diameter = 1 mm) as shown in Fig. 2.9a. The feeder electrodes were gold

plates, stuck to the internal walls of both cuvettes and connected to the power supply. The distance between these two feeder electrodes was 5 cm. The bipolar electrode (i.e. the substrate to be modified being in this case the organic crystals) was placed inside the capillary while the cell was filled with an electrolytic solution of metal salt precursor. The latter is reduced to the corresponding metal during the course of the bipolar electrodeposition experiment.

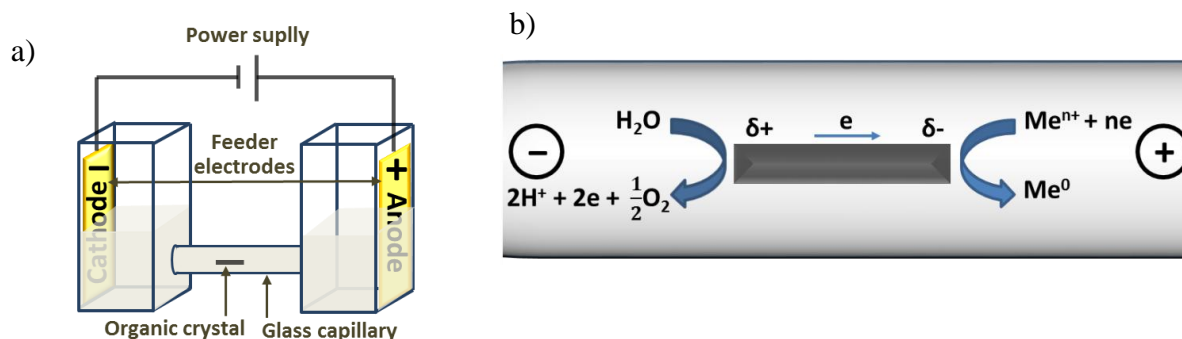


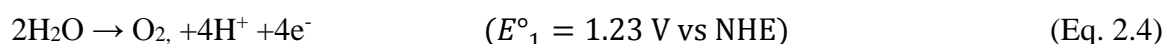
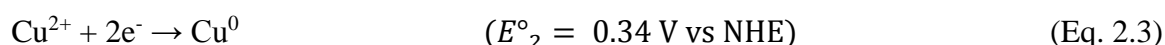
Fig. 2.9. Schematic illustration of (a) the experimental set-up for the bipolar electrodeposition of metal at one side of organic crystals (b) the reduction and oxidation processes on a conductive object in the capillary during bipolar electrochemical process leading to metal cluster deposition at the cathodic extremity.

To ensure electroneutrality, two redox reactions need to be coupled at both extremities of the BE. For instance, electrons released during the oxidation reaction at one extremity of the bipolar electrode are transported across and are involved in the reduction reaction occurring at the opposite extremity. The simplest way to achieve bipolar deposition is the reduction of a metal salt at the cathodic side of the BE, which is coupled with the oxidation of the solvent (water in the case of aqueous solutions) at the anodic pole. The schematic illustration of this process is depicted in Fig. 2.9b. In addition, bipolar electrodeposition can only take place when the electric field strength is large enough to promote the two redox reactions involved at both extremities of the conductive object. As described in the first chapter, the necessary electric field value ( $\mathcal{E}$ ) is directly related to the potential difference ( $\Delta V$ ) between the two redox couples involved (Eq. 2.1) and the length of the BE, (Eq. 2.2).

$$\Delta V_{min} = E_1^\circ - E_2^\circ \quad (\text{Eq. 2.1})$$

$$\mathcal{E} = \frac{\Delta V_{min}}{l_e} \quad (\text{Eq. 2.2})$$

In a first experiments, copper reduction from its cupric salt solution (Eq. 2.3) at the cathodic side was combined with water oxidation (Eq. 2.4) at the anodic pole of the BE:



The standard potential of each reaction is given in brackets versus the normal hydrogen electrode. To achieve the expected bipolar electrochemical process, the minimal polarization potential ( $\Delta V_{min}$ ) between both poles of the BE should be at least equal to the difference of potentials of the involved reactions, i.e.:  $1.23 \text{ V} - 0.34 \text{ V} = 0.89 \text{ V}$ . Then, if one considers a typical length of the crystal of 1 mm, the minimum value of applied electric field should be



$0.89 \text{ V} / 0.1 \text{ cm} = 8.9 \text{ V cm}^{-1}$ . Moreover, the distance between both feeder electrodes was fixed at 5 cm, meaning that the difference of potentials applied to the cell must be at least  $\sim 45 \text{ V}$  in order to reach this electric field value. The series of experiments was performed in the cell presented in fig. 2.10a, with the organic crystal positioned inside the central glass capillary and the whole cell filled with an aqueous 10 mM  $\text{CuSO}_4$  solution.

Bipolar electrodeposition was performed on both  $(\text{TMTTF})_2\text{PF}_6$  and  $(\text{TMTSF})_2\text{PF}_6$  crystals, and the corresponding experiments were monitored *in situ* by optical microscopy while applying the electric field (Fig. 2.10a and 2.10b, respectively). During the first set of experiments, the coloration of the initially colorless electrolyte (yellow for TMTTF and red for TMTSF) near the left side of the organic crystals was observed. This side of the crystals corresponds to the anodic pole of BE. The colored electrogenerated species seem to migrate towards the feeder cathode, showing that they are positively charged molecules.

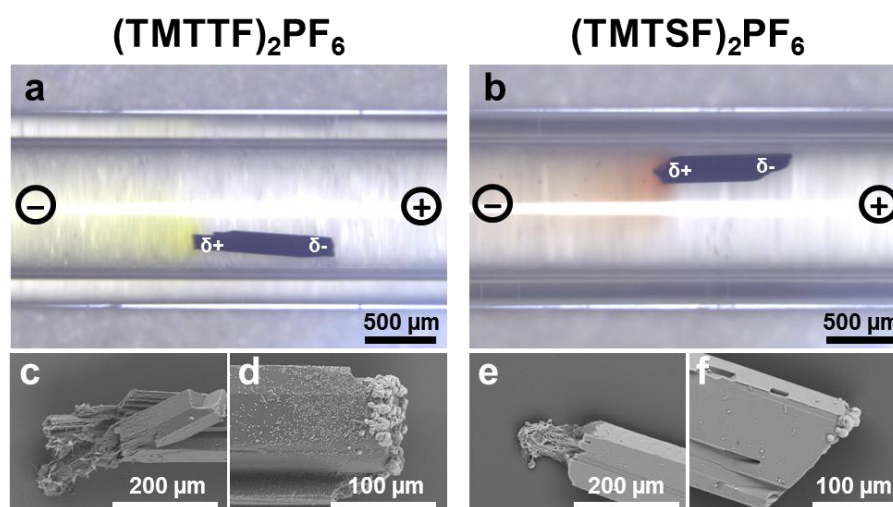


Fig. 2.10. Bipolar electrodeposition experiments performed on organic crystals. (a) Optical image of an organic crystal of  $(\text{TMTTF})_2\text{PF}_6$  positioned inside a glass capillary filled with 10 mM  $\text{CuSO}_4$  aqueous solution and exposed to an electric field of  $5 \text{ V cm}^{-1}$ . The polarity of both feeder electrodes is indicated. (b) Same experiment with a crystal of  $(\text{TMTSF})_2\text{PF}_6$  and an electric field of  $6.5 \text{ V cm}^{-1}$ . Scanning electron micrographs of the (c) left and (d) right extremities of the  $(\text{TMTTF})_2\text{PF}_6$  organic crystal damaged at the anodic side and modified with copper at the cathode side. (e, f) Idem in the case of  $(\text{TMTSF})_2\text{PF}_6$ . Adapted from ref.<sup>14</sup>.

For further characterization, the crystals were taken out from the capillary and observed with scanning electron microscopy (SEM) as shown in Fig. 2.10c-f. These images show that electrodeposition of Cu as discrete clusters (size  $< 10 \mu\text{m}$ ) did occur at the cathodic extremity of both crystals (Fig. 2.10d and 2.10f, respectively). On the other hand, the anodic pole of the crystal was clearly damaged during BPE, and the corresponding images show an extended portion of the crystals where an electro-induced dissolution took place (Fig. 2.10c and 2.10e, respectively). This oxidative degradation of both TMTTF- and TMTSF-based crystals, observed with the tested BPE conditions, encouraged us to further investigate the electrochemical behavior of these two donors. It is noteworthy that absolutely no degradation was observed without applying the electric field, meaning that both crystals are indeed stable at open-circuit potential.

To better address this stability issue and determine the corresponding potential window, an electrochemical characterization of both organic donors was performed to determine the oxidation potentials of TMTTF and TMTSF. The electrochemical behavior of the donor moieties was studied by cyclic voltammetry (CV). Due to low solubility of fulvalenes in water, CVs were recorded in aprotic organic solvents. Acetonitrile was used as a solvent for TTF and dichloromethane for TMTSF. Both CV are essentially comparable. Fig. 2.11 shows the CVs recorded at several scan rates obtained from a 1 mM TTF solution in CH<sub>3</sub>N containing 0.1 M Bu<sub>4</sub>NPF<sub>6</sub> as supporting electrolyte. Analogous experiments were repeated with a 1 mM TMTSF solution in CH<sub>2</sub>Cl<sub>2</sub>, and the corresponding CVs are shown in Fig. 2.14.

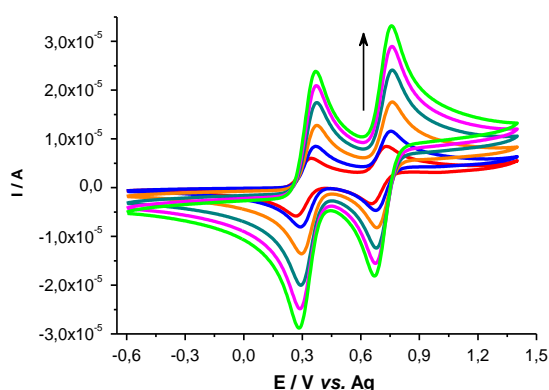


Fig. 2.11 Cyclic voltammograms of 1 mM TTF in CH<sub>3</sub>CN with 0.1 M Bu<sub>4</sub>NPF<sub>6</sub> as supporting electrolyte recorded with a gold disc working electrode at various scan rates ( $v = 0.05, 0.10, 0.250, 0.50, 0.75$ , and  $1.00 \text{ V s}^{-1}$ , respectively). The counter electrode was a platinum mesh, and a silver wire was used as pseudo-reference.

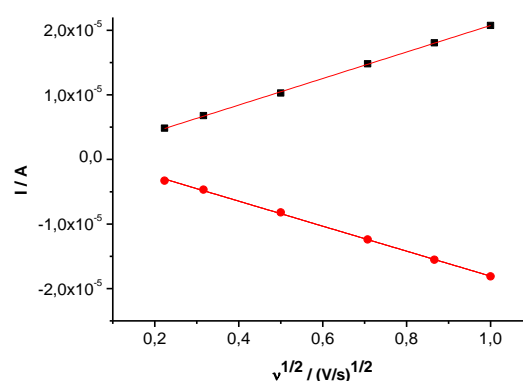


Fig. 2.12. Amplitude of the first oxidation peak (black line) and first reduction peak (red line) of TTF as a function of the square root of scan rate.

$$I_1 = 2.02E-6 + 2.06E-5 \cdot \sqrt{v}; R^2 = 0.9997$$

$$I_2 = -1.29E-6 - 1.94E-5 \cdot \sqrt{v}; R^2 = 0.9991$$

The cyclic voltammograms feature two well-defined reversible processes corresponding to two stepwise monoelectronic oxidations of the tetrathia- or tetraselenafulvalene moiety (Fig. 2.13).

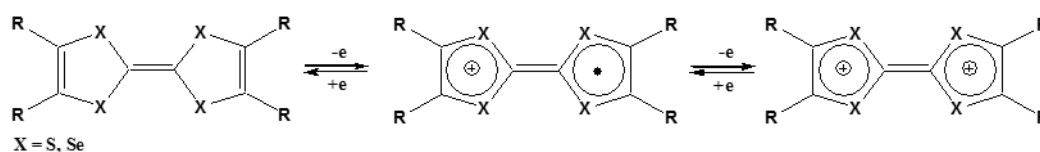
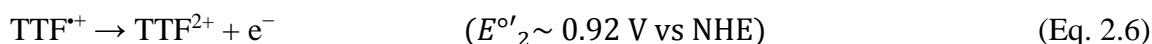
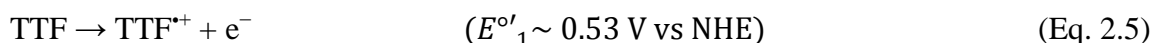


Fig. 2.13. Schematic representation of the two step oxidation process of tetrathia- or tetraselenafulvalenes.<sup>39</sup>.

For TTF, the first oxidation is centered at 0.33 V versus a silver pseudo-reference, corresponds to the removal of an electron from TTF to form a radical cation (Eq. 2.5), whereas the second one occurs at 0.72 V and is assigned to the formation of a dication (Eq. 2.6):



The formal potentials of these electrochemical reactions were recalculated versus NHE in order to facilitate further comparison. These values are fully consistent with previously reported data (0.33 and 0.70 V versus SCE for TTF in CH<sub>3</sub>CN)<sup>40</sup>. In addition, the linear dependence of the peak current with respect to the square root of scan rate (Fig. 2.12) corresponds as expected to a reversible electron transfer reaction, limited by the diffusion of electroactive species towards the working electrode surface.

Similar data were obtained for the TMTSF molecule (Fig. 2.14, 2.15). The first oxidation (Eq. 2.7) is centered at 0.36 V versus a silver pseudo-reference and the second one occurs at 0.83 V (Eq. 2.8) that corresponds again to the formation of the radical monocation and the dicationic species respectively:

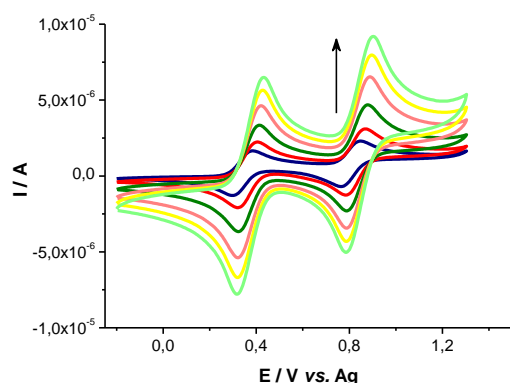
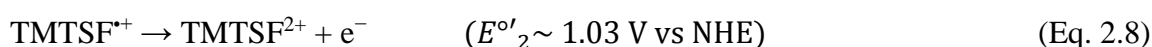
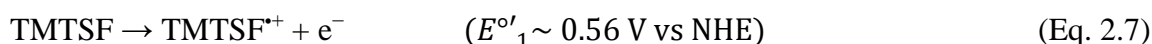


Fig. 2.14. Cyclic voltammograms of 1 mM TMTSF in CH<sub>2</sub>Cl<sub>2</sub> with 0.1 M Bu<sub>4</sub>NPF<sub>6</sub> as supporting electrolyte recorded with a gold disc working electrode at various scan rates ( $\nu = 0.05, 0.10, 0.250, 0.50, 0.75$ , and  $1.00 \text{ V s}^{-1}$ , respectively). The counter electrode was a platinum mesh, and a silver wire was used as pseudo-reference. Adapted from ref. <sup>14</sup>.

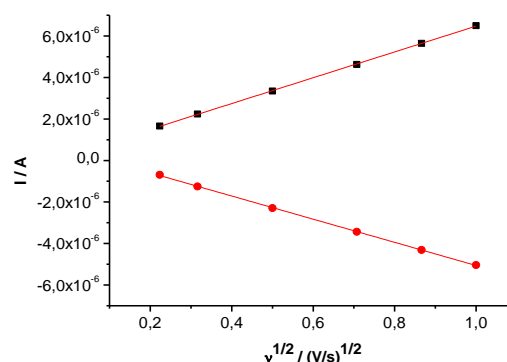


Fig. 2.15. Amplitude of the first oxidation peak (black line) and second reduction peak (red line) of TMTSF as a function of the square root of scan rate.

$$I_1 = 2.55E-7 + 6.22E-6 \cdot \sqrt{\nu}; R^2 = 0.99988$$

$$I_2 = 5.21E-7 - 5.58E-6 \cdot \sqrt{\nu}; R^2 = 0.99979$$

Comparing the obtained electrochemical data of TTF and TMTSF (eq. 2.5 – 2.8) with the standard potential of water oxidation (eq. 2.4) we can conclude that oxidation of the crystals should occur at the anodic pole during BPE. This is the reason why the first set of tested BPE conditions led to a degradation of these organic crystals (Fig. 2.10). Indeed, the reduction of Cu<sup>2+</sup> at the cathodic pole is coupled with the oxidation of the crystal at the anodic side, leading to an electro-induced dissolution (Fig. 2.16).

It is also noteworthy that the changes in color observed by optical microscopy (Fig. 2.10 a,b) are attributed to the electro-oxidation of TMTTF<sup>0/+</sup> or TMTSF<sup>0/+</sup> into the corresponding dications. The corresponding absorption properties are self-consistent with literature data reported previously for *in situ* visible absorption spectroelectrochemistry with TTF.<sup>41</sup>

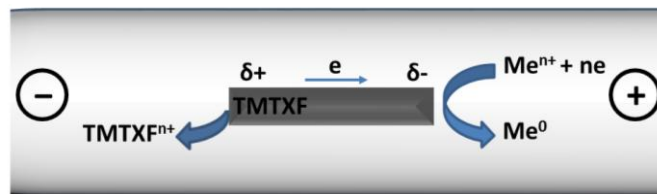
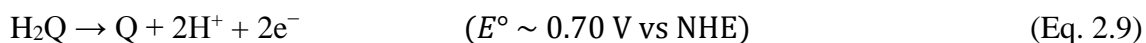


Fig. 2.16. Schematic illustration of the reduction and oxidation reactions occurring on the TMTXF charge transfer crystal during bipolar electrochemistry. This leads to metal deposition at one extremity and dissolution of the bipolar electrode at the other extremity.

To avoid the oxidative degradation that affects the integrity of the crystals, a supplementary sacrificial reactant can be advantageously used. The sacrificial co-reactant should have a lower oxidation potential than the undesirable oxidation process. In our case, we need an electroactive species, which is easier to oxidize than the donor moiety involved in the organic charge transfer crystal. In another context, hydroquinone ( $\text{H}_2\text{Q}$ ) has already been used to decrease the oxidation potential of the reaction occurring at the anodic side of a BE. In that case, the idea was to avoid water oxidation at bipolar objects.<sup>42</sup>  $\text{H}_2\text{Q}$  was selected, because it exhibits appropriate redox properties ( $E^\circ \sim 0.70$  V vs NHE) with a formal oxidation potential less positive than the oxidation of water ( $E^\circ \sim 1.23$  V vs NHE).



The same strategy was therefore applied in our experiments, relying on a comparison of oxidation potential values of fulvalenes ( $E^\circ_2 \sim 1.0$  V vs NHE) and hydroquinone ( $E^\circ \sim 0.70$  V vs NHE). It is clear, that  $\text{H}_2\text{Q}$  oxidation will take place at lower potentials and prevent the oxidation of the fulvalene's donor into the dicationic forms  $\text{TMTTF}^{2+}$  or  $\text{TMTSF}^{2+}$ .

To confirm experimentally this hypothesis, the electrochemical characterization of a  $\text{H}_2\text{Q}$  as well as  $\text{CuSO}_4$  solution was recorded versus the same reference electrode (Ag pseudo-reference) in order to determine the formal oxidation potential under the same conditions. A pH value of 1 was used to perform CV in order to stabilize  $\text{Cu}^{2+}$  ions in solution and to facilitate copper reduction. The corresponding CV are presented in Fig. 2.17.

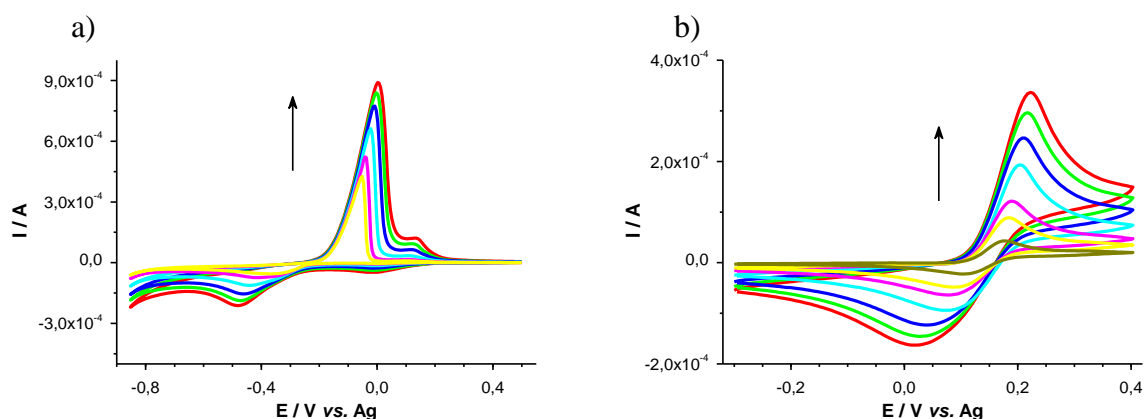


Fig. 2.17. Cyclic voltamperograms of (a) 10 mM  $\text{CuSO}_4$ ; (b) 10 mM  $\text{H}_2\text{Q}$  at pH 1 recorded with a gold working electrode at various scan rates ( $\nu = 0.01, 0.05, 0.10, 0.250, 0.50, 0.75$ , and  $1.00 \text{ V s}^{-1}$ , respectively). The counter electrode was a platinum mesh, and a silver wire was used as pseudo-reference.

Consequently, the two redox half reactions, involved during the bipolar electrochemical electrodeposition, are copper reduction at the cathodic extremity and hydroquinone oxidation at the anodic side. Since the latter reaction has a mild oxidation potential, the necessary electric field to couple both electrochemical processes will be much lower than previously. The difference of formal potentials of the two involved reactions is only  $0.70\text{V} - 0.34\text{V} = 0.36\text{V}$ . For a typical length of the crystal of 1 mm, the applied electric field on the crystal should be at least  $0.36\text{ V}/0.1\text{ cm} = 3.6\text{ V cm}^{-1}$ . Therefore, a new series of BPE tests was conducted using a mixture of 10 mM  $\text{H}_2\text{Q}$  and 10 mM  $\text{CuSO}_4$  by applying an electric field of typically  $3 - 4\text{ V cm}^{-1}$ . The solution of 10 mM  $\text{H}_2\text{Q}$  and 10 mM  $\text{CuSO}_4$  was prepared directly before electrodeposition experiments to prevent an eventual slow spontaneous reaction between these two components. The corresponding modified crystals (length  $\geq 1\text{ mm}$ ) were characterized by SEM imaging (Fig. 2.18).

As one can see in the corresponding micrographs, such an approach, which takes advantage of a sacrificial redox co-reactant, is successful. The cathodic edge was indeed correctly modified with copper (Fig. 2.18, left parts) while the anodic side remained undamaged (Fig. 2.18, right parts). In this series of experiments, the applied electric field was varied in a narrow window in order to focus the copper deposit at the very edge of organic crystal. In addition, the time of bipolar electrodeposition was increased up to 60 min. Also, to ensure the presence of enough electroactive species in solution for this duration, the mixture containing 10 mM of  $\text{H}_2\text{Q}$  and 10 mM of  $\text{CuSO}_4$  was refilled regularly (every 10 min).

In one case, a low electric field of  $2.6\text{ V cm}^{-1}$  was applied and this experimental condition resulted in a metal deposit that is well-focused at the very edge of the organic crystal (Fig. 2.18d). This special case was related to the shape of the crystal itself, which exhibited an arrow-like edge acting as an ideal point for copper deposition with the nucleation point located at the point of maximum polarization.

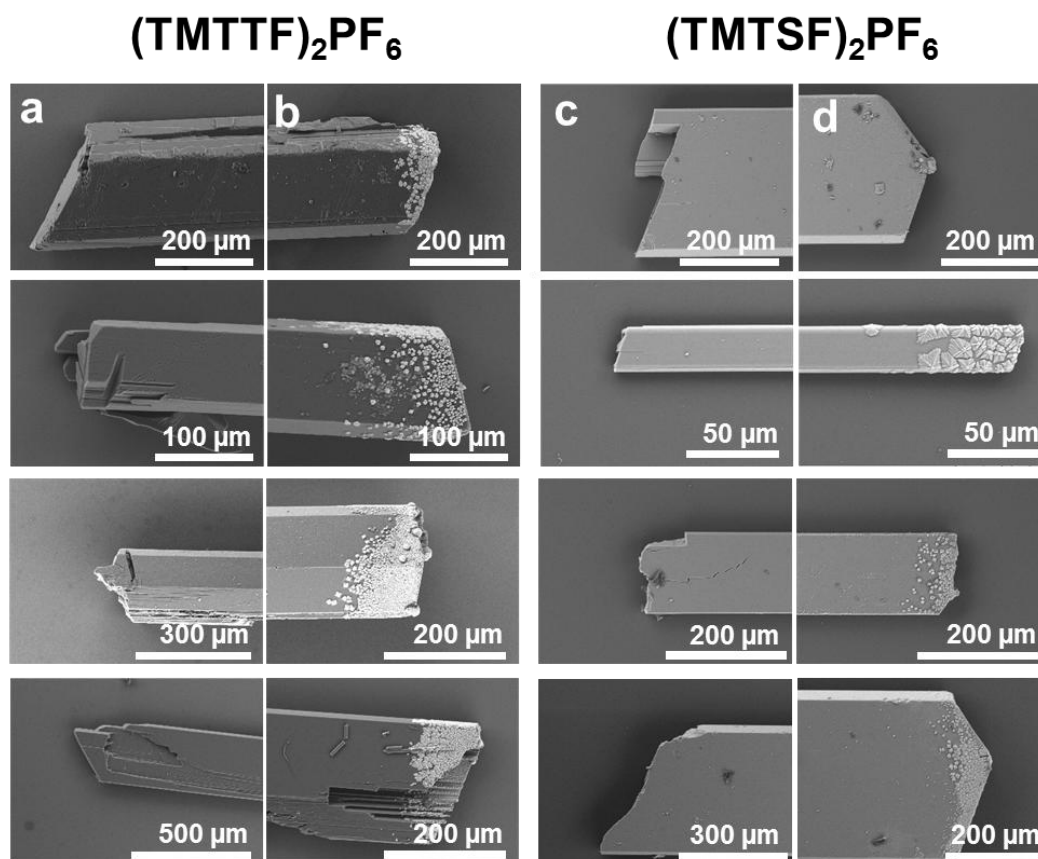


Fig. 2.18. Scanning electron micrographs of the left and right extremities of  $(\text{TMTTF})_2\text{PF}_6$  and  $(\text{TMTSF})_2\text{PF}_6$  organic crystals, whereas the cathodic side is modified with copper and the anodic side remains undamaged (due to the addition of hydroquinone as a sacrificial coreactant).

Another set of experiments was performed by varying in a wider range the electric field value. A selection of SEM images was recorded to show the cathodic side of the crystals (Fig. 2.19). One can see from these images that increasing the electric field strength definitely affects both the size of the copper clusters as well as the corresponding density.

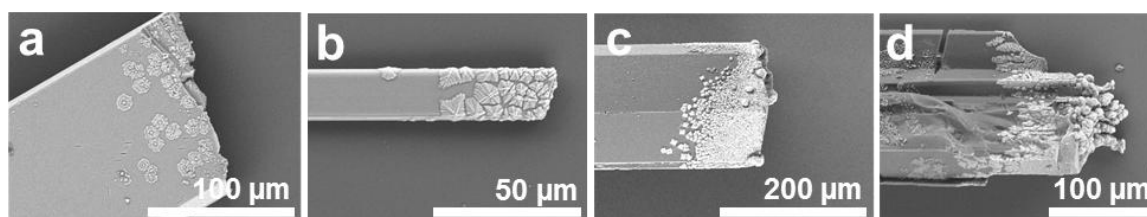


Fig. 2.19. Scanning electron microscopy images of the right extremities of  $(\text{TMTTF})_2\text{PF}_6$  and  $(\text{TMTSF})_2\text{PF}_6$  organic crystals modified with copper. Various morphology gradients of the deposit are observed as a function of the applied electric field.

In addition, we can see very different morphologies of the deposit. A slow nucleation process resulting in small discrete clusters of copper deposits at low electric fields (Fig. 2.19a). With increasing electric field amplitude, the morphology changes from clusters to a more homogeneous amorphous copper coating until the appearance of dendrites (Fig. 2.19b-d).

It is noteworthy that the same typical dependence of metal layer morphologies was already observed and reported on other substrates such as carbon fibers.<sup>26</sup> A small electric field value

provides lower overpotentials at the edges of the bipolar electrode (Fig. 2.20). When increasing the electric field value, the surface of the bipolar electrode is more polarized and this polarization increases from the center to the edges (Fig. 2.20). If the arising potential difference between the two extremities of the conductive object ( $\Delta V_e$ ) is much larger than the minimum threshold potential corresponding to the two redox reactions ( $\Delta V_{\min}$ ), then the reaction can take place alongside a longer portion of the bipolar electrode and create a deposit gradient (Fig. 2.20a). On the other hand, if  $\Delta V_e$  is smaller than the necessary  $\Delta V_{\min}$ , then the electrochemical reactions cannot be coupled on the bipolar electrode and therefore no deposition is observed (Fig. 2.20b). Of course, if the value  $\Delta V_e$  is very close to  $\Delta V_{\min}$ , then the redox reactions only take place at the edges of the bipolar electrode where the polarization is sufficient (Fig. 2.20b).

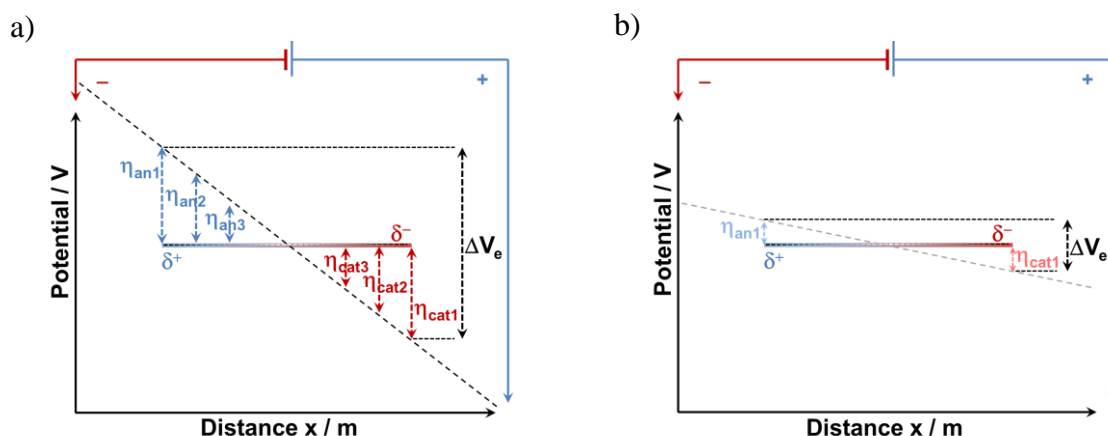


Fig. 2.20. Schematic representation of the polarization potential drop established alongside a conducting object exposed to an increasing electric field strength (from left to right).

Besides copper, bipolar electrodeposition of silver and nickel on these organic crystals was also tested. The reduction of silver ions on the bipolar organic crystal can take place when combined with the oxidative degradation of TMTTF or TMTSF (Fig. 2.21). However, in the case of silver, hydroquinone cannot be used as a sacrificial chemical species, because it directly reduces silver via a homogeneous redox reaction. In contrast, for nickel deposition, hydroquinone was employed without undesired reactivity occurring in solution, but no deposition was observed. This can be related to a competition between several reactions on the edges of the bipolar electrode. Indeed, the value of the potential difference related to water reduction/hydroquinone oxidation ( $0.70\text{V} - 0\text{V} = 0.70\text{V}$ ) is significantly smaller than the potential difference of nickel cation reduction/hydroquinone oxidation ( $0.70\text{V} - (-0.25\text{V}) = 0.95\text{V}$ ). Therefore, the first pair of reactions is electrochemically favorable, thus preventing the deposition of nickel unless a much larger electric field is applied. This highlights the necessity to select precisely the nature of the chemical reactants in order to achieve metal deposition. This is due to the interplay between several reaction pathways involving the metal precursor, the solvent, the sacrificial co-reactant and the crystal itself.

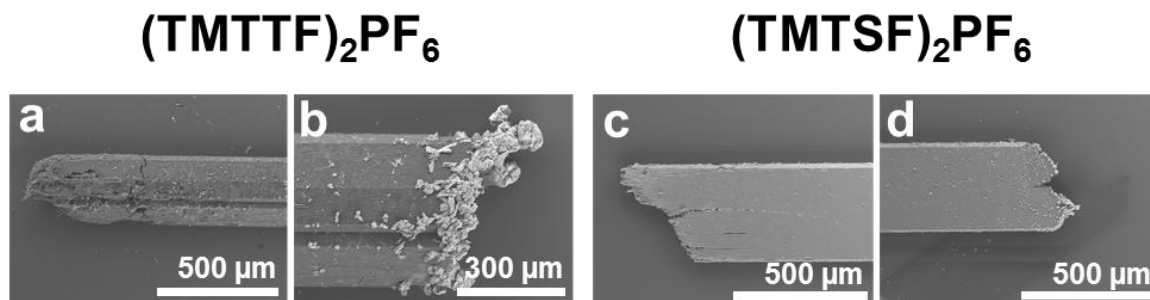


Fig. 2.21. Scanning electron images of the left and right extremities of  $(\text{TMTTF})_2\text{PF}_6$  and  $(\text{TMTSF})_2\text{PF}_6$  organic crystals, where the cathodic side is modified with silver but the anodic side is degraded.

Therefore, bipolar electrodeposition of copper was chosen for generating asymmetric metal organic substrates exhibiting potentially anisotropic properties. A large number of asymmetric objects of various lengths were prepared according to the procedure described above, and as expected, a longer deposition zone was observed when using the longest crystals available (2.5–3.0 mm) such as the one shown in Figure 2.22a. These long single crystals were then selected for further electrical characterization as they are also easier to handle manually.

### 2.3.3. Metal-organic hybrid materials

There is a great interest in metal-hybrid semiconductor materials. This is based on the fact that they can retain simultaneously the physical and chemical properties of the individual metal and semiconductor parts. Also, they can exhibit unique properties due to synergetic effects. These hybrid materials can potentially be exploited for new applications. For instance, such metal-semiconductor materials are interesting in the frame of possible photocatalytic or photovoltaic properties. Therefore, asymmetric copper-organic crystals were further tested for photovoltaic applications.

### 2.3.4. Electrical characterization (asymmetric photovoltage generation)

Photovoltage measurements were recorded to demonstrate the influence of the localized deposit on the physical properties of the newly prepared metal-organic hybrid material.

Due to the intrinsic fragility of these organic crystals, different approaches have been used to achieve electric measurements via a connection to a voltmeter. First, the organic substrate, modified or not modified, was glued on a coverslip with double-sided scotch tape and the connection was ensured with thin needles in a typical probe station configuration. The disadvantages of such a set-up is that the electric contact is established only at one point and is potentially very sensitive to the quality of the contact with a very often significant noise level. In addition, the pressure exerted on the crystals very often leads to irreversible damage such as cracking and/or breaking. Therefore, a new and softer approach was established. A simpler experimental setup was chosen where the organic crystal is simply positioned between two carbon-tape stripes (Fig. 2.22a), which are connected to a voltmeter by crocodile clips. In this



case, the nature of the tape surface is softer allowing to absorb the mechanical constraints and to reduce significantly the risk of fracture. Moreover, it was possible to establish a reproducible electric contact with the copper deposit by using a macroscope. As shown on the optical image below (Fig. 2.22c), the copper layer that covers the right part of the crystal is in contact with the conducting carbon stripe.

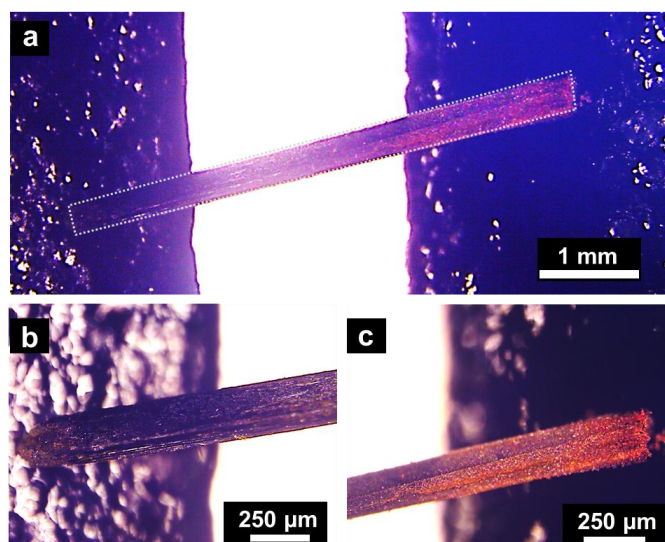


Fig. 2.22. Optical images of the Janus  $(\text{TMTSF})_2\text{PF}_6$  copper modified crystal on carbon stripe. (a) Hole length  $(\text{TMTSF})_2\text{PF}_6$  modified with copper at the right end; (b) zoom on the left side of the crystal; (c) zoom on the right side of the crystal modified with copper.

The voltage was then measured while illuminating either one side or the other of the asymmetric materials with a red laser ( $\lambda = 650 \text{ nm}$ ). A representative time evolution of the photovoltage generated across a modified  $(\text{TMTSF})_2\text{PF}_6$  crystal as a function of the light excitation side is shown in Figure 2.23c.

Here, the geometry of the device is similar to a metal/semiconductor/metal (MSM) photodetector architecture, i.e., a semiconductor material in between two metal electrodes. It means that in this configuration two metal/semiconductor Schottky contacts are generated, and therefore the photovoltage polarity depends on the illumination side. Indeed, the intensity of the photovoltage was found to be asymmetric with a different amplitude depending on whether the excitation was focused on the modified versus unmodified side of the crystal (Fig. 2.23). The photovoltage generated with a copper-modified organic crystal was observed to have different amplitude, being twice larger when illuminating the copper side, compared to an illumination of the unmodified side (Fig. 2.23a, c). This is assigned to the different nature of the contact (and corresponding work functions) between the right and left sides with or without the presence of copper. A control experiment was also recorded with a pristine crystal. In this case, the amplitude of the photovoltage has the same value independently of the illumination side. (Fig. 2.23b, d). Such an asymmetric photovoltage behavior was also reported recently in the case of Janus graphene sheets<sup>43</sup> and is observed here for the first time on a more complex Janus organic single crystal conductor. Finally, the comparison between a modified and an

unmodified crystal confirms also that the copper electrodeposition did not alter the chemical integrity of the Bechgaard salt.

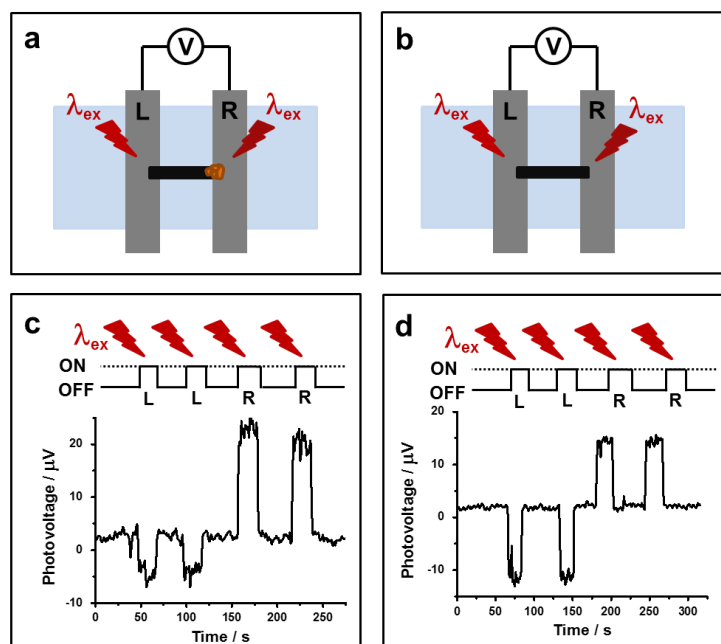


Fig. 2.23. Schematic illustration of the experimental photovoltage set-up with (a) a copper modified organic crystal, (b) an unmodified crystal. Two carbon electrodes are connected to a voltmeter, the light source is a red laser directed alternatively towards the left (L positive polarity) and right (R negative polarity) side of the electrode/crystal contact. (c) Sequence of illumination pulses and corresponding photovoltage recorded with Janus, and (d) unmodified (i.e., symmetric) organic crystals respectively. Adapted from ref. <sup>14</sup>.

### 2.3.5. Conclusions

Using BPE has already proven to be successful for the fabrication of various asymmetric Janus particles. So far, the strategy was typically based on the site-selective electrodeposition of a redox-active precursor at one extremity of either carbon or metal bipolar electrodes. The choice of these substrates is straightforward because they are efficient conductors that are usually employed as electrode materials for conventional electrochemistry. In an effort to extend the scope and potentialities of BPE, Fabre and Bechgaard salts based on TMTTF and TMTSF moieties were selected and used as bipolar electrodes. This is the first demonstration of the use of organic single crystal conductors in bipolar electrochemistry for which copper metal electrodeposition was successfully achieved. This approach opens the route to new families of Janus particles that can be prepared by BPE in the bulk and therefore potentially at a large scale. The corresponding asymmetric objects were characterized by optical imaging and electron microscopy revealing that the edge of the crystal acting as an anode is very sensitive to electro-dissolution. This drawback has been circumvented by the addition of a sacrificial co-reactant with an appropriate redox potential in order to carry out bipolar electrodeposition without altering the chemical structure of the crystal. Finally, asymmetric photovoltage generation could be observed as a result of the intrinsic break of symmetry provided by the site-selective metal deposition. We anticipate that this kind of new functional hybrid materials could be

employed for applications in organic electronics and/or photocatalysis, as well as for electronic displays or photoactive electronic devices. Moreover, other, more elaborated, TTF-based conducting crystals with different functionalities can be considered as possible BPE organic electrodes.<sup>44,45</sup>

## 2.4. Introduction to transition metal dichalcogenides

In this chapter, we demonstrate that transition metal dichalcogenide (TMDCs) single crystals could constitute a new class of BEs. TMDCs are two-dimensional materials and they have recently been reported as efficient catalysts for the hydrogen evolution reaction (HER).<sup>46–48</sup>

Since the recent discovery of graphene<sup>49</sup>, two-dimensional (2D) materials have attracted a significant interest due to their original physical, chemical, mechanical and electronic properties.<sup>50,51</sup> Among the 2D family, TMDCs are one of the most widely studied structures and therefore one representative of this group was considered in order to address in this chapter the suitability to be used as a BE. TMDCs currently attract a major interest both in fundamental studies as well as for technological applications due to their wide range of properties that can vary from semiconductors and metals to superconductors. In addition, they exhibit a unique crystal structure, that can be changed by reducing dimensions or intercalations and consequently the physical and chemical properties of TMDCs can be effectively tuned. Also by controlling the stoichiometric ratio in the chemical vapor deposition growth of alloys, the optical and electrical properties of the thin layers can be rather different. Due to the flexible tuning of the resulting properties, TMDCs have become attractive candidates for a variety of applications including electronics, optoelectronics, catalysis and energy storage.<sup>52</sup> Some TMDCs are also promising for fuel cells and in water-splitting applications because of photocatalytic properties of their reactive edge sites. Recent findings have also revealed that TMDCs could be practical and inexpensive alternatives to noble metals such as Pt for the electrochemical production of hydrogen by water electro-reduction. The most studied examples of 2D TMDCs are molybdenum disulfide (MoS<sub>2</sub>), molybdenum diselenide (MoSe<sub>2</sub>), tungsten disulfide (WS<sub>2</sub>) and tungsten diselenide (WSe<sub>2</sub>). These materials, in particular MoS<sub>2</sub> and WS<sub>2</sub> nanosheets are particularly relevant in the context of HER.

### 2.4.1. Crystal structure

The building blocks of TMDCs are monolayers that consist of three atomic layers: the layer of transition metal atoms is sandwiched between two layers of chalcogen atoms to maintain the X-T-X composition where X = chalcogen atoms and M = transition metal atoms as shown in the crystal structure (Fig. 2.24). In all dichalcogenides, chalcogen-metal intra-layers are coupled

by strong covalent bonding whereas van der Waals forces are holding together the planar two-dimensional monolayers.

Due to the strong covalent character of the chalcogen/metal interaction within a single layer compared to the much weaker van der Waals forces between layers, it is relatively easy to exfoliate them and obtain ultimately monolayers. The physical properties of TMDCs are anisotropic, because of directionality inherent of the layered structure, i.e. the properties are significantly different in orthogonal planes. Consequently, the electrical conductivity is quite high along one or two directions, while it is smaller by several orders of magnitude along the perpendicular directions. Such an anisotropy does strongly influence the charge transport within the structure.

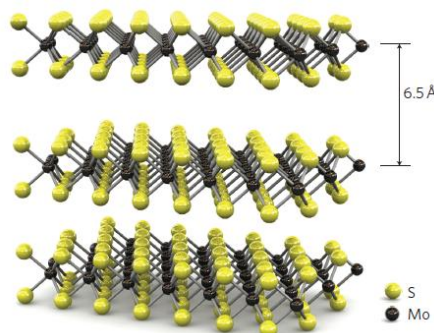


Fig. 2.24. Structural representation of a  $\text{MoS}_2$  crystal, which is similar for all TMDCs. The distance between two single layers is about 6.5 Å. Adapted from ref <sup>53</sup>

On TMDCs, two types of surface sites can be highlighted: terrace sites on the basal planes and edge sites on the side, respectively. Experimentally the edge sites of  $\text{MoS}_2$  were found to be the active sites for HER, rather than terrace sites.<sup>48</sup> This is the reason explaining why bulk  $\text{MoS}_2$  is not an active catalyst for HER since there are not enough edge sites exposed to the surrounding aqueous media.

## 2.5. Bipolar electrochemistry with macroscale $\text{MoSe}_2$ crystals

### 2.5.1. Asymmetric modification by different metals with BPE

In this chapter, for the first time we demonstrate that TMDCs, in particular  $\text{MoSe}_2$  single crystals can be used as BE.

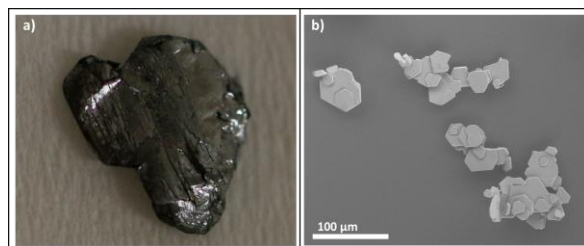


Fig. 2.25. (a) Photograph of a  $\text{MoSe}_2$  macrocrystal and (b) SEM image of  $\text{MoSe}_2$  microcrystals.

BPE was employed first for metal electrodeposition on large MoSe<sub>2</sub> crystals exhibiting typically a macroscale dimension. The bipolar electrodeposition of metals on conductive objects could be achieved when two redox reactions take place at the opposite sides of the BE. Experimentally, the bipolar object is immersed in an aqueous solution containing a metal salt and when a sufficient electric field is applied, the reduction of the metal precursor occurs at the cathodic pole and is coupled with water oxidation at the anodic pole of the BE.

The cell used to perform bipolar metal electrodeposition on MoSe<sub>2</sub> is presented in figure 2.26. The feeder electrodes were positioned at a distance of 3.5 cm from each other and were connected to the power supply (Keithley 6517B electrometer). A sufficient potential difference was applied between the feeder electrodes, depending on the nature of the metal considered and therefore the corresponding thermodynamic conditions.

The aqueous solutions of different metal salts were prepared with CuSO<sub>4</sub>, Ag<sub>2</sub>SO<sub>4</sub>, H<sub>2</sub>AuCl<sub>4</sub> and NiSO<sub>4</sub> at a concentration of 5 mM as precursors for the deposition of copper, silver, gold and nickel, respectively.

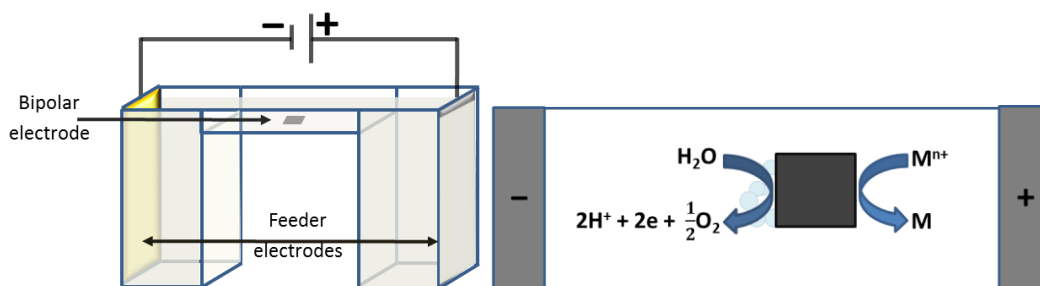
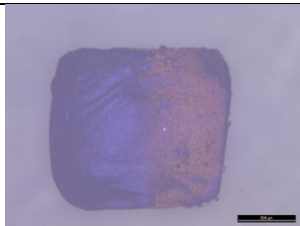
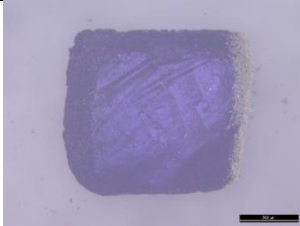
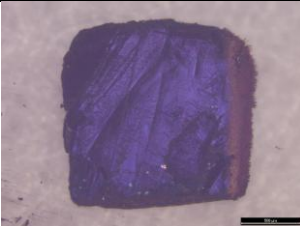
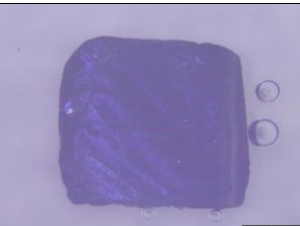


Fig. 2.26. (a) Scheme of the set-up used for metal deposition on MoSe<sub>2</sub> by BPE. (b) Schematic illustration of the involved bipolar redox reactions.

The bipolar electrodeposition of metals was monitored *in situ* with a Leica MSV266 microscope, during the application of the electric field across the cell. Each metal necessitates a different electric field value to be electrodeposited on the BE as it depends on the respective standard potential of the involved chemical species. The following order is observed in the series of tested metals:  $E^\circ (\text{AuCl}_4^-/\text{Au}) > E^\circ (\text{Ag}^+/\text{Ag}) > E^\circ (\text{Cu}^{2+}/\text{Cu}) > E^\circ (\text{Ni}^{2+}/\text{Ni})$ . The minimum polarization potential ( $\Delta V_{\text{min}}$ ) is equal to the difference of standard potentials of water oxidation and metal salt reduction. This value increases in the aforementioned order from gold to nickel (Table 2.1). Therefore, by keeping the inter-feeder electrode distance constant inside the BPE cell, gold deposition occurs at a significantly smaller electric field, whereas an incrementally higher electric field is necessary for silver, copper and nickel. The typical theoretical and experimental values needed for bipolar electrodeposition are gathered in Table 2.1. This series of data allows to establish the conditions for a successful metal deposition on MoSe<sub>2</sub> crystals. The length of the deposit depends directly on the electrochemical characteristics of each metal and can be readily adjusted by tuning the value of the electric field. For example, for gold deposition, a minimum electric field value of 1.5 V cm<sup>-1</sup> is needed. However a larger electric field value promotes a larger polarized area of the crystal and consequently a more extended metal deposit on that area. In the same time, an applied electric

field value just beyond the threshold value ( $\Delta V_{\min}$ ) causes metal deposition only at the edges of the BE as observed in the case of silver and copper depositions. A significantly higher voltage is necessary for the deposition of nickel, resulting in a possible competition with proton reduction since the polarization potential is about the same when these two redox reactions are involved: the calculation leads to  $\Delta V_{\min} = 1.43\text{V}$  for coupling water oxidation and nickel reduction, and  $\Delta V_{\min} = 1.23\text{V}$  in the case of water oxidation / proton reduction, respectively. That's why we observed  $\text{H}_2$  bubbles formation together with nickel reduction at the negatively polarized side of the crystal as shown in the last line of Table 2.1. This first series of results demonstrate without ambiguity that  $\text{MoSe}_2$  is indeed a suitable substrate for BPE experiments (Table 2.1).

Table 2.1. Standard potentials of redox couples involved. Minimum polarization potential ( $\Delta V_{\min}$ ), based on the difference of standard potentials of the metal reduction and water oxidation redox couples and typical electric field values necessary to trigger the bipolar electrodeposition on a 1.5 mm-long  $\text{MoSe}_2$  crystal.

Redox couple	$E^\circ$ (V vs NHE)	$\Delta V_{\min}$ (V)	Electric field (V/cm)	Optical image
$\text{O}_2(\text{g})/\text{H}_2\text{O}$	+1.23			
$[\text{AuCl}_4]^-/\text{Au}(\text{s})$	+0.99	+0.24	1.6	 2.8 V/cm, 20 min
$\text{Ag}^+/\text{Ag}(\text{s})$	+0.80	+0.43	2.9	 4.3 V/cm, 3 min
$\text{Cu}^{2+}/\text{Cu}(\text{s})$	+0.34	+0.89	5.6	 5.7 V/cm, 20 min
$\text{Ni}^{2+}/\text{Ni}(\text{s})$	-0.26	+1.49	9.3	 11.4V/cm, 5 min

### 2.5.2. Wireless hydrogen production on a single crystal

The advantage of BPE is that we can combine very different reactions on the edges of the BE. Since MoSe<sub>2</sub> is widely known for its electrocatalytic activity towards HER, the next task was to exploit this property with BPE. MoSe<sub>2</sub> has recently received a lot of attention as a Pt substitute in the context electrocatalytic hydrogen production. We were interested by using BPE for hydrogen production on this material in a wireless manner. The aim was to achieve water splitting, i.e. water oxidation and water reduction at the opposite edges of a single MoSe<sub>2</sub> crystal in comparison with carbon material addressed by BPE. In order to assess this behavior, pieces of carbon and MoSe<sub>2</sub> samples of comparable size (length ~ 1.5 mm) were immersed in a  $1 \times 10^{-3}$  mol L<sup>-1</sup> NaCl aqueous solution and submitted to an increasing electric field value, ranging from 7.1 to 20.0 V cm<sup>-1</sup> (Fig. 2.27). The substrates were imaged *in situ* in order to visualize the production of gas bubbles due to the electrochemically driven proton reduction to form hydrogen gas at the cathodically-polarized side of the crystal. In this set of experiments, when an increasing potential is applied (Fig. 2.27) bubble formation occurs much faster and more efficiently on the MoSe<sub>2</sub> crystal than on carbon material. The formation of hydrogen bubbles was observed on the carbon sheet only above an electric field of 14.3 V cm<sup>-1</sup> and after quite a long time. On the other hand, it occurs at much lower potentials (starting from 7.4 V cm<sup>-1</sup>) and immediately on MoSe<sub>2</sub>. During the application of an electric field of 17.1 V cm<sup>-1</sup> bubbles form immediately and very intensively on MoSe<sub>2</sub> substrate, while only very tiny bubbles were barely visible on carbon sheet, and started to grow only after 30 s. Finally, hydrogen production on the carbon-based material starts to be unambiguously observed when applying the largest electric field value tested, 20.0 V cm<sup>-1</sup> (Fig. 2.27f). These data confirm that it is much easier to initiate proton reduction at the MoSe<sub>2</sub> bipolar electrode compared to the carbon one. In addition, the BPE configuration allows to carry out these reactions without any electrical connection to the crystal. This ability might be used for example for the separation of gas during water splitting operated in a closed BPE configuration in order to obtain pure hydrogen and oxygen gases in the two separated compartments.



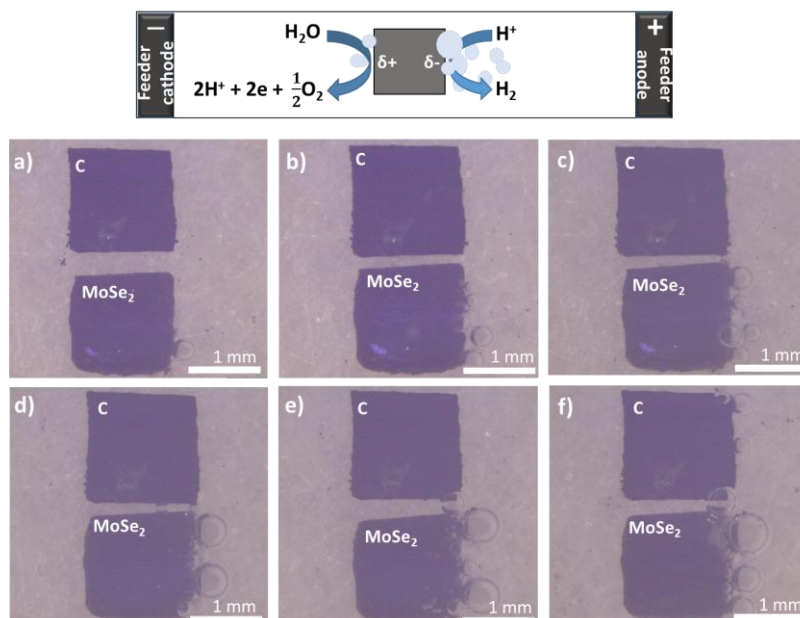


Fig. 2.27. Bipolar electrochemical hydrogen bubble production. Optical micrographs of carbon (top) and MoSe<sub>2</sub> (bottom) under an electric field of (a) 7.4 V cm<sup>-1</sup>; (b) 8.6 V cm<sup>-1</sup>; (c) 11.4 V cm<sup>-1</sup>; (d) 14.3 V cm<sup>-1</sup>; (e) 17.1 V cm<sup>-1</sup>; (f) 20.0 V cm<sup>-1</sup> in 1 mM NaCl aqueous solution.

A superior electrocatalytic activity for proton reduction was also confirmed by investigating the behavior of MoSe<sub>2</sub> with conventional cyclic voltammetry when using either carbon or MoSe<sub>2</sub> as working electrode. A much larger faradaic current is observed for MoSe<sub>2</sub> compared to a C electrode with the same geometric size (Fig. 2.28). In addition, it is thermodynamically easier to trigger these reactions on MoSe<sub>2</sub> material.

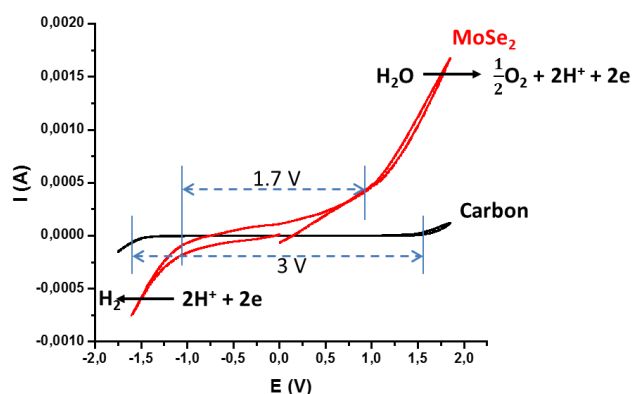


Fig. 2.28. Cyclic voltamperograms obtained by using as working electrode either carbon material (black curve) or MoSe<sub>2</sub> (red curve) in 1 mM NaCl aqueous solution at a scan rate of 100 mV s<sup>-1</sup>.

These results confirm that bipolar reactions involving proton reduction are much easier on MoSe<sub>2</sub> allowing to work at lower applied electric fields in the BPE configuration. At the same time, the other involved electrochemical reaction of water oxidation for O<sub>2</sub> bubble formation at the anodic pole of the BE has limited yield on both materials. Theoretically, the quantity of oxygen bubbles formed must be two times lower than the quantity of hydrogen gas according to the stoichiometry of these reactions. However, O<sub>2</sub> bubble formation was rarely observed at



both materials. This can be explained due to different requirements for bubble formation of  $O_2$  compared to  $H_2$ . Oxygen is more soluble, and might be continuously dissolved in the aqueous solution without significant nucleation of bubbles. In order to verify the nature of the counter reaction, a control experiment was performed by adding a universal pH indicator to the solution (Fig. 2.29). The formation of pH gradients was indeed observed on both sides of the  $MoSe_2$  bipolar electrode with red and blue colorations of the initially yellow pH indicator solution, confirming the consumption and generation of protons at the opposite edges of the BE.

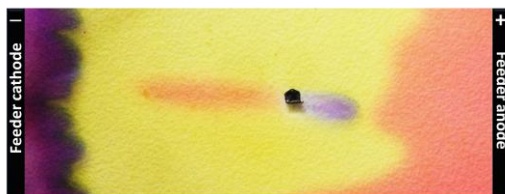


Fig. 2.29. Direct visualization of pH gradients promoted on a  $MoSe_2$  bipolar electrode. In unbuffered conditions, the presence of a universal pH indicator reveals the formation of  $OH^-$  at the cathodic extremity (right side) and the formation of  $H^+$  at the anodic pole (left side) of the  $MoSe_2$  bipolar electrode.

Since the reaction of proton reduction toward hydrogen gas formation is very efficient on the  $MoSe_2$  crystal, it can be used for many different applications in a BPE configuration. First of all, this material could be used for hydrogen gas production like in conventional electrochemistry. Second, it is also possible to couple it with any other oxidation reaction of interest in the bipolar mode.

### 2.5.3. Bipolar electrochemical decontamination with macro-particles of $MoSe_2$

Thus, the possible application to electrochemical decontamination by BPE with a  $MoSe_2$  single crystal was studied with model organic and inorganic molecular systems.

First, the electrochemical redox indicator Ferroin ( $[Fe(phen)_3]^{2+}$ , where phen is the abbreviation for 1,10-phenanthroline) was used for this purpose. This inorganic ferrous complex is an electrochromic species that can be oxidized to the corresponding ferric derivative,  $[Fe(phen)_3]^{3+}$  with color-switching from red to blue (Fig. 2.30).

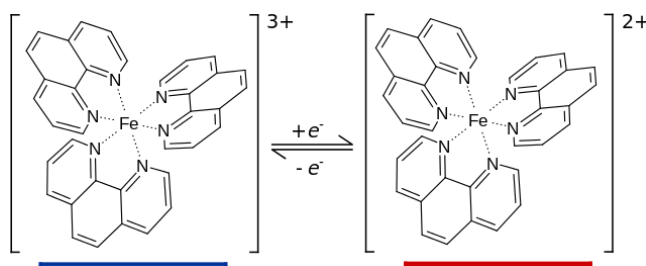


Fig. 2.30. Chemical structure of Ferroin: oxidized form  $[Fe(phen)_3]^{3+}$ , which has a blue color and reduced form  $[Fe(phen)_3]^{2+}$ , red color).

Electrochemical and spectral characterization of this molecule are presented in Fig. 2.31.

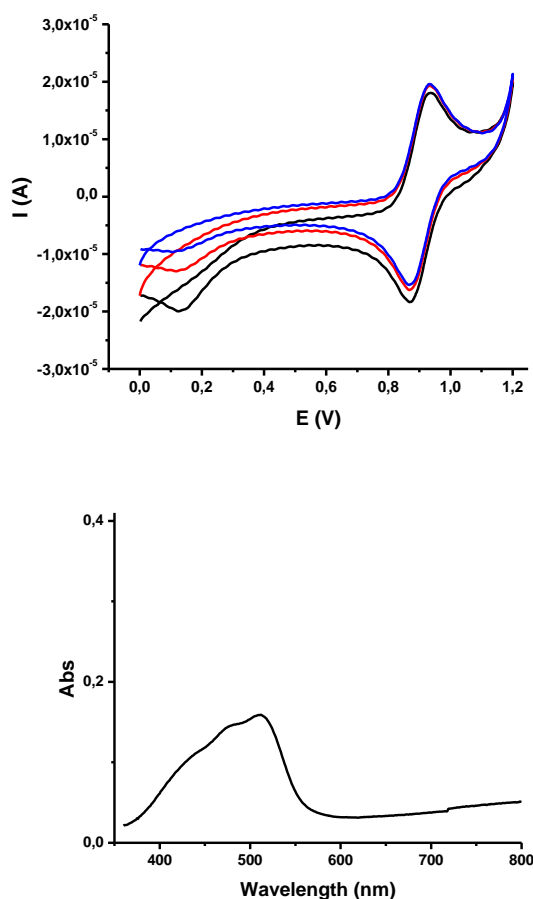


Fig. 2.31. (a) Cyclic voltammograms of 1.4 mM Ferroin in 0.1 M NaCl recorded with a carbon working electrode, a platinum mesh as the counter electrode and a silver/silver chloride reference electrode. (b) Absorption spectra of 14.4  $\mu$ M Ferroin,  $\lambda_{\text{max}} = 510$  nm.

The CV shows that the ferroin/ferrin redox system is reversible and rapid. The formal potential of this redox couple was determined to be  $\sim 0.9$  V versus Ag/AgCl which is consistent with previous literature<sup>54</sup> data reporting a mid-potential of 0.87 V. The absorption spectrum reveals a typical MLCT band in the visible region with a maximum absorbance of the reduced form at a wavelength of 510 nm. It is noteworthy that the corresponding Iron III complex solution does not absorb significantly at 510 nm in the green, but in the orange instead ( $\lambda_{\text{max}} \sim 650$  nm, responsible for a light blue color).

This redox indicator was used in BPE experiments with macroscale MoSe<sub>2</sub> crystals.

For this purpose, a MoSe<sub>2</sub> crystal with a size of  $\sim 0.3$  cm was inserted inside a small capillary positioned between two compartments with the feeder electrodes. The distance between both feeder electrodes was 3.0 cm and the BE cell was filled with a 1 mM NaCl solution containing 0.28 mM Ferroin.

An electric field of  $15 \text{ V cm}^{-1}$  was applied to the cell in order to try to combine the reduction of protons at one side of BE and the oxidation of ferroin at the opposite side.

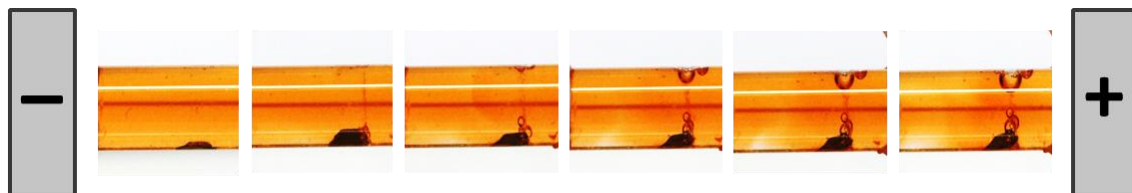


Fig. 2.32. Evolution of bipolar electrochemical reactions with time at a MoSe<sub>2</sub> bipolar electrode. The left side of the crystal is polarized positively where the [Fe(phen)<sub>3</sub>]<sup>2+</sup> oxidation takes place. The migration of colorless fraction towards the feeder cathode is observed at the bottom of the capillary. The right side of the crystal is polarized negatively, where proton reduction reaction takes place. An increasing evolution of hydrogen bubbles is observed with time.

Fig. 2.32 gathers a series of images taken at a regular interval while the potential is applied to the cell. We can observe a large amount of H<sub>2</sub> bubbles that increases with time at the cathodic edge of the bipolar MoSe<sub>2</sub> crystal. At the same time, a slight color change is observed near the anodic side of the crystal. In addition, this fraction of pale blue/colorless solution seems to migrate with time from the MoSe<sub>2</sub> crystal towards the feeder cathode. This processes obviously relates to the redox conversion of ferroin from [Fe(phen)<sub>3</sub>]<sup>2+</sup> to [Fe(phen)<sub>3</sub>]<sup>3+</sup> and changes in color respectively from red to blue (in diluted solution colorless). Since the formed species [Fe(phen)<sub>3</sub>]<sup>3+</sup> are charged positively, their electrophoretic flow directs them towards the negative feeder cathode. Therefore, we observe a migration of the oxidized form of ferroin during the BPE process.

To avoid such an undesirable migration of redox species, another redox indicator being neutral in its oxidized state was selected.

For this purpose, Amplex® Red dye (AR) which is a N-protected 10-Acetyl-3,7-dihydroxyphenoxazine was chosen. The color of this molecule changes depending on the oxidation state, which is favorable for optical detection. In addition, the mild potential of oxidation is suitable for BPE experiments.

In fact, AR is a commercially available fluorogenic probe that is widely used in many bioassays. The molecule is colourless in its initial form, but a deep pink coloration ( $\lambda_{\text{abs}} = 570 \text{ nm}$ ,  $\epsilon = 51,000 \text{ M}^{-1} \text{ cm}^{-1}$ ) is observed upon oxidation to the corresponding 7-hydroxy-3H-phenoxazin-3-one (also known as resorufin, RF) (Fig. 2.33).

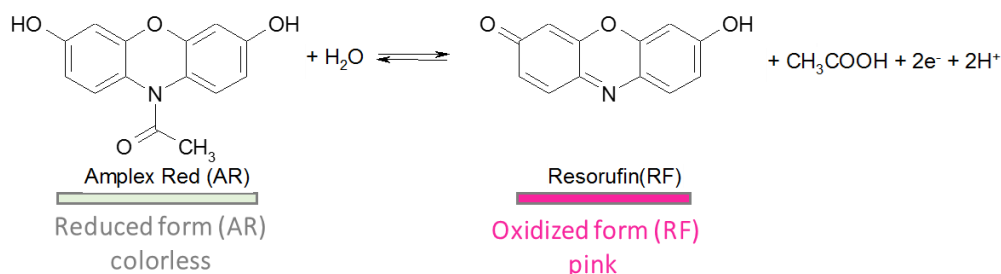


Fig. 2.33. Chemical structure of Amplex Red (AR) and electrochemical oxidation of AR to Resorufin (RF)

The first experiment was performed at the macroscale, with a piece of MoSe<sub>2</sub>. The single crystal with a length of  $\sim 0.3 \text{ cm}$  was immersed inside a capillary filled with a 5 mM AR solution and 1 mM NaCl in a mixture of DMSO/H<sub>2</sub>O (Fig. 2.34b).

To promote two redox reactions at the opposite edges of the bipolar electrode, a sufficient electric field should be applied to the cell.

Theoretically, the value of the electric field needed depends on the potential difference of the two reactions involved,  $\Delta V$  and the size of the bipolar electrode,  $l_e$  (Eq. 2.10). The reactions involved at the bipolar electrode consist of proton reduction ( $E_1^\circ = 0.0$  V) and AR oxidation ( $E_2^\circ = 0.5$  V) at opposite edges, meaning that the overall redox process will be the following:  $AR + H_2O = RF + CH_3CO_2H + 2H^+$ . Thereby the minimum electric field value can be calculated as:

$$\varepsilon = \frac{\Delta V_{min}}{l_e} = \frac{E_1^\circ - E_2^\circ}{l_e} = \frac{0.5 \text{ V}}{3 \cdot 10^{-1} \text{ cm}} = 1.7 \text{ V cm}^{-1} \quad (\text{Eq. 2.10})$$

Nevertheless, a much larger electric field value above  $25 \text{ V cm}^{-1}$  was found to be optimal for a better observation of hydrogen evolution as well as RF formation.

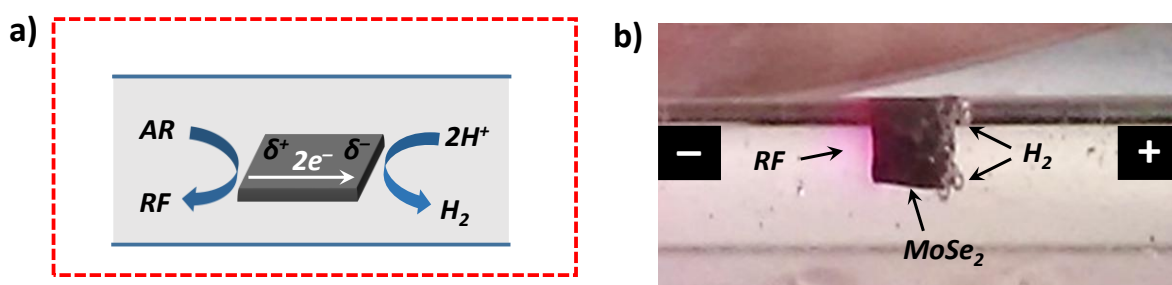


Fig 2.34. (a) Scheme showing the coupling between AmplexRed (AR) oxidation into resorufin (RF) and proton reduction at the edges of a BE. (b) Photograph of a  $3 \times 3 \text{ mm}^2$   $\text{MoSe}_2$  crystal placed inside the capillary and exposed to an electric field of  $26.7 \text{ V cm}^{-1}$ . Capillary filled with 5 mM AR solution and 1 mM NaCl in DMSO/ $\text{H}_2\text{O}$  (1/1).

Consequently, during the potential application, we did observe an effective  $\text{H}_2$  bubble formation at the cathodic side of the molybdenum diselenide and a persistent pink coloration surrounding the anodic side of the crystal due to the electro-oxidation of AR to RF (Fig. 2.34b).

However, it is noteworthy that this experiment was difficult to reproduce. It is due to the fact that the electrogenerated RF is indeed pH-sensitive, exhibiting thus different colors depending on the local pH. Thereby, by applying an electric field above  $25 \text{ V cm}^{-1}$ , the competitive reaction of water oxidation could also occur at the anodic side of the bipolar  $\text{MoSe}_2$  crystal. This process results in the production of protons that can locally change the pH. In such acidic conditions, RF color is pale yellow, which is rather difficult to observe.

Nevertheless, these experiments show that the  $\text{MoSe}_2$  crystal can definitely serve as a material for selective electrochemical oxidation that can be used potentially in decontamination applications. Therefore, the same principle can be applied simultaneously to several  $\text{MoSe}_2$  micro-particles in order to achieve a quantitative BPE-assisted electrochemical conversion. In that configuration, BPE processes can occur simultaneously at the level of each individual particle, providing electrochemical conversion in the bulk that could be used, for example for the oxidative decontamination of aqueous solutions polluted by organic molecules.

#### 2.5.4. Bulk bipolar electrochemical decontamination with micro-particles of MoSe<sub>2</sub>

BPE is indeed based on the generation electrochemical reactions at the opposite poles of a conductive object exposed to an electric field.<sup>12,55</sup> This phenomenon was successfully demonstrated by performing redox reactions on macroscopic bipolar electrodes, exhibiting a typical size of several cm or mm.<sup>14,16,19,42,56</sup> But the same behavior can be carried out with conductive particles of micrometric dimensions.<sup>57–59</sup> The key-advantage of BPE compared to other classic electrochemical methods is the possibility to address in a wireless way individual electrodes or ensembles of electrodes without a direct contact between the bipolar electrode and the power supply. Such a feature enables the promotion of electrochemical reactions on many conductive particles dispersed in solution.<sup>57</sup> In this manner, a BPE process can be carried out simultaneously on many microparticles.<sup>58,59</sup> For example, the work of M. Sentic et al.<sup>59</sup> demonstrated that a sufficient electric field promotes ECL of [Ru(bpy)<sub>3</sub>]<sup>2+</sup> dye at individual micro- and nano-objects that are homogeneously dispersed in solution and lead to bulk ECL generation inside a capillary tube filled with particles.

In this part of the thesis, MoSe<sub>2</sub> micro-crystals with sizes of about 30-100  $\mu\text{m}$  (Fig. 2.35) were used in a bulk configuration. For that purpose, MoSe<sub>2</sub> micro-particles were mixed with redox indicator AR dissolved in H<sub>2</sub>O/DMSO, with a 1/1 ratio, NaCl and agarose. An agarose gel was used to avoid the sedimentation and aggregation of the particles and to keep them well separated during the BPE process. This is very important to have well-suspended particles, because aggregates can act as single BE at lower potential due to a bigger size in comparison to a discrete single micro-particle. On another hand, NaCl was added to the jellifying part as supporting electrolyte to preserve a sufficient ionic conductivity inside the gel.

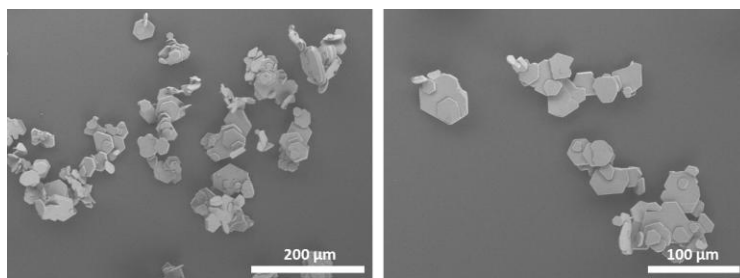


Fig. 2.35. The SEM images of MoSe<sub>2</sub> micro-crystals.

Approximately 0.02g of MoSe<sub>2</sub> particles were suspended in 1 mL of the preheated mixture of AR, NaCl and dissolved agarose, filled inside the glass capillary (outer diameter 3 mm, length 2 cm) between two feeder electrodes. (Fig. 2.36) and left for 10 min for jellifying. The final composition of the mixture in the capillary contains 5 mM of AR, 1 mM of NaCl and 1.4% of agarose. The glass capillary was then placed between two compartments of a bipolar cell, containing the graphite feeder electrodes and filled with 1 mM NaCl (Fig. 2.36).

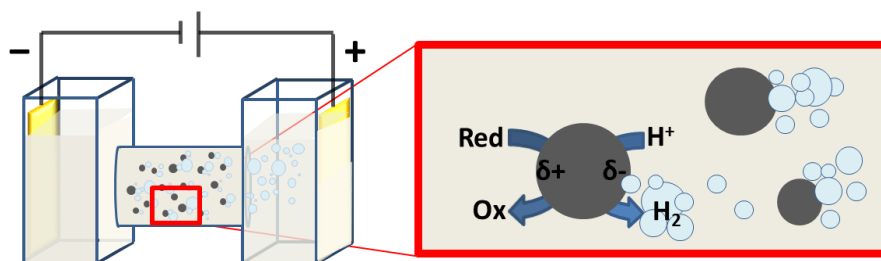


Fig. 2.36. Schematic illustration of the set-up for BPE in the bulk.

The scheme of the set-up used in this experiment is given in Fig. 2.36. As before, an electric field was applied across the cell by applying a voltage between both feeder electrodes. A potential gradient is created between the surface of each microparticle and the surrounding solution. It results in a polarization voltage difference between the opposite poles of individual MoSe<sub>2</sub> microparticles. When this polarization voltage is large enough, the desired redox reactions can occur at each microparticle. In this case, an overall electrochemical conversion of organic dye molecules can take place leading to the previously observed change in color in the entire volume of the solution where the particles are suspended.

The theoretical threshold value for the applied electric field in order to promote bipolar electrochemical reactions on MoSe<sub>2</sub> micro-particles was calculated to be about 133 V cm<sup>-1</sup>. This value was obtained on the basis of the fundamental equations of BPE as reported in the previous chapter.<sup>12</sup>

The AR oxidation occurs around +0.5 V vs Ag/AgCl on the anodically polarized side of the particles, whereas the reduction of protons takes place at potentials around 0 V vs Ag/AgCl. This means, that a minimum potential difference of 0.5 V is needed between the two edges of a particle to promote these redox reactions simultaneously. Taking into account the smallest particles size of about 30-40 μm, an electric field of about 133 V·cm<sup>-1</sup> should be present in the cell in order to observe BPE reactions even at the smallest particles. A DC generator (Heinzinger) was used to apply the electric field. The images were recorded with a digital camera (Canon 70D) equipped with macroobjective (Canon 100 mm-1:2.8).

Images were recorded during the first minute of the experiment, because at longer times ohmic heating and basic gradients near feeder cathode occur that can lead to a melting of the agarose gel and therefore sedimentation of the suspended particles. Representative images of the whole cell before and after BPE process, with and without MoSe<sub>2</sub> micro-particles are displayed in Fig. 2.37.

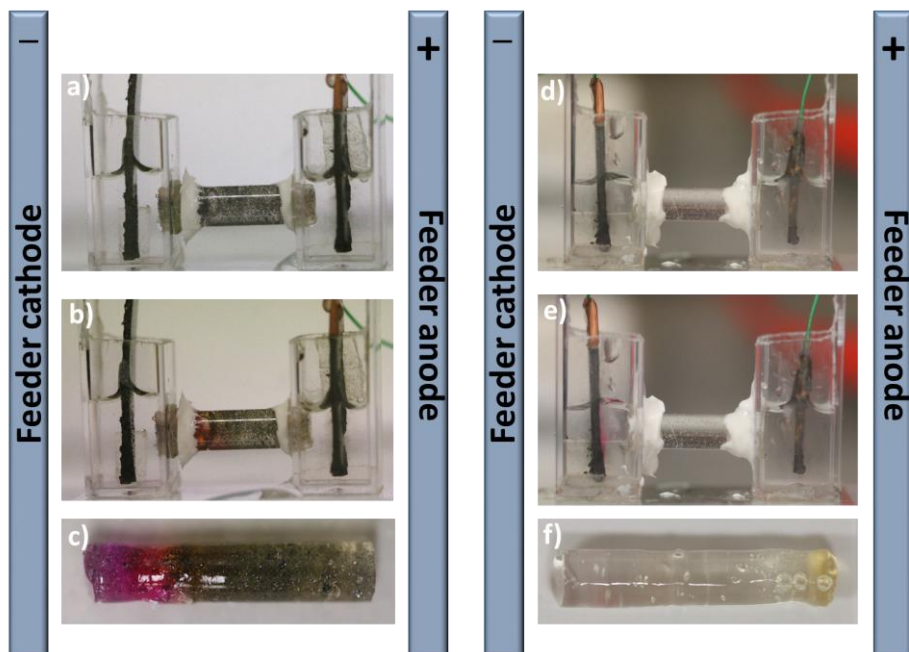


Fig. 2.37 Bipolar electrochemistry with MoSe<sub>2</sub> microparticles (average dimension 50  $\mu\text{m}$ ). In all cases the capillary is filled with 1.4% agarose gel in 1mM NaCl with 5mM AR in DMSO/H<sub>2</sub>O (1/1) ratio. (a – c) MoSe<sub>2</sub> microparticles immobilized in agarose gel; (d – f) control experiment, without MoSe<sub>2</sub> microparticles. (a, d) Before application of the electric field, (b, e) after application of 133 V cm<sup>-1</sup> for one minute. (c, d) Gels extracted from the capillary after BE experiments.

The high-viscosity of the agarose gel makes it possible to extract it smoothly from the capillary at the end of the experiment for better optical characterization. It is obvious that the electrochemical conversion is different in the presence of MoSe<sub>2</sub> particles and without (Fig. 2.37c, f). The recorded images reveal that the conversion is apparently not homogeneous inside the capillary (Fig. 2.37). This can be due to fact that the electric field generates an electro-osmotic flow (EOF), which induces motion of both species, the initial AR and the converted RF, towards the feeder cathode. Since the color of RF depends on the pH value of the solution and because the migration of H<sup>+</sup> and OH<sup>-</sup> is possible from the feeder electrodes into the capillary (Fig. 2.38), the electro-formed RF can be colored differently from yellow at acidic pH to pink at basic pH. This is the reason why we observe the migration of the involved chemical species and a difference of coloration along the capillary. The deep pink coloration is localized only in the left part of the capillary facing the feeder cathode, which is most likely related to the increased pH value in this area.



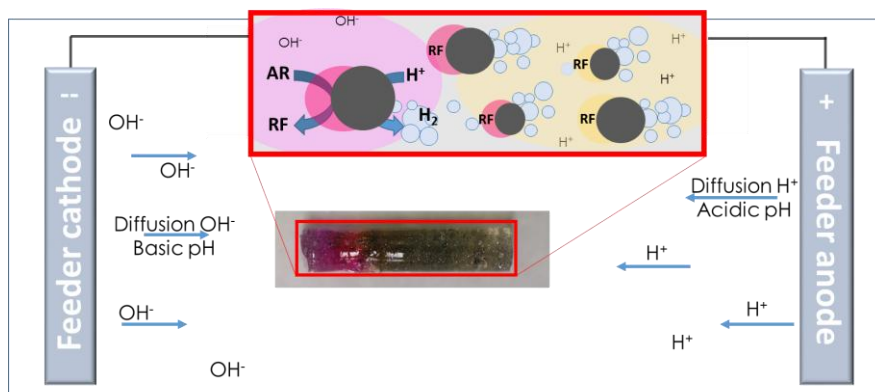


Fig. 2.38. Schematic illustration explaining the observed color change inside the gel due to the pH variations.

At the same time, the MoSe<sub>2</sub> particles remain immobilized inside the viscous reaction compartment. Thus, the approach might be potentially coupled with a fluidic device in order to achieve continuous flow-through electrochemical conversion.

A control experiment was performed under the same conditions, but without MoSe<sub>2</sub> crystals in the electrochemical cell. As expected, AR electrochemical transformation was not observed and the solution color remained unchanged (Fig. 2.37f). Only a slightly yellowish coloration can be seen, which can be related to traces of RF that are very often present in AR solution. No diffusion of a pink coloration at the left side of capillary was observed, confirming that indeed MoSe<sub>2</sub> micro-crystals are responsible for the electrochemical oxidation of AR to RF with a significant conversion rate.

In order to rationalize the pH effect on RF absorption, pH-titration was monitored by UV-vis absorption (Fig. 2.39).

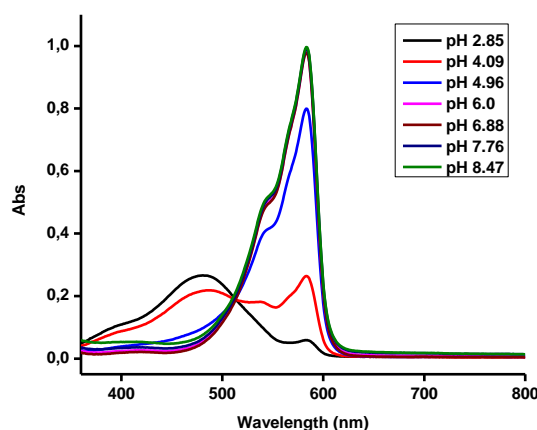


Fig. 2.39. Absorption spectra of 10  $\mu$ M Resorufin in DMSO/H<sub>2</sub>O (1/1) at different pH values.

However, AR may not be a perfect choice as redox indicator in bipolar configurations as it can be easily photo-oxidized to RF even under ambient room light<sup>60</sup>. In addition different pathways of AR oxidation are possible. Firstly, AR can be oxidized to RF initiated by trace amounts of



RF presented in the AR stock solution according to the formation of a radical intermediate. This effect depends on the duration of light exposure and the quantity of oxygen in the solution.<sup>60</sup> The authors proposed a photochemical mechanism of oxidation where RF does form a triplet excited state (RF\*) under illumination. Then, electron transfer from AR to RF\* generates an AR cation radical and RF anion radical. In our experimental conditions, the generation of these species can introduce more complexity in the mechanism and render further characterizations more difficult. Due to all these factors, it is not straightforward to conclude about the exact molecular mechanism of conversion on the bipolar electrode and to estimate the yield of conversion. Nevertheless, the comparison with the control experiment (without MoSe<sub>2</sub> microparticles) clearly demonstrates a significant difference. It means that MoSe<sub>2</sub> particles are good candidates as particles for selective electrochemical conversion.

### 2.5.5. Conclusions

In conclusion, in this chapter, we report that inorganic metal dichalcogenide crystals can be used as bipolar electrodes in a straightforward way. This is exemplified at various scales with a series of large substrates employed for proof-of-concept experiments and also with MoSe<sub>2</sub> microparticles. Electrodeposition of various metal layers is observed as a first demonstration of bipolar activity. Furthermore, a superior efficiency of this material compared to carbon can be demonstrated with respect to HER under BPE conditions. In addition, an ensemble of microparticles were collectively addressed in order to carry out an accelerated oxidation of an organic model compound. The electrochemical oxidation of the redox indicator AR in the bulk was combined with the reduction of protons. Each MoSe<sub>2</sub> microparticle is addressed electrochemically by BPE and generates the oxidation of this redox indicator, which results in local changes of color where particles are suspended. Such a fast electrolysis is impossible with one or even several macroscale bipolar electrodes. Therefore, it could be potentially used as an appropriate set-up for flow-through decontamination of waste water or unwanted organic impurities after organic synthesis.

## References

- (1) Delhaes, P.; Coulon, C.; Amiell, J.; Flandrois, S.; Toreilles, E.; Fabre, J. M.; Giral, L. *Mol. Cryst. Liq. Cryst.* **1979**, *50* (1), 43–58.
- (2) Bechgaard, K.; Jacobsen, C. S.; Mortensen, K.; Pedersen, H. J.; Thorup, N. *Solid State Commun.* **1980**, *33* (11), 1119–1125.
- (3) Shaikh Yasin, S. Electron spin resonance in low-dimensional spin chains and metals, 2008.
- (4) Granier, T.; Gallois, B.; Ducasse, L.; Fritsch, A.; Filhol, A. *Synth. Met.* **1988**, *24*, 343–356.
- (5) Quasi one dimensional charge transfer salts [http://www.pi1.uni-stuttgart.de/forschung/organic/one\\_dimen/index.en.html](http://www.pi1.uni-stuttgart.de/forschung/organic/one_dimen/index.en.html).
- (6) Bechgaard, K.; Carneiro, K.; Olsen, M.; Rasmussen, F. B.; Jacobsen, C. S. *Phys. Rev. Lett.* **1981**, *46* (13), 852–855.
- (7) Walther, A.; Müller, A. H. E. *Soft Matter* **2008**, *4* (4), 663.
- (8) Perro, A.; Reculosa, S.; Ravaine, S.; Bourgeat-Lami, E.; Duguet, E. *J. Mater. Chem.* **2005**, *15* (35–36), 3745.
- (9) Jiang, S.; Chen, Q.; Tripathy, M.; Luijten, E.; Schweizer, K. S.; Granick, S. *Adv. Mater.* **2010**, *22* (10), 1060–1071.
- (10) Loget, G.; Kuhn, A. *J. Mater. Chem.* **2012**, *22* (31), 15457.
- (11) Pawar, A. B.; Kretzschmar, I. *Macromol. Rapid Commun.* **2010**, *31* (2), 150–168.
- (12) Fosdick, S. E.; Knust, K. N.; Scida, K.; Crooks, R. M. *Angew. Chem. Int. Ed.* **2013**, *52* (40), 10438–10456.
- (13) Loget, G.; Zigah, D.; Bouffier, L.; Sojic, N.; Kuhn, A. *Acc. Chem. Res.* **2013**, *46* (11), 2513–2523.
- (14) Malytska, I.; Mézière, C.; Kielar, M.; Hirsch, L.; Wantz, G.; Avarvari, N.; Kuhn, A.; Bouffier, L. *J. Phys. Chem. C* **2017**, *121* (23), 12921–12927.
- (15) Warakulwit, C.; Nguyen, T.; Garrigue, P.; Limtrakul, J.; Kuhn, A. *Nano Lett.* **2008**, *8* (2), 500–504.
- (16) Roche, J.; Loget, G.; Zigah, D.; Fattah, Z.; Goudeau, B.; Arbault, S.; Bouffier, L.; Kuhn, A. *Chem. Sci.* **2014**, *5* (5), 1961–1966.
- (17) Kong, S.; Fontaine, O.; Roche, J.; Bouffier, L.; Kuhn, A.; Zigah, D. *Langmuir* **2014**, *30* (11), 2973–2976.
- (18) Kumsapaya, C.; Bakaï, M.-F.; Loget, G.; Goudeau, B.; Warakulwit, C.; Limtrakul, J.; Kuhn, A.; Zigah, D. *Chem. - A Eur. J.* **2013**, *19* (5), 1577–1580.
- (19) Loget, G.; Roche, J.; Gianessi, E.; Bouffier, L.; Kuhn, A. *J. Am. Chem. Soc.* **2012**, *134* (49), 20033–20036.
- (20) Yadnum, S.; Roche, J.; Lebraud, E.; Négrier, P.; Garrigue, P.; Bradshaw, D.; Warakulwit, C.; Limtrakul, J.; Kuhn, A. *Angew. Chem. Int. Ed.* **2014**, *53* (15), 4001–4005.
- (21) Fattah, Z.; Roche, J. J.; Garrigue, P.; Zigah, D.; Bouffier, L.; Kuhn, A. *ChemPhysChem* **2013**, *14* (10), 2089–2093.

- (22) Loget, G.; Larcade, G.; Lapeyre, V.; Garrigue, P.; Warakulwit, C.; Limtrakul, J.; Delville, M.-H. H.; Ravaine, V.; Kuhn, A. *Electrochim. Acta* **2010**, *55* (27), 8116–8120.
- (23) Fattah, Z.; Loget, G.; Lapeyre, V.; Garrigue, P.; Warakulwit, C.; Limtrakul, J.; Bouffier, L.; Kuhn, A. *Electrochim. Acta* **2011**, *56* (28), 10562–10566.
- (24) Ulrich, C.; Andersson, O.; Nyholm, L.; Björefors, F. *Angew. Chem. Int. Ed.* **2008**, *47* (16), 3034–3036.
- (25) Ramakrishnan, S.; Shannon, C. *Langmuir* **2010**, *26* (7), 4602–4606.
- (26) Tisserant, G.; Gillion, J.; Lannelongue, J.; Fattah, Z.; Garrigue, P.; Roche, J.; Zigah, D.; Kuhn, A.; Bouffier, L. *ChemElectroChem* **2015**, *3* (3), 387–391.
- (27) Ongaro, M.; Roche, J.; Kuhn, A.; Ugo, P. *ChemElectroChem* **2014**, *1* (12), 2048–2051.
- (28) Tiewcharoen, S.; Warakulwit, C.; Lapeyre, V.; Garrigue, P.; Fourier, L.; Elissalde, C.; Buffière, S.; Legros, P.; Gayot, M.; Limtrakul, J.; Kuhn, A. *Angew. Chem. Int. Ed.* **2017**, *56* (38), 11431–11435.
- (29) Mishra, N. In *Semiconductor Photocatalysis - Materials, Mechanisms and Applications*; Cao, W., Ed.; InTech, 2016; Vol. 3, pp 403–424.
- (30) Mokari, T.; Rothenberg, E.; Popov, I.; Costi, R.; Banin, U. *Science* **2004**, *304* (5678), 1787–1790.
- (31) Zhao, N.; Liu, K.; Greener, J.; Nie, Z.; Kumacheva, E. *Nano Lett.* **2009**, *9* (8), 3077–3081.
- (32) Dutta, S. K.; Mehetor, S. K.; Pradhan, N. *J. Phys. Chem. Lett.* **2015**, *6* (6), 936–944.
- (33) Costi, R.; Saunders, A. E. E.; Banin, U. *Angew. Chem. Int. Ed.* **2010**, *49* (29), 4878–4897.
- (34) Batail, P.; Boubekeur, K.; Fourmigué, M.; Gabriel, J.-C. P. *Chem. Mater.* **1998**, *10* (10), 3005–3015.
- (35) Moser, J.; Gabay, M.; Auban-Senzier, P.; Jérôme, D.; Bechgaard, K.; Fabre, J. M. *Eur. Phys. J. B* **1998**, *1*, 39–46.
- (36) Nad, F.; Monceau, P.; Carcel, C.; Fabre, J. M. *Phys. Rev. B* **2000**, *62* (3), 1753–1756.
- (37) Fattah, Z.; Garrigue, P.; Goudeau, B.; Lapeyre, V.; Kuhn, A.; Bouffier, L. *Electrophoresis* **2013**, *34* (14), 1985–1990.
- (38) Loget, G.; Lapeyre, V.; Garrigue, P.; Warakulwit, C.; Limtrakul, J.; Delville, M.-H.; Kuhn, A. *Chem. Mater.* **2011**, *23* (10), 2595–2599.
- (39) Schukat, G.; Fanghaenel, E.; Fanghänel, E. *Synthesis, Reactions, and Selected Physico-Chemical Properties of 1,3- and 1,2-tetrachalcogenafulvalenes*; 2003; Vol. 24.
- (40) Coffen, D. L.; Chambers, J. Q.; Williams, D. R.; Garrett, P. E.; Canfield, N. D. *J. Am. Chem. Soc.* **1971**, *93* (9), 2258–2268.
- (41) Huchet, L.; Akoudad, S.; Levillain, E.; Roncali, J.; Emge, A.; Bäuerle, P. *J. Phys. Chem. B* **1998**, *102* (40), 7776–7781.
- (42) Loget, G.; Kuhn, A. *Nat. Commun.* **2011**, *2*, 535.
- (43) Zuccaro, L.; Kuhn, A.; Konuma, M.; Yu, H. K.; Kern, K.; Balasubramanian, K. *ChemElectroChem* **2016**, *3* (3), 372–377.

- (44) Pop, F.; Auban-Senzier, P.; Frąckowiak, A.; Ptaszyński, K.; Olejniczak, I.; Wallis, J. D.; Canadell, E.; Avarvari, N. *J. Am. Chem. Soc.* **2013**, *135* (45), 17176–17186.
- (45) Pop, F.; Auban-Senzier, P.; Canadell, E.; Rikken, G. L. J. A.; Avarvari, N. *Nat. Commun.* **2014**, *5*, 3757.
- (46) Hinnemann, B.; Moses, P. G.; Bonde, J.; Jørgensen, K. P.; Nielsen, J. H.; Horch, S.; Chorkendorff, I.; Nørskov, J. K. *J. Am. Chem. Soc.* **2005**, *127* (15), 5308–5309.
- (47) Tsai, C.; Chan, K.; Abild-Pedersen, F.; Nørskov, J. K. *Phys. Chem. Chem. Phys.* **2014**, *16* (26), 13156–13164.
- (48) Jaramillo, T. F.; Jørgensen, K. P.; Bonde, J.; Nielsen, J. H.; Horch, S.; Chorkendorff, I. *Science* **2007**, *317* (5834), 100–102.
- (49) Novoselov, K. S.; Geim, A. K.; Morozov, S. V.; Jiang, D.; Zhang, Y.; Dubonos, S. V.; Grigorieva, I. V.; Firsov, A. A. *Science* **2004**, *306* (5696), 666–669.
- (50) Bonaccorso, F.; Colombo, L.; Yu, G.; Stoller, M.; Tozzini, V.; Ferrari, A. C.; Ruoff, R. S.; Pellegrini, V. *Science* **2015**, *347* (6217), 1246501.
- (51) Das, S.; Robinson, J. A.; Dubey, M.; Terrones, H.; Terrones, M. *Annu. Rev. Mater. Res.* **2015**, *45* (1), 1–27.
- (52) Gao, M.-R.; Xu, Y.-F.; Jiang, J.; Yu, S.-H. *Chem. Soc. Rev.* **2013**, *42* (7), 2986.
- (53) Radisavljevic, B.; Radenovic, A.; Brivio, J.; Giacometti, V.; Kis, A. *Nat. Nanotechnol.* **2011**, *6* (3), 147–150.
- (54) Takahashi, K.; Kusu, F. *Electrochemistry* **2006**, *74* (2), 192–196.
- (55) Loget, G.; Zigah, D.; Bouffier, L.; Sojic, N.; Kuhn, A. *Acc. Chem. Res.* **2013**, *46* (11), 2513–2523.
- (56) Loget, G.; Roche, J.; Kuhn, A. *Adv. Mater.* **2012**, *24* (37), 5111–5116.
- (57) Chow, K.-F.; Mavr , F.; Crooks, J. A.; Chang, B.-Y.; Crooks, R. M. *J. Am. Chem. Soc.* **2009**, *131* (24), 8364–8365.
- (58) de Poulpique, A.; Diez-buitrago, B.; Milutinovic, M. D.; Sentic, M.; Arbault, S.; Bouffier, L.; Kuhn, A.; Sojic, N. *Anal. Chem.* **2016**, *88*, 6585–6592.
- (59) Sentic, M.; Arbault, S.; Bouffier, L.; Manojlovic, D.; Kuhn, A.; Sojic, N. *Chem. Sci.* **2015**, *6* (8), 4433–4437.
- (60) Zhao, B.; Summers, F. A.; Mason, R. P. *Free Radic. Biol. Med.* **2012**, *53* (5), 1080–1087.

## Chapter III. Bipolar electrochemistry with biological material

### 3.1. DNA charge transport and studies of DNA conductivity

#### 3.1.1. Introduction to DNA structure

The discovery of the double helical structure of DNA opened a new era in molecular biology and biochemistry. From a historical point of view, the Swiss biologist F. Miescher first isolated an unknown substance from the nucleus of cells in 1868 that led later to the discovery of deoxyribonucleic acid (DNA).<sup>1</sup> He described this substance as an important nuclear substance being neither a protein nor a lipid and that contained large amounts of phosphorous. After decades, P. Lavegne identified the chemical constituents of DNA and proposed an hypothesis about the way in which they are joined with each other.<sup>2</sup> Later, E. Chargaff has established a quantitative relationship between different types of nitrogenous bases.<sup>3</sup> More specifically, he found, that the amount of guanine should be equal to cytosine and the amount of adenine should be equal to thymine.

Based on all these preliminary results, J. D. Watson and F. H. C. Crick were the first scientists who correctly formulated and described in detail a double-helical structure of DNA in 1953.<sup>4</sup> Nowadays, DNA is well-known as the carrier of genetic information in cells. However, not everybody knows that DNA has also some very unique physical properties and other biological functions that are not fully explored and understood.

The DNA double helix is composed of a stacked array of heterocyclic aromatic base pairs, wrapped within a helical chain of negatively charged sugar phosphate backbone (Fig. 3.1). The two strands are held together by the pairing of complementary nucleotide bases on opposite DNA strands. The helix is formed when two single strands combine by hydrogen bonding between the complementary bases and is stabilized by the  $\pi$ -stacking interactions between base pairs.

Figure 3.1 shows a schematic illustration of the DNA structure. The nucleotide bases are planar molecules and form hydrogen bonds between adenine (A, shown in green) – thymine (T, shown in red) and guanine (G, shown in blue) – cytosine (C, shown in orange) inside the helix.<sup>5</sup> Therefore, two strands of DNA molecules are complementary and form a double-helical structure. The distance between two base pairs is 0.34 nanometers. The length of one turn of the double-helix is 3.4 nanometers. The width of the DNA molecule is about 2 nanometers. The DNA double helix represents a well-defined molecular  $\pi$ -stack of planar paired base units that forms a one-dimensional structure.

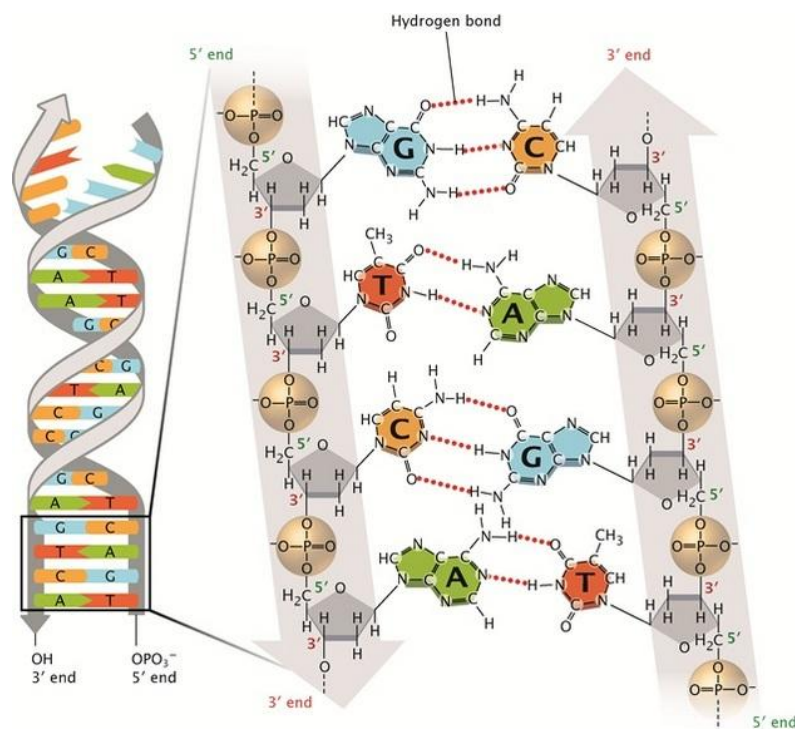


Fig. 3.1. Schematic illustration of the chemical structure of the DNA double helix. The sugar-phosphate backbone arranged in an antiparallel manner that twist to form a double helix is shown in grey. Phosphate groups are depicted within light brown spheres, and the sugars are represented by grey pentagons. The nitrogenous bases from the two DNA strands interact in the center, where two hydrogen bonds connect T to A and three hydrogen bonds connect G to C, respectively. Adapted from ref.<sup>5</sup>

Therefore, it was postulated by scientists, that a DNA molecule might behave as a one-dimensional aromatic crystal and could exhibit  $\pi$ -electron driven conductivity along its main axis.<sup>6,7</sup>

Theoretically, the molecular  $\pi$ -stack of the DNA double helix has a similar structure to solid-state stacked materials; however critical differences exist. For example, unlike solid state  $\pi$ -stacked systems, DNA is a highly dynamic molecule, and continuously undergoes dynamic motion.<sup>8,9</sup> The structure of DNA is also balanced by the close interaction of water molecules and counter-ions. Consequently, the charge transport (CT) in DNA is highly dependent on the DNA's conformational dynamics and could be much more complicated than in solid state materials.<sup>10</sup>

Studies on the ability of DNA to promote CT are controversial,<sup>11</sup> and there is still a debate whether DNA is a conductor,<sup>12</sup> semiconductor,<sup>13,14</sup> or an insulator.<sup>15,16</sup>

### 3.1.2. DNA charge transport

Nature is truly incredible and has still many secrets remaining unattainable to human understanding. Until about 100 years ago, humanity did not know about the existence of such a small molecule as DNA that encodes genetic information of all living organisms. The discovery of the structure of DNA has contributed to the understanding of the key-role of this molecule and its biological function. However, this discovery may not be the final step of understanding, because of remaining not yet known functions of this molecule. One of such

exotic properties of DNA molecule, that scientists are trying to understand over the last 30 years, is electronic properties of DNA and particularly CT capability.

DNA conductivity is an important parameter, which probably plays a major role in biological processes and could be exploited for medical applications and also in the field of nanoelectronics.

It is not studied yet, but nature possibly uses DNA as a kind of electrical wire for detecting the constantly occurring genetic damages and all kinds of errors that, if not properly repaired, can lead ultimately to diseases. DNA could use its electrical properties to give a signal to a certain protein for urgent repairs when needed. If the DNA molecule no longer conducts an electrical signal or the conductivity is noticeably lowered, this could serve as an immediate alert for proteins to begin to work.

From a practical point of view, the transmission of an electrical signal via DNA can be the basis for developing new diagnostic methods or electrical biosensors that can detect potentially dangerous DNA damages, as well as assess the level of risk of different diseases. Therefore, potential applications of DNA-mediated CT could be used in DNA chips for DNA sequencing, disease screening, or gene expression analysis. Also, if DNA displays a sufficient conductivity, a sequence could be read out electronically instead of visually without the necessity to employ fluorescent labels as done currently. Differences in CT for ssDNA and dsDNA could be the basis of such a signal. The single strands of DNA are insulating, but well-stacked double stranded DNA after successful hybridization with a complementary strand could be significantly more conducting, thus allowing an electronic readout.

In addition, DNA-based templates may find important applications in nanoelectronics. Using a DNA molecule could enable a new generation of electronic circuits and electrical devices at the nanoscale.

After the discovery of the double-helical structure of DNA, the scientists D. Eley and D. Spivey noted that stacked DNA base pairs show resemblance to stacked graphite sheets<sup>17</sup>. The same planarity as well as a comparable inter-plane stacking distance of 3.4 Å of nucleic acids as aromatic molecules. Therefore, they suggested that  $\pi$  stacking in double stranded DNA structure could be efficient for one dimensional CT.

Several experimental approaches such as photo-oxidation studies, spectroscopy, and electrochemistry have been used over decades to study CT via DNA molecules. DNA-mediated CT has been probed in solution, on surfaces and also with single molecule techniques. The major difficulty is to perform reproducible and interpretable experiments at nanoscale dimensions. Other problems arise from the large variety of experimental conditions that are difficult to control at the nanoscale and which can influence the corresponding results obtained. The most direct and easiest way is to perform physical measurement of current flow through a DNA wire.<sup>12</sup> It consists in measuring the electrical current as a function of the potential applied across a DNA molecule.

Different complicated approaches were used to investigate DNA conductivity. Among them atomic force microscopy (AFM), that consists of probing charge transport by a conducting AFM tip with a gold nanoparticle attached to the DNA (Fig. 3.2a).<sup>18,19</sup> Scanning tunneling

microscopy (STM) was also used in a configuration where a gold STM tip is brought into contact with thiol-modified DNA allowing to construct a histogram of conductance over different orientations (Fig. 3.2b).<sup>20,21</sup> Also conductivity measurements with a single DNA molecule were performed in a carbon nanotube gap with the DNA biomolecule fixed in between (Fig. 3.2c).<sup>14,22</sup> In this method, individual DNA molecules functionalized with terminal amines were covalently attached within the gap by using amide bond chemistry. These robust devices can then be used to measure the current flow in the nanotube containing the covalently attached molecule of interest versus the current in the original nanotube.

The resistance generated in the gap with a DNA duplex inserted was found to be  $\sim 1 \text{ M}\Omega$  for a  $\sim 6 \text{ nm}$  gap, similar to that expected for a stacked graphite insert.<sup>22</sup>

The variability in experimental results with these methods could be due to the not fully controlled structure and integrity of DNA under the used conditions of these different measurements.

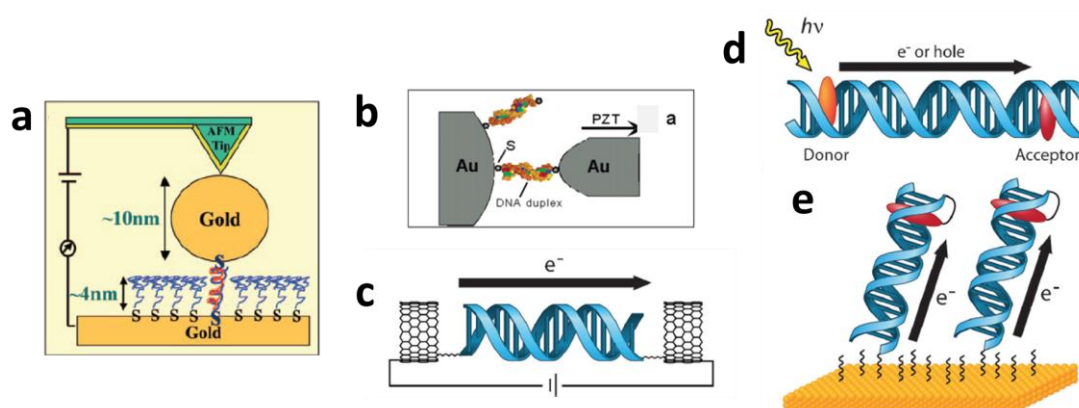


Fig. 3.2. Different approaches to study DNA CT. (a) AFM measurements of current through dsDNA molecules chemically connected on both ends to a gold substrate and to a gold nanoparticle. The connection is established by hybridization of complementary strands, one ssDNA attached to the gold surface and another to a gold nanoparticle on an AFM tip, adapted from Ref<sup>18</sup>. (b) STM conductivity measurements of DNA molecules covalently attached to two electrodes in aqueous solutions, adapted from Ref<sup>21</sup>. (c) DNA conductivity studies with DNA duplex that bridges a gap, reprinted from Ref<sup>23</sup>. (d, e) Studies of DNA CT in solution. (d) Photo-oxidation studies of donor acceptor molecules, incorporated into opposite ends of a DNA duplex, reprinted from Ref<sup>23</sup>. (e) Electrochemical studies of a redox active probe intercalated into DNA layers covalently attached to the surface, reprinted from Ref<sup>23</sup>.

Another type of experiments to explore CT in DNA is based on photochemical and photophysical methods. Such approaches, unlike physical measurements, rely on well-defined oligonucleotide assemblies under physiological conditions. In these cases, oligonucleotides are prepared with intercalated redox probes (charge donors and charge acceptors). The rate of electron transfer and yield are measured through fluorescence quenching as a function of the distance between these molecules inside a DNA duplex (Fig. 3.2d).

J. Barton and co-workers started to study DNA conduction by observing charge transfer between DNA-intercalated transition-metal complexes.<sup>24</sup> Metallo-intercalators were covalently attached to the DNA duplex. The donor and acceptor molecules exhibit aromatic ligands that allow them to intercalate into the DNA  $\pi$ -stack. The DNA molecule was labeled at one terminus with  $[\text{Ru}(\text{phen})_2\text{dppz}]^{2+}$  (dppz = dipyrdo[3,2-a:2',3'-c]phenazine; phen = 1,10-phenanthroline),



with the excited state acting as an electron donor, and  $[\text{Rh}(\text{phi})_2\text{phen}]^{3+}$  ( $\text{phi}$  = 9,10-phenanthrenequinone diimine) at the opposite terminus acting as an electron acceptor. In the absence of the electron acceptor, the ruthenium complex is luminescent. However, upon incorporation of the rhodium complex, the luminescence is completely quenched due to rapid CT to the acceptor. The authors demonstrated oxidative quenching of a DNA-bound metal complex through the DNA base stack and suggested that DNA is an efficient medium for coupling electron donors and acceptors over long distances (40 Å). However, this method is critical regarding base pair stacking. Small perturbations in base stacking can lead to a significant loss in CT efficiency.

Also, DNA conductivity was studied by using an electrochemical device with a DNA-modified electrode with intercalated donor/acceptor systems in the DNA (Fig. 3.2e). Traditionally, DNA-modified electrodes are formed from self-assembled thiolated DNA molecules on a gold substrate, containing redox reporters at the opposite end for electrochemical monitoring by cyclic voltamperometry. Such DNA CT sensors are based on the flow of electrons from the redox-active reporter through the DNA base stack to the electrode surface. An intercalating probe is essential to monitor a DNA-mediated reaction within the film. Daunomycin or Methylene Blue are intercalators that are typically used. An intercalator can covalently cross-link to guanine residues and serves as a site specific redox reporter.<sup>25,26</sup>

The variability of results obtained with these different methods can be influenced by various factors. The sequence, length and character of the DNA molecule (ropes or single molecules), perturbations such as base mismatches and its 3-dimensional structure (coiled or stretched) are important. In addition, the whole environment of DNA should be considered. The water molecules and counterions can exert non-negligible forces on the electrons in the base pair stack. Freestanding DNA molecules or surface-bound ones can also behave differently. The nature of the donor and acceptor molecules, as well as the rate and efficiency of the reaction must equally be considered.

### 3.1.3. Mechanism of charge transport

Many experimental and theoretical studies were carried out to study DNA conductivity, resulting in the distinction between three possible mechanisms of DNA-mediated CT. All these mechanisms involve an electron moving from a donor (D) orbital to an acceptor (A) orbital (Fig. 3.3). The CT through DNA molecules was measured over a short distance as well as in long range transport. The variations could arise from the location of the orbitals that mediate this transition and the pathways that are coupled to it. The DNA sequence is important for the pathway of charge, because the intrinsic energy level of the G-C and A-T base pairs are different.

One of the most important feature is that a hole (i.e. positive charge) is more stable on a G-C base pair than on A-T base pair. It is related to the fact that the hole has a lower energy on G-C sites and will therefore be preferentially localized on G-C base pairs. On the opposite, the A-T base pair has a higher energy and acts as a barrier for hole transfer. However, the hole can move from one G-C pair to the next by coherent tunneling through the A-T sites. The overall motion

from the first base pair to the last is based on a hopping mechanism in which the charge carrier is localized along the path.<sup>7</sup>

The scientific community considers generally three basic mechanisms of charge transport: the tunneling mechanism (or super-exchange), hopping mechanism and combined domain hopping mechanism (Fig. 3.3) through the DNA bridge between the bound donor and acceptor.

For the tunneling mechanism, the charge tunnels through high energy bases (A-T base pairs) without formally occupying it. The rate of this process decreases exponentially with the distance between the charge donor and acceptor. In the hopping mechanism, charge migrates by transiently occupying the low energy sites in the  $\pi$ -stack and hopping from one to the next, involving short-distance tunneling intervals (Fig. 3.3).<sup>27</sup>

The domain hopping model combines two basic charge transport mechanisms, in which charge migrates through the DNA bridge via delocalized energetically lower domains and tunneling through intervening T-A (Fig. 3.3c).

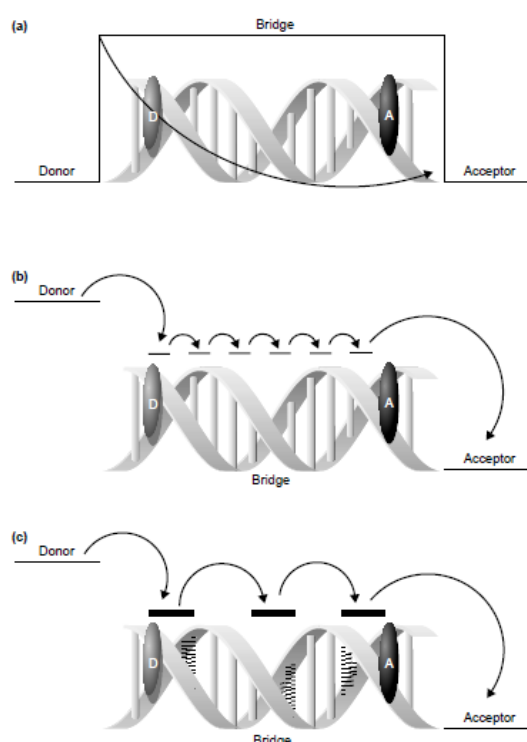


Fig. 3.3. Schematic representation of possible mechanisms for charge transport through DNA. (a) Super-exchange: the charge tunnels from the donor (D) to the acceptor (A) through the bridge, in which the rate of CT decreases exponentially with increasing bridge length. (b) Hopping: the charge occupies the bridge hopping between discrete molecular orbitals. If hopping is faster than radical trapping, the charge should be able to migrate over long distances along the bridge. (c) Domain hopping: the charge occupies the bridge by delocalizing over several bases, or a domain. This domain hops along the bridge to travel from donor to acceptor. The charge should be able to travel long distances before getting trapped. Adapted from ref. <sup>27</sup>

### 3.2. Bipolar electrochemistry for the asymmetrical modification of DNA by metal particles

In contrast to all previous approaches that have been used to study DNA conductivity, BPE represents a simple method that can be also useful for this purpose. The advantage of BPE is

that this method does not need any direct contact between the DNA molecule and the measuring device, which simplifies studies at the nanoscale.

BPE can be used not only for the synthesis of asymmetrical objects but might also be employed for investigating intrinsic properties of different (bio)-objects, such as DNA conductivity.

Visualization of redox reactions performed by BPE on a single DNA filament could be a direct prove of CT via a DNA molecule and consequently, a validation of such intrinsic conductivity. Thereby, by using a DNA molecule as a BE and performing bipolar metal electrodeposition from a solution containing a given metal salt could be a direct and easy way to study the conductivity. The formed metal deposit on the cathodic edge of the substrate would be the confirmation of a CT process.

This strategy was used in this work to investigate the possibility to use BPE for studying DNA conductivity.

Based on the principle of BPE (Chapter 1), under specific experimental conditions, the oxidation and reduction reactions may occur at both extremities of a DNA molecule. In the presence of metal cations  $M^{n+}$  in solution, their reduction can occur and lead to the formation of a metal deposit at the cathodic pole of DNA (Fig. 3.4).

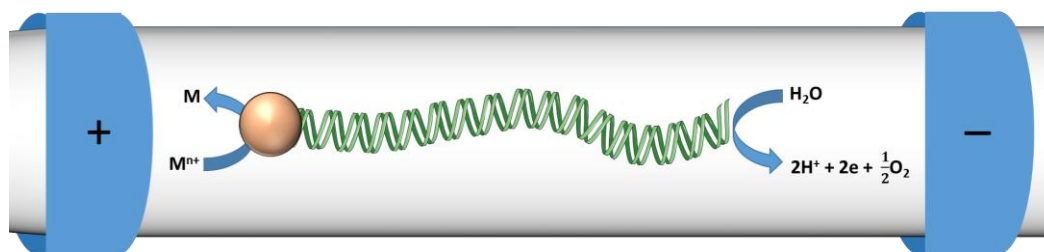


Fig. 3.4. Schematic illustration of possible faradaic processes on a dsDNA molecule due to BPE phenomenon. If DNA has a sufficient conductivity, typically higher than the ionic conductivity of the surrounding medium, the reduction of metal precursors can occur during BPE, resulting in the formation of a metal cluster at one extremity of the molecule.

For the bipolar experiments with DNA, a capillary-assisted bipolar electrodeposition (CABED) set-up was used first. This technology was briefly described in the first chapter for the preparation of asymmetric particles by BPE.

In this chapter will be given a detailed description of the instrument used and the corresponding results.

### 3.2.1. Instrument description

The CABED approach uses a capillary electrophoresis set-up for bipolar electrodeposition in the bulk. Capillary electrophoresis (CE) is normally used as an analytical tool for the separation of analytes. The separation is based on the difference in migration speed of analytes due to different charge and the size of the molecules.

The rate with which the analytes moves is directly proportional to the applied electric field. The higher the field strength, the higher the speed. In addition, the ions experience the influence of two forces. The first force is induced by the electrophoretic flow (EPF), which is the flow of charged species to the electrode of opposite charge. The second force is generated by

electroosmotic flow (EOF), which is induced by the motion of the charges along the electric double layer of the capillary wall. The capillary wall is made out of glass with negatively charged silanol groups that cause a proton flow at the interface, directing the EOF towards the cathode. These protons can be considered as a stationary phase that will direct the motion of the ions towards the cathode under the influence of the applied electric field. These two forces promote separation of analytes in solution. Thereby, the analytes with a larger positive charge will move faster than others species and the speed will be larger than the rate of EOF due to electrophoretic attraction. Neutral species will travel slowly inside the capillary, with the rate of EOF. Negatively charged species will be the slowest due to the electrophoretic attraction to the anode, which is the opposite direction compared to the EOF.

In Figure 3.5 is presented a schematic illustration of a CE instrument. It consists of two vials containing the running buffer, with an anode in the inlet, and a cathode in the outlet vials, respectively. The electrodes are conical Pt wires where the capillary is inserted (Fig. 3.5). A UV-visible detector is positioned before the cathode compartment in front of the capillary window for monitoring flow of species. The CE equipment provides a voltage of up to 30 kV, which induces an electric field of 100 kV/m when using a 30 cm-long capillary.

The possibility to use high voltages with CE makes it an interesting tool for BPE experiments with micro-objects. In addition, the presence of the liquid flow, generated by EOF, continuously pumps the substrate of interest from the inlet compartment to the outlet. Moreover, the small inside diameter (100  $\mu\text{m}$ ) of the capillary allows efficient dissipation of the heat generated by the application of such high voltages, and provides a resistive current pathway that is valuable for faradaic reactions to occur.

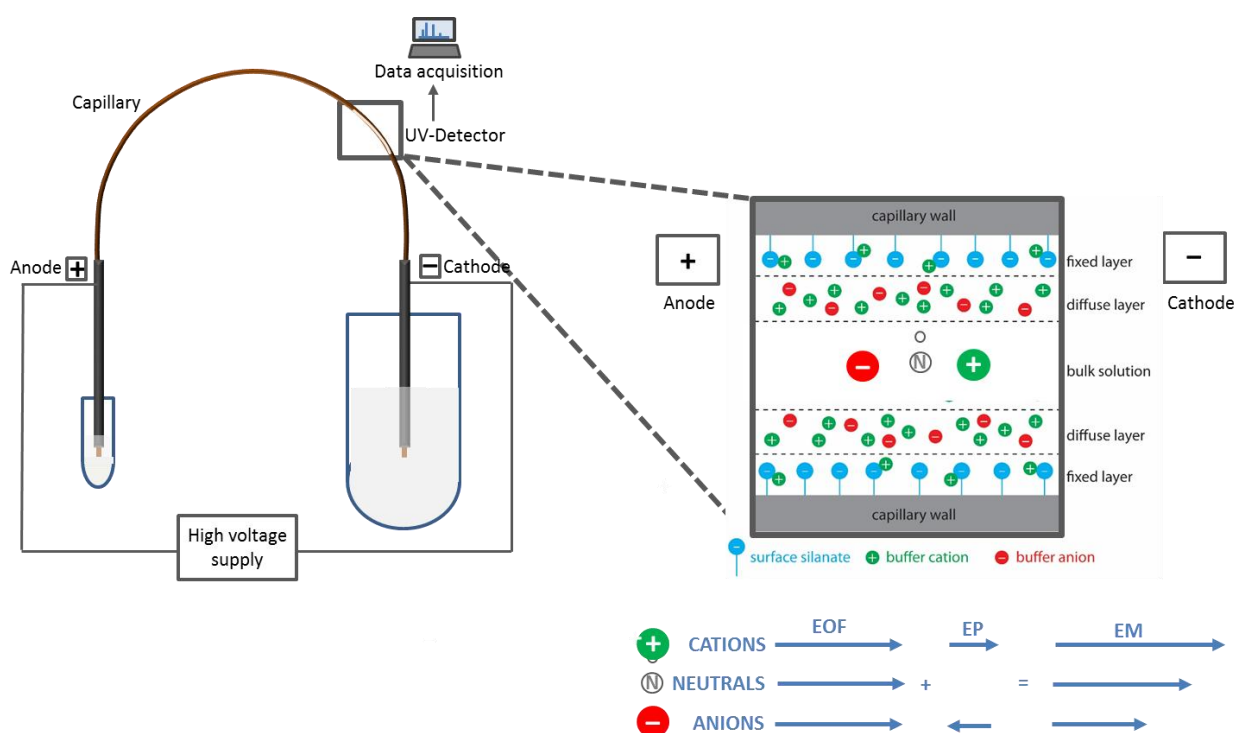


Fig. 3.5. Schematic illustration of CE equipment, used in CABED experiments.

The CABED process is based on the modification of particles during their journey through the capillary. A suspension of conducting particles to be modified and electro-deposable precursor is injected into the anodic compartment. Application of the electric field polarizes the conductive particles and generates the EOF of the electrolyte that carries the particles towards the cathodic vial. The BPE process takes place at the level of each individual particle inside the capillary. They can be monitored in situ by the detector and then collected for further characterization.

The aim of this chapter is to enlarge the application of BPE to different bio-relevant topics such as the study of the intrinsic conductivity of DNA as well as the development of a new BPE sensing approach for the detection of DNA hybridization.

### **3.2.2. CABED for asymmetrical metal deposition on DNA**

The CABED setup was widely used for bipolar modification of CMTs that has been described in chapter 1. At the same time, this tool can be adapted to many different microscale objects. Therefore, in this section we employed the CABED method for asymmetrical site-selective modification of DNA molecules with metal particles. As previously reported, electric fields enable the control of the alignment of anisotropic objects<sup>28</sup> parallel to the field lines. Therefore during the course of a CABED experiment, DNA strands could be stretched, providing thus a suitable shape for bipolar electrodeposition as elongated filaments. The electrochemical reaction of copper reduction from cupric salt solution was chosen because the metal cluster formed could be easily detected and further characterized. This reduction reaction was coupled with water oxidation, because it has a suitable formal potential value and does not need the addition of any co-reactant. Bipolar electrodeposition of metal on DNA could potentially occur while it travels through the capillary, leading to a localized metal reduction at the cathodic pole and water oxidation at the anodic pole of the molecule (Fig. 3.4).

Commercially available double-stranded lambda DNA with a suitable length (a few tens of  $\mu\text{m}$ ) was selected for a series of experiments in order to achieve a larger polarization and easier visualization. After CABED experiments, the samples were collected directly from the capillary and characterized by Transmission Electron Microscopy (TEM). Lambda DNA is a relatively long molecule that contains typically 48502 bps, corresponding to a length of  $\sim 16.5 \mu\text{m}$ . The Lambda DNA used is isolated from *E. coli* stain and provided at a concentration of 462  $\mu\text{g/mL}$  in 10 mM Tris-HCl (pH 7.5), 10 mM NaCl and 1 mM EDTA from Promega, France.

For the CABED experiments, the initial solution of DNA was simply diluted in water or mixed with an aqueous copper sulfate solution. Before being injected for CE, solution was vortexed and sonicated for 30 s in order to disperse the DNA strands. An electric field value ranging from  $0.7 \text{ kV cm}^{-1}$  to  $1.0 \text{ kV cm}^{-1}$  was tested in different experiments. Also in all these experiments, a glass capillary with a typical length of 30 cm and 100  $\mu\text{m}$  in diameter was used. The electric field was applied for different durations from 1 min to 10 min before collection of the resulting sample. DNA absorbance was monitored with the UV detector at  $\lambda = 260 \text{ nm}$ . At

the end of the experiments, the solution filling the capillary was directly dropped onto a TEM grid (200 mesh, Agar scientific), left for 1 min to settle down. Then, the supernatant was removed from the bottom side of the grid by using a filter paper and the grid was washed several times with 10  $\mu\text{L}$  droplets of water using the same procedure stepwise. The dried samples were characterized with a high-resolution TEM microscope (JEOL-1400, kindly provided at PLACAMAT – UMS 3626, University of Bordeaux/CNRS).

Prior to CABED experiments, the initial DNA was diluted and visualized with TEM. DNA was founded essentially as packed bundles (several DNA molecules attached together) and not totally stretched, as can be seen from the corresponding representative micrographs in figure 3.6.

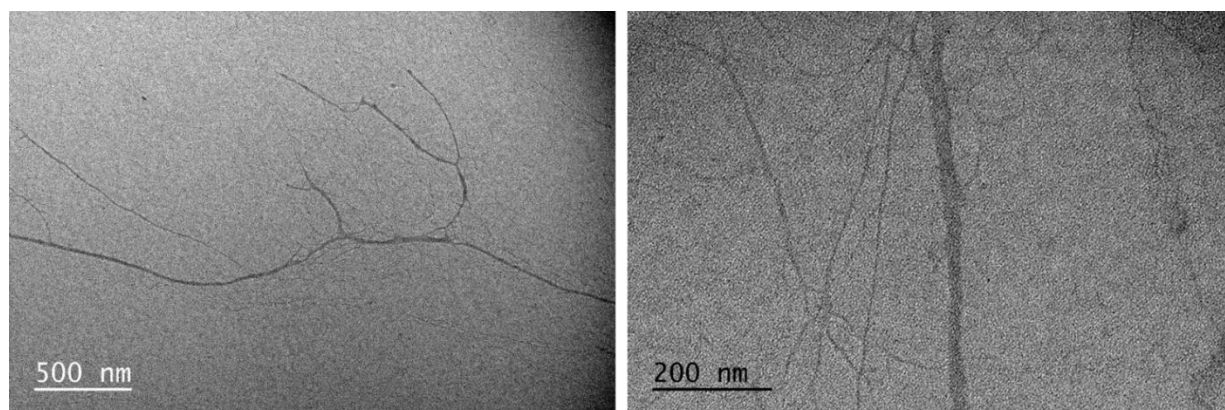


Fig. 3.6. TEM micrographs of DNA bundles prior to their exposure to the electric field.

For metal deposition, copper sulfate was chosen among other metal salts because it is readily reduced to copper metal. The following electrochemical reactions can occur at the extremities of the bipolar object:

Copper reduction at the cathodic pole:



Water oxidation at the anodic pole:



Considering the length of one double stranded DNA ( $\sim 16 \mu\text{m}$ ), the minimum electric field needed to achieve the coupling of both redox reactions can be calculated:

$$\varepsilon = \frac{\Delta V_{\min}}{l_e} = \frac{E_2^\circ - E_1^\circ}{l_e} = \frac{(1.23 - 0.34) \text{ V}}{16 \cdot 10^{-4} \text{ cm}} = 0.5 \frac{\text{kV}}{\text{cm}} \quad (\text{Eq. 3.3})$$

In order to fulfill the condition  $\Delta V > \Delta V_{\min}$  (chapter 1.2), an electric field of at least  $0.7 \text{ kV cm}^{-1}$  and up to  $1.0 \text{ kV cm}^{-1}$  was applied for 3-4 min, during which the DNA motion could be followed by UV-detection.

For the initial bipolar electrodeposition of copper, the solution for injection contained  $92.4 \mu\text{g/mL}$  DNA and  $5 \text{ mM}$   $\text{CuSO}_4$ . This mixture was injected inside the capillary by hydrodynamic injection during different times (5 s, 10 s, 15 s, respectively). The longest injection time led to plugging of the capillary. The passage of DNA was followed by recording

the absorbance, and as soon as a signal was observed (typically 2-3 min), the sample was collected on a TEM grid according to the previously described protocol.

Characterization of the collected samples shows clearly several DNA filaments with black clusters (i.e. high electron absorption in transmission microscopy). As we can see from the figure 3.7a a big black deposit is attached to the bundle of DNA. It is very likely a metal cluster as its morphology reminds dendritic growth that is typical for copper electrodeposition. Copper dendrites are usually observed with BEs when the applied electric field is much larger than the threshold value. One hypothesis is that several DNA molecules gathered together in such bundles are more stable and may favor electron transfer compared to a single dsDNA molecule and these bundles act as stable conductive wire, promoting thus the formation of such big deposits. Another bundle observed in the micrograph of fig. 3.7c has also several black particles localized only at its very extremity. In the case of other DNA filaments, nanoparticles were also found alongside the DNA backbone instead of at the extremity, (Fig. 3.7b, c, Fig. 3.9c). Such nanoparticles might be formed when the DNA strand is folded during its journey through the capillary of the CE or eventually when the integrity of the DNA is damaged causing a localized loss of conductivity. In such cases, the deposition is possible, if the longer part of the folded or conductive portion of the DNA experiences a sufficient polarization.

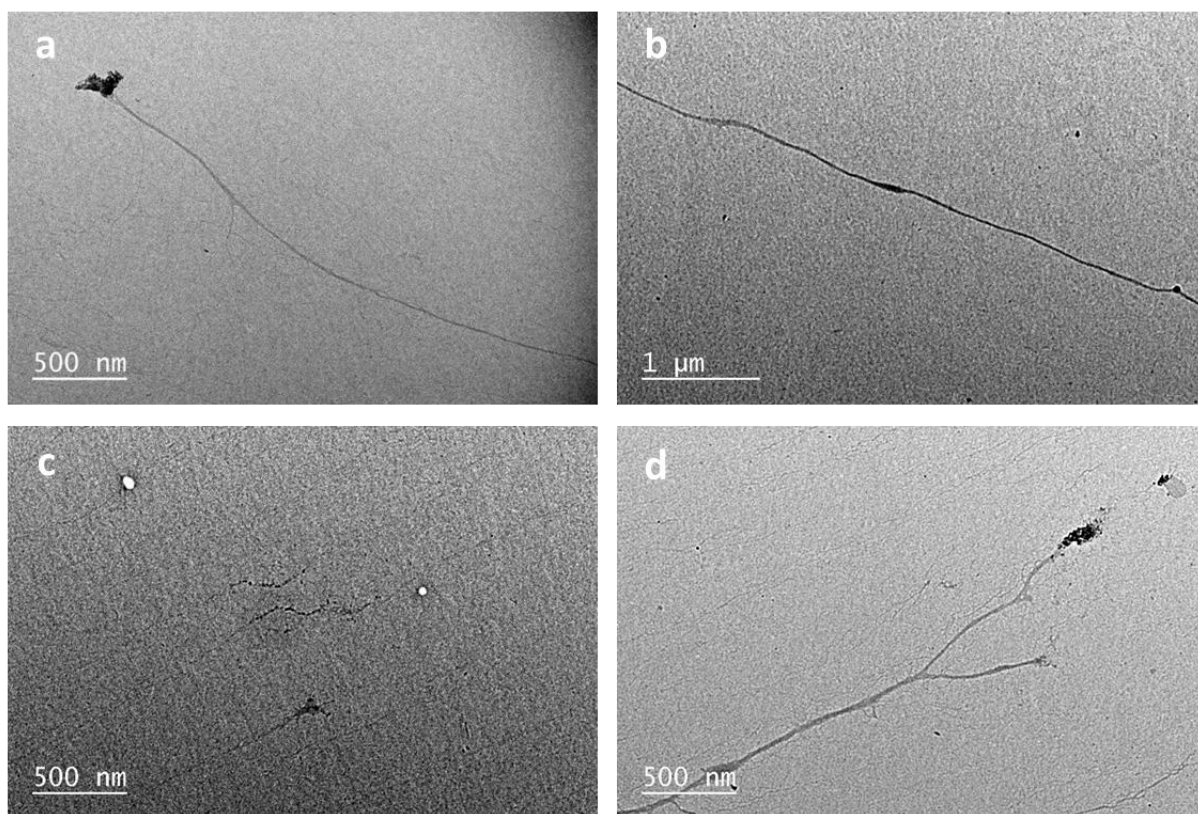


Fig. 3.7. TEM micrographs showing DNA filaments and bundles after their polarization using capillary electrophoresis in the presence of  $\text{CuSO}_4$ .

It is noteworthy that investigation of these DNA samples showed sometimes different results. In many cases, DNA filaments were observed still as bundles and in others – almost no filaments were observed. We were in fact interested to demonstrate the possibility to use BPE-induced modification of single dsDNA molecules with electrodeposited nanoparticles. The



complexity to observe single molecule of dsDNA was sometimes also due to TEM microscope limitations, a good focus and contrast conditions are crucial for observation of such small objects.

Nevertheless, from all the TEM images, one can see stretched structures of DNA filaments, confirming that the CE process facilitates the straightening of the DNA molecules under the influence of the applied electric field (Fig. 3.8).

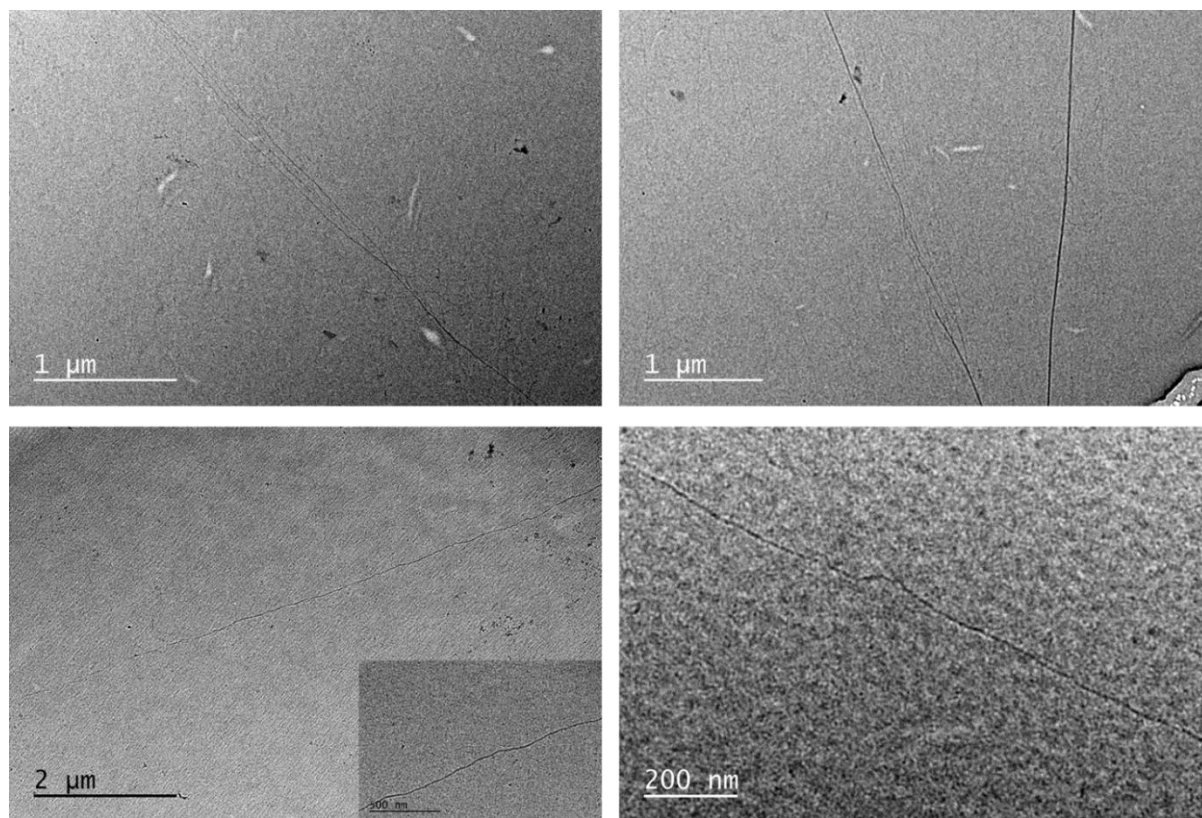


Fig. 3.8. TEM micrographs showing DNA filaments after polarization using capillary electrophoresis in the presence of  $\text{CuSO}_4$ .

A control experiment was also performed by mixing 92.4  $\mu\text{g/mL}$  DNA and 5 mM  $\text{CuSO}_4$  without applying any electric field. Under such negative control conditions, absolutely no deposit was observed on the DNA filaments, confirming that the metal clusters observed previously on the DNA molecules was solely due to the bipolar electrochemical process.

In order to obtain a lower amount of bundles and therefore a larger number of single dsDNA filaments, the concentration of DNA in the injected solution was decreased to 46.2  $\mu\text{g/mL}$  DNA and mixed with 5 mM  $\text{CuSO}_4$  (dilution of DNA concentration by a factor of 2). TEM characterization of these samples, collected after CE, revealed the the dsDNA was often well-separated and nicely stretched. In addition, the majority of the DNA molecules, but not all in a single sample, was found to exhibit metal nanoparticles at their extremity (Fig. 3.9). However, it was difficult to follow a single DNA filament from one extremity to the other, due to unsufficient contrast during TEM acquisition.

Different morphologies of the collected DNA samples were observed under the TEM. Deposits that are just localized at the extremity of the DNA (Fig. 3.9) as well as a nanoparticle positioned



along the single DNA wires could be detected, as previously for the DNA bundles. These images suggest that single dsDNA molecule could indeed behave as an electrical wire and redox reactions can be performed at its extremities with BPE. However, among all the observed filaments, some were modified whereas others were not, revealing a non-quantitative modification yield.

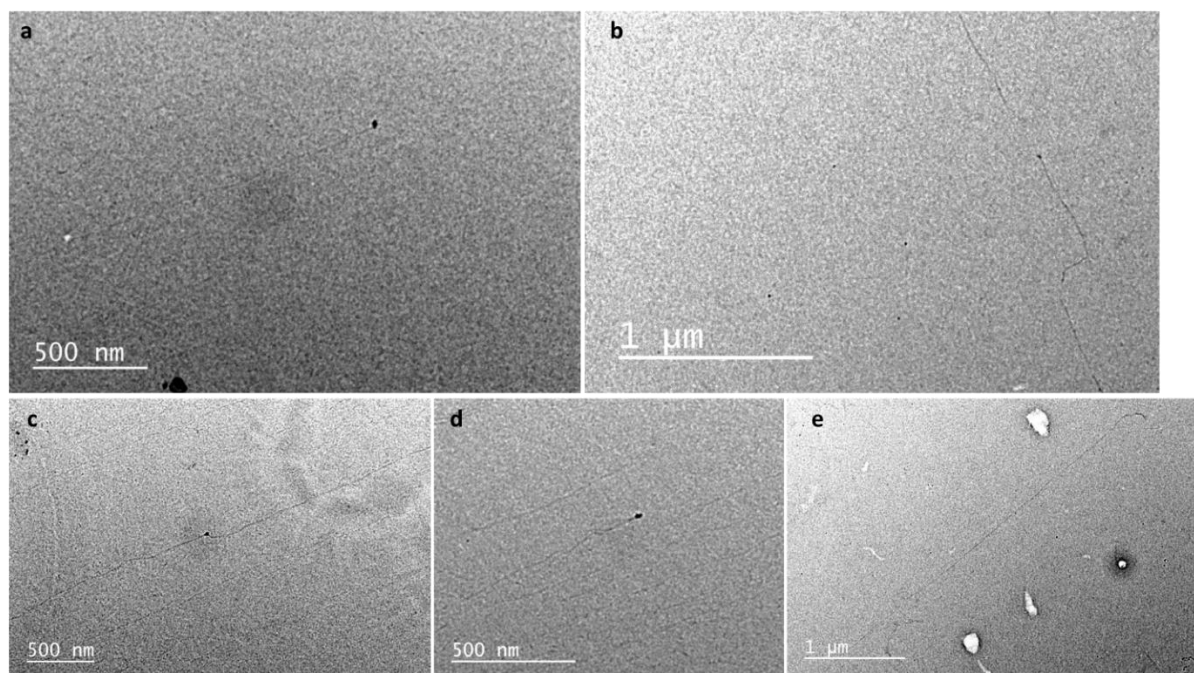


Fig. 3.9. TEM images of stretched single dsDNA molecules modified with black metal nanoparticles.

Different experimental conditions were also explored by changing the DNA or copper sulfate concentration in the injected solution, changing the time of injection, as well as using a diluted DNA/CuSO<sub>4</sub> solution as a running phase. Copper sulfate solution was also tested as a running phase after injection of the DNA-containing fraction in order to ensure the availability of Cu<sup>2+</sup> ions inside the capillary throughout the CE. However, several problems were observed during CE experiments, causing difficulties to summarize and/or interpret the obtained results. First of all, it was difficult to understand the whole processes that occurred inside the capillary. Sometimes marked current changes were observed during the course of CE, which means that changes in the corresponding EOF and residential time inside the capillary occurred, leading to the impossibility to obtain reproducible results. This issue might be due to local pH changes, plugging of the capillary during injection or local heating due to Joule effect during the experiment. In addition, since different retention times were also observed during CE, it was difficult to collect systematically the good fraction containing a sufficient number of DNA molecules, and therefore the experiments showing modified DNA molecules were poorly reproducible. On the other hand, during TEM characterization, it was sometimes difficult to maintain a good contrast when increasing the magnification for observing and following DNA filaments at high resolution. In fact, the low percentage of clearly reproducible samples is the major problem that we are facing during these series of CE experiments.

Despite that, CABED method helped us to demonstrate for the first time the possibility of single-molecule DNA modification by BPE approach. The moderate yield of modified filaments and low reproducibility of these experiments forced us to look for alternatives. We decided to use another approach whereas the DNA molecules were first immobilized and stretched on an insulating surface prior to BPE experiment for DNA functionalization. A realization of such approach is described in following paragraphs.

### 3.2.3. Deposition of DNA molecules on the surface for BPE

DNA in its natural state usually adopts a coiled conformation. To unfold and align it to single filament, so called “combing DNA method”<sup>29,30</sup> is well known and described in literature. During this process, one end of the DNA molecules is attached to a solid surface and the filaments are extended and aligned by a receding air-water interface (Fig. 3.10a). These combed molecules are usually detected by microscopy by using fluorescent dyes that are intercalated inside DNA. However, in our experiments, in order to visualize the metal deposit after BPE, we choose Atomic Force Microscopy (AFM) for further characterization of the samples.

#### 3.2.3.1. Preparation of the surface for combing DNA and AFM characterization

For this new approach, several conditions must be fulfilled. For AFM analysis, the surfaces must be perfectly smooth, and at same time not conductive for the subsequent BPE experiments. In addition, for a good elongation of the DNA molecules, a sufficient air-water meniscus is necessary, therefore a control of hydrophobic/hydrophilic properties of the surfaces is needed.

To fulfill these criteria, a mica surface was selected as a convenient surface. Mica by itself is a hydrophilic surface, but can be eventually switched to a hydrophobic behavior upon covering the surface with a thin layer of self-assembled units of organo-alkoxysilane molecules. This process is indeed known as silanization.

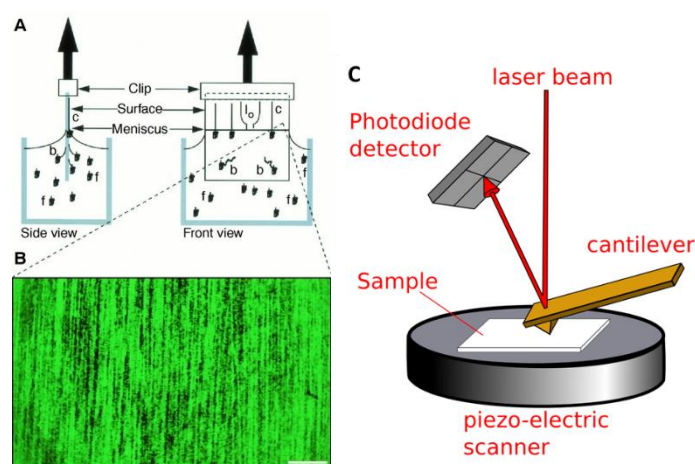


Fig. 3.10. (a) Schematic illustration of the DNA combing process, (b) combed human genomic DNA, observed with an epifluorescence microscope, scale bar 25  $\mu\text{m}$ . Adapted from ref.<sup>31</sup> (c) Schematic illustration of AFM detection.

Surface preparation is a key step for imaging DNA at high resolution with AFM. Thereby, silanization of the mica samples was performed in the vapor phase. It has two advantages: no contact with the solution and therefore no contamination of the surface by impurities dissolved in this solution. The second advantage is that silanization takes place evenly, so that in principle smooth layers are formed at the surface which is an essential criterion for AFM characterization.

On the other hand, for arranging and stretching DNA molecules on the surface, specific binding of its extremities more than the midterm chain is required. For this purpose, different approaches are presented in the literature such as binding via specific biochemical interactions (for example biotin – streptavidin), binding by chemical reaction or pH-depended specific binding of DNA via its extremities.<sup>30,32,33</sup> Additional forces at the air-water meniscus can unfold DNA chains, leading to a linear fully-extended conformation. To keep our approach simple enough we decided to avoid chemical modification of DNA molecules and their covalent grafting and to use only the pH-depending properties of DNA.

One approach of mica silanization, described in the literature, utilizes 3-aminopropyl-triethoxysilane (APTES) to obtain a smooth surface<sup>34</sup>. According to this method, authors used aminosilanes for functionalization of the surface, which is positively charged over a broad pH range (pKa ~ 10) and therefore negatively charged DNA adheres strongly through electrostatic interactions. It should be kept in mind that at low pH, the surface charge will be very high due to a complete protonation of all NH<sub>2</sub> groups (NH<sub>3</sub><sup>+</sup>) and DNA molecules will adsorb too strongly and in a non-specific way, thus it will be not possible to stretch them. At high pH the surface will lose its charge (NH<sub>2</sub>) and DNA will be adsorbed too weakly or not at all so it will be dragged away by the receding meniscus<sup>32,33</sup>. In between there exists an optimal pH range (4 – 7) for which DNA binds to the surface strongly enough and specifically by its extremities and therefore these conditions were used in our experiments.

#### ***3.2.3.1.1. Silanization of mica with APTES***

The procedure for mica functionalization with APTES in the vapor phase was adapted from reference<sup>34</sup>(section 3.3.2). Briefly, APTES functionalization experiments were carried out in a plastic pot, closed with a rubber stopper, where freshly cleaved mica slides were attached to the walls (Fig. 3.11a). The air was pumped out with a syringe connected to the hose pump during a minute, filled with Ar from the balloon and this procedure was repeated several times. The reagents for silanization, APTES and DIPEA (ratio 1:3), were placed in small plastic cups at the bottom of the pot with a syringe positioned through the septa. After 3 – 4 h of evaporation, the cups with reagents were removed, the reactor was filled with Ar as described above and was left for 2 – 3 days.

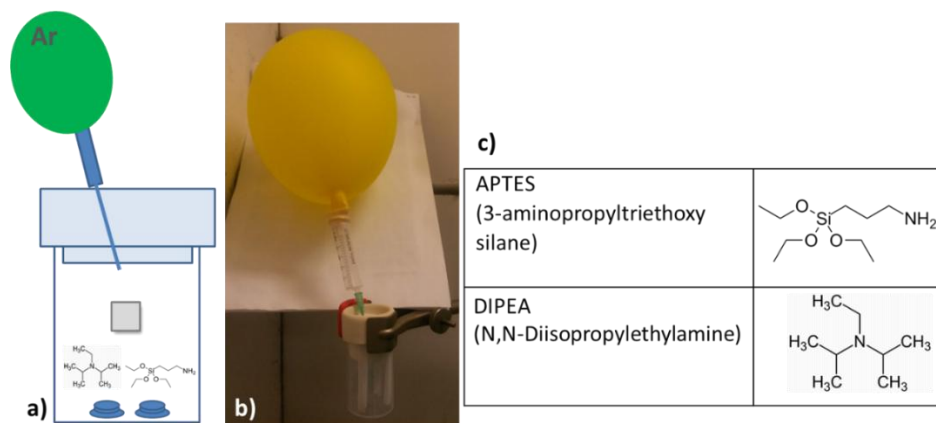


Fig. 3.11. (a) Schematic illustration and (b) photograph of the experimental setup for mica functionalization with APTES. (c) Structural formulas of organic molecules used for silanization.

All AFM characterizations were carried out in the user-friendly ScanAsyst mode in air. As is illustrated by the AFM image in fig. 3.12, the surface of the modified mica is relatively flat, with a roughness of 1 – 2nm. One can see that the coating layer exhibits a thickness of about 0.5 – 1.0 nm. In addition, the hydrophobicity of the surface was significantly increased.

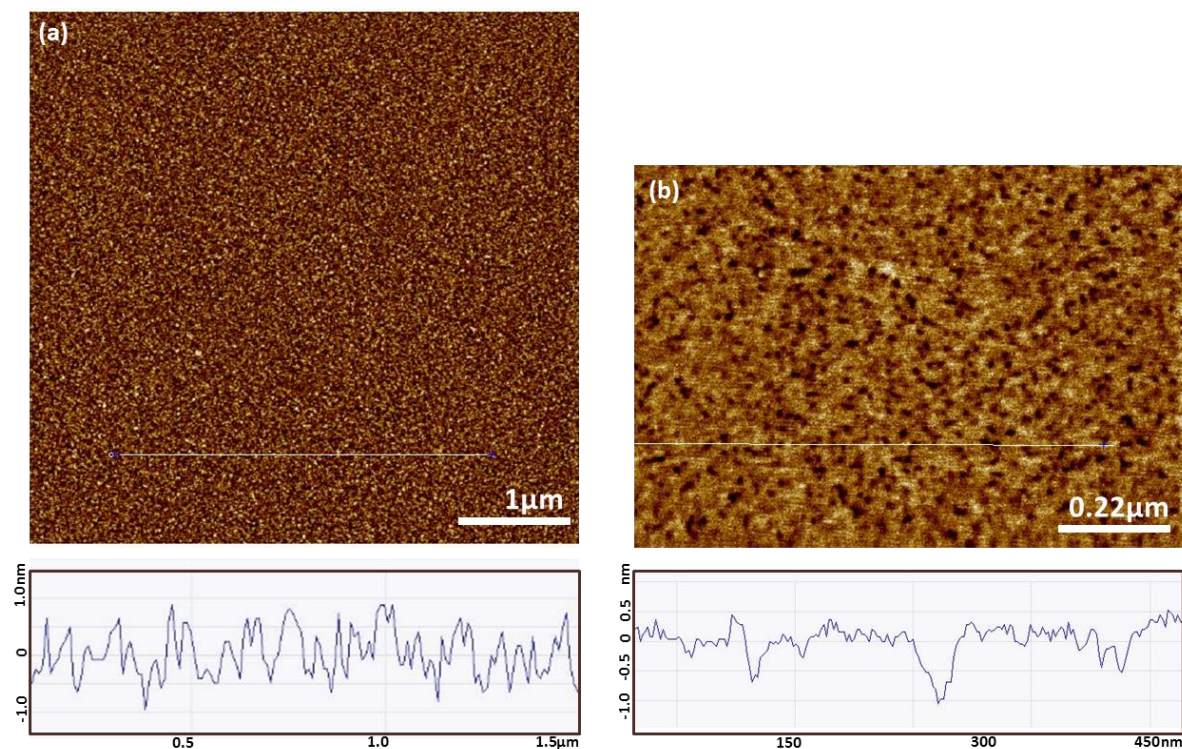


Fig. 3.12. AFM images of APTES-modified mica and corresponding cross-sections. Image size: (a) 5.0 μm; (b) 1.1 μm.

The combing procedure was performed manually by inclination of the surface that causes the movement of the solution droplet<sup>30</sup>. The alignment procedure occurs in two major steps. First, a droplet of DNA solution is deposited on the hydrophobic surface. Then, DNA molecules settle down on the surface and their extremities specifically adsorb onto the surface allowing the anchoring the DNA molecules. Second, by inclining the surface, the forces exerted by the receding meniscus of the droplet stretch DNA molecules on the surface.



As stated before, combing DNA from different pH solutions was performed on APTES silanized mica surfaces. A solution of lambda-DNA in TE buffer, pH 8 was dropped on the surface. After 2 minutes, the droplet was set into motion by inclining the surface manually. The DNA molecules observed on such samples were typically in a coiled configuration (Fig. 3.13). Other combing experiments were performed with a DNA solution prepared in phosphate buffer, pH 5.5. In this latter case, two different configurations were observed, combed DNA molecules as well as a majority of coiled DNA (Fig. 3.14).

This problem might originate from the not perfectly controlled conditions, like for example the speed of the droplet motion, and/or from the type of silane (aminosilane) that was used.

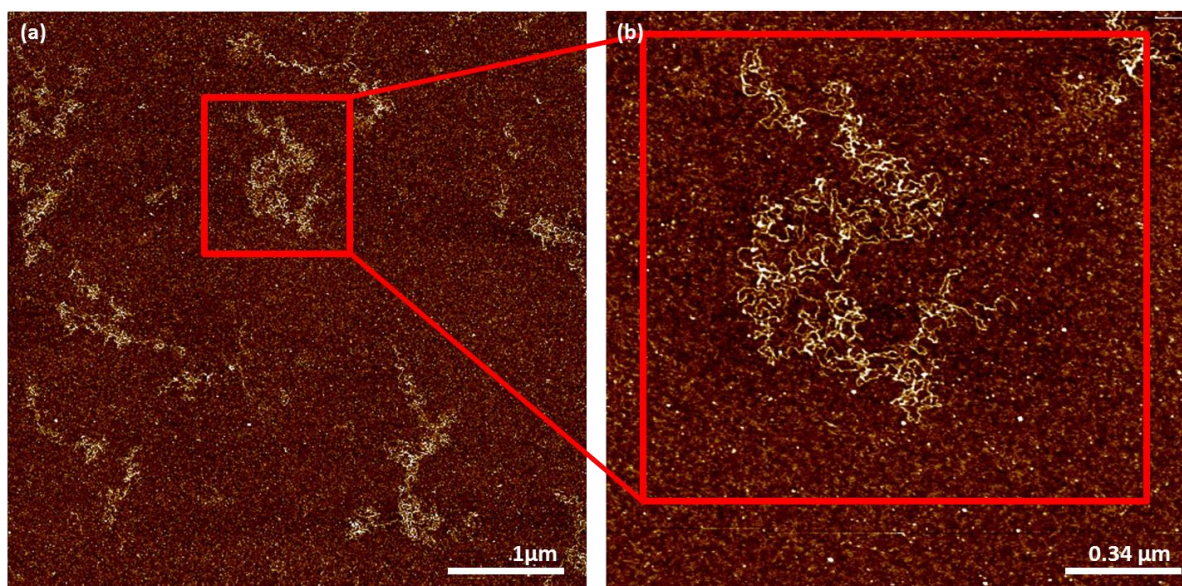


Fig. 3.13. AFM images of DNA on APTES modified mica. Images size : (a) 5.0 μm; (b) 1.7 μm. 40 μl of 1.0 μg/ml DNA solution in Tris buffer, pH 8, deposited on the surface.

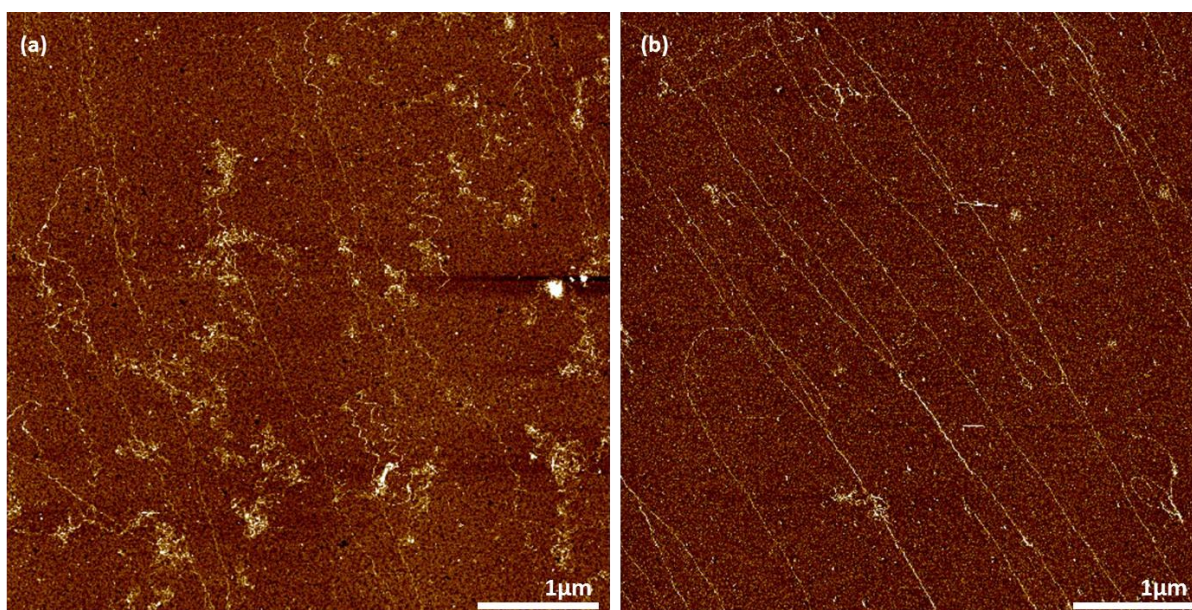


Fig. 3.14. AFM images of DNA on APTES modified mica, images size: 5.0 μm. 40 μl of 1.0 μg/ml DNA solution in phosphate buffer, pH 5.5 deposited on surface.

However, the better coverslips where stretched DNA molecules could be observed were selected for BPE experiments. Nevertheless, after positioning these surfaces in a solution for electrochemical modification the molecular resolution of the AFM images was totally lost thus preventing the subsequent observation of DNA filaments.

### ***3.2.3.1.2. Silanization of mica with 7-octenyltrichlorosilane***

Another methodology for DNA combing is proposed by the DNA Combing Facility group, IGMM, UMR 5535, University of Montpellier/CNRS, France. This service is currently performing patented DNA combing on glass coverslips with detection by fluorescence methods. Since glass surfaces are too rough for AFM observation, we started a collaboration to adapt this technology to mica surfaces.

The same procedure of silanization and combing was performed with mica instead of glass coverslips. The silanization was carried out with the 7-octenyltrichlorosilane (OCTS) in a vapor phase. Before silanization, the coverslips were subjected to UV/Ozone treatment and then placed in the reactor. The reactor is heated and before introducing the silane, 3 cycles of vacuum/argon is performed.

The silanization is performed with the 7-octenyltrichlorosilane (OCTS) in a vapor phase typically during 18 h with glass coverslips. After the silanization, the coverslips are washed with ethanol and cyclohexane, respectively. The combing is performed with an automated system, where coverslips are lifted out from the DNA solution at a constant rate in order to obtain a good reproducibility.

For the first experiments, the mica coverslips were silanized following the existing protocol and DNA filaments were observed either by fluorescence of DNA stained with YOYO dye or by immunodetection of DNA. The same samples were than characterized with AFM. In a first case, with fluorescence detection, the DNA filaments were rare but it was possible to find some of them in different areas of the mica (Fig. 3.15b). As illustrated in fig 3.15 a,b, DNA strands were observed by fluorescence as well as by AFM. However, in a second case, with imunodetection of DNA, AFM analysis could not be realized due to very rough and contaminated surfaces (data not shown).

However, at the condition of 18 h silanization the undulating surface roughness is observed (Fig. 3.15b, c, d) which is undesirable and interferes with DNA observation. At bigger magnification DNA filaments are better visible (Fig. 3.15e).

Therefore, the silanization conditions as well as DNA combing need to be optimized prior to AFM analysis. First of all, different silanization time were tested (6 h, 12 h, 18 h) in order to decrease the silane quantity and therefore the surface roughness (Fig. 3.15b,d, Fig. 3.16). The combing of DNA was performed with solutions at different concentrations of  $0.3 \mu\text{g ml}^{-1}$ ,  $0.6 \mu\text{g ml}^{-1}$ ,  $1.0 \mu\text{g ml}^{-1}$ , as well as at different pH 5.2; 5.7, 6.2, 7.0 and 8.0 in order to find the best conditions to reach a good distribution of stretched DNA on the surface. Control



experiments without DNA were also performed for each condition, showing the same roughness, confirming that it originates from the silanization step and not from the combing.

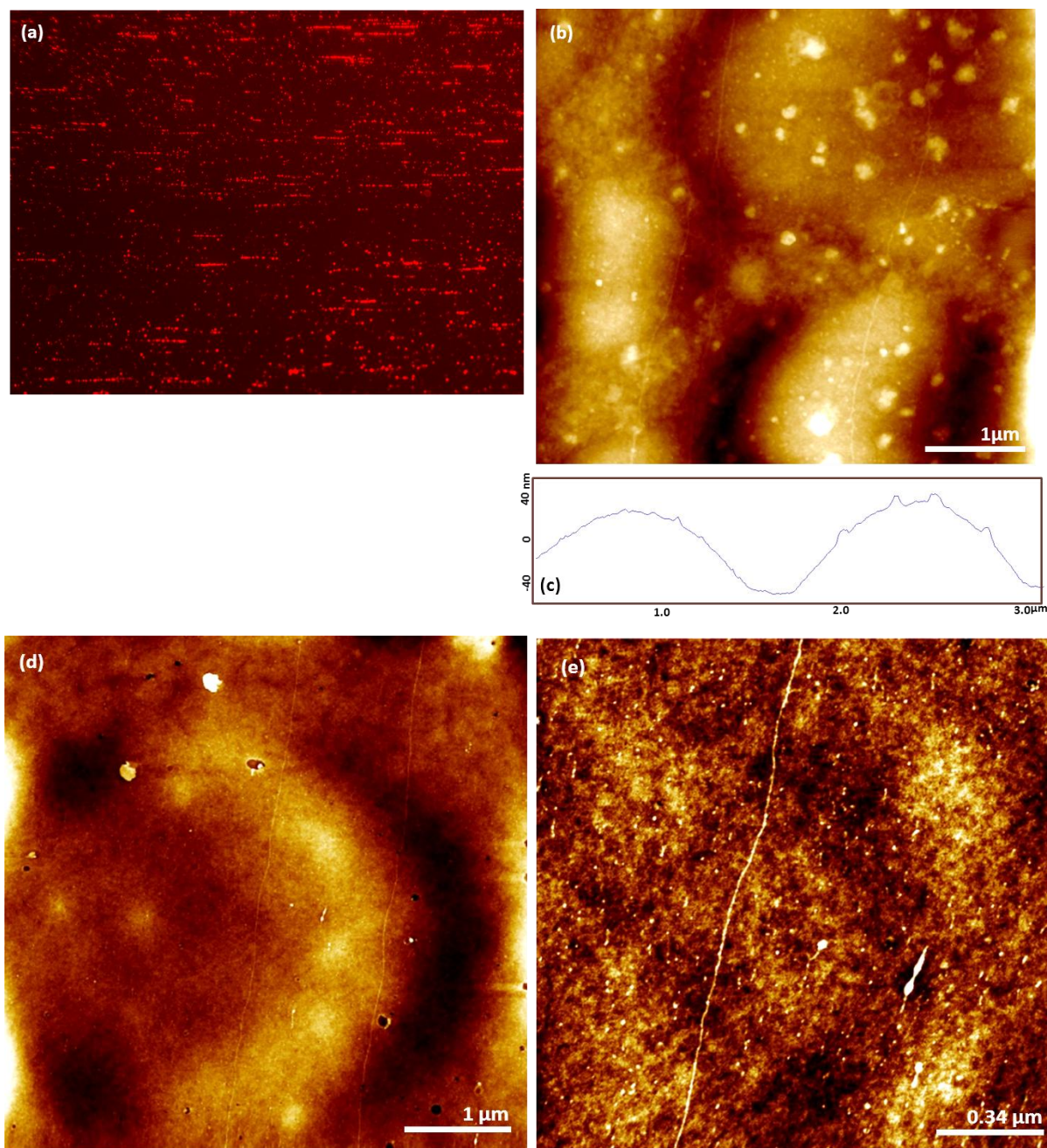


Fig. 3.15. (a) Fluorescent microscopy image of YOYO-stained DNA molecules on OCTS-modified mica at 18 h silanization, combed at pH 5.7. (b, d, e) AFM images of the same sample, where some DNA filaments could be observed, (b, d) images size 5.0 μm, (e) image size 1.7 μm. (c) Height profile of the surface, showing the undulating roughness.

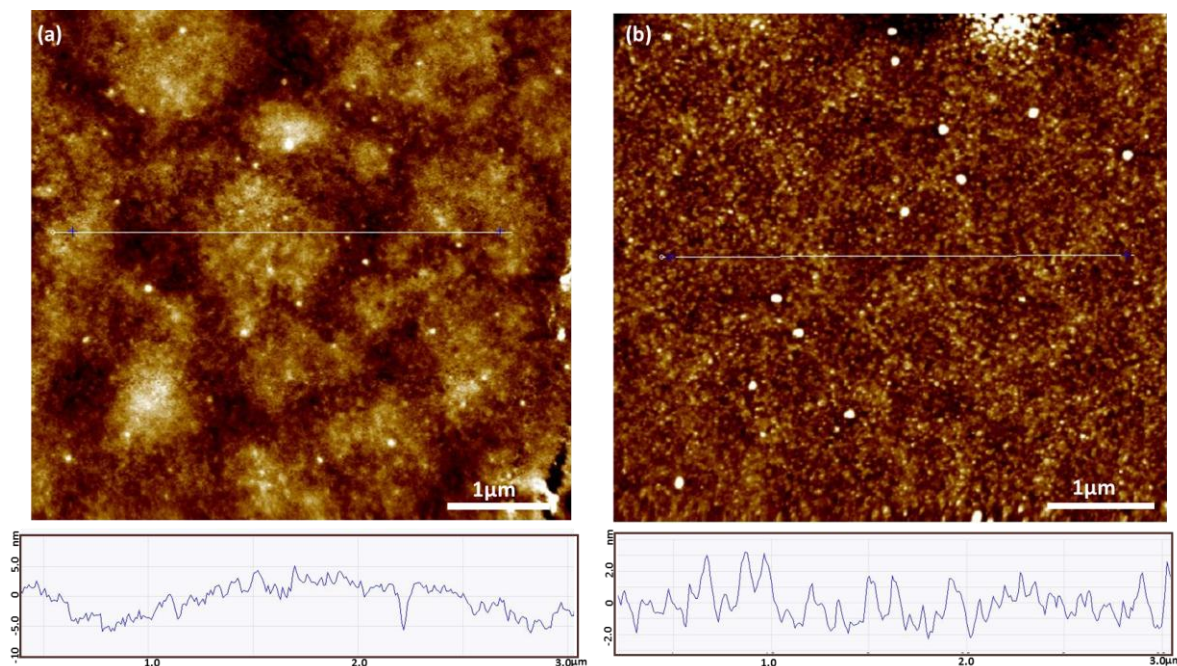


Fig. 3.16. AFM images of OCTS modified mica surfaces at (a) 12 h silanization, (b) 6 h silanization and their height profiles of the surfaces respectively. Images size: 5.0  $\mu\text{m}$ .

Finally, a reasonable roughness of 2-4 nm was obtained when the silanization time is reduced to 6 h. However, a distribution of unidentified spots with a size of about 10 nm in diameter are observed and only very few DNA filaments, thus complicating the AFM analysis. Nevertheless, several coverslips were selected for the BPE experiments.

### 3.2.3.2. Design of new set-up for BPE experiments on mica

For BPE experiments with DNA deposited on coverslips, a new electrochemical cell was designed. It consists of two containers with feeder electrodes attached to its walls and a bridge in between (Fig. 3.17). The coverslips were deposited in the bridge area. The similar redox reactions as in case of CABED were coupled such as copper reduction at cathodic side and water oxidation at anodic side (eq. 3.1 – 3.3).

Taking into account the smaller distance between feeder electrodes (6.0 cm) and the high potential needed for redox reactions to be performed (3 – 4 kV), this can lead to important Joule heating of the solution due to high ionic currents passing through the electrolyte solution.

In order to decrease this side-effect, two approaches have been used. First, diluted solutions of the metal ion precursor  $\text{CuSO}_4$  were used (1 mM; 0.1 mM) to decrease the ionic strength and corresponding current generated in the electrochemical cell. To ensure a sufficient  $\text{Cu}^{2+}$  concentration during these experiments, copper feeder electrodes were also employed, assuming that  $\text{Cu}^{2+}$  can be produced at the anode feeder electrode throughout the experiment. Second, to decrease the ionic current, the solution thickness in the bridge area was minimized by covering the mica coverslip with DNA with another glass slide at the top (Fig. 3.17). In this case, a thin layer of solution is sandwiched between the two slides causing a smaller current in



the cell. This is indeed a crucial condition, because based on the principle of bipolar electrochemistry, the conductivity of the substrate should be higher than that of its surrounding medium in order to achieve a sufficient polarization of the substrate behaving as a BE.

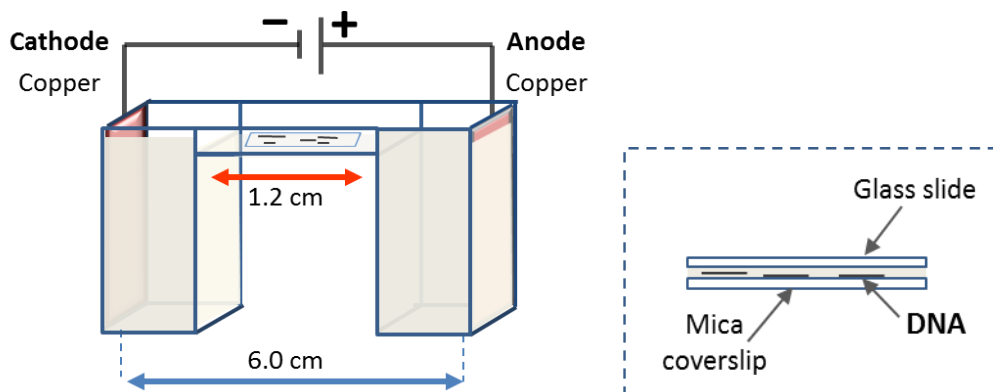


Fig. 3.17. Schematic illustration of the cell used in the BPE experiments with DNA.

In addition, in such a configuration the part of the solution where the major potential drop occurs is focused in the bridge area. Therefore, we can assume that the potential drops at the feeder electrode/solution interface and along both feeder compartments are negligible and the majority of the potential drops linearly through the solution in the bridge area (Fig. 3.17). Considering this assumption, the necessary potential needed to apply to the cell for coupling the redox reactions on the BE was calculated based on a distance of 1.2 cm.

Control experiments to verify the validity of this experimental configuration were performed for copper deposition on carbon microtubes (CMTs). The result shows that a copper deposit on 15 – 20  $\mu\text{m}$ -long CMTs is formed by applying only 0.2 – 0.4  $\text{kVcm}^{-1}$  to the cell, due to a maximum of potential drop in bridge area, while it should be formally 0.7  $\text{kVcm}^{-1}$  (Fig. 3.18).

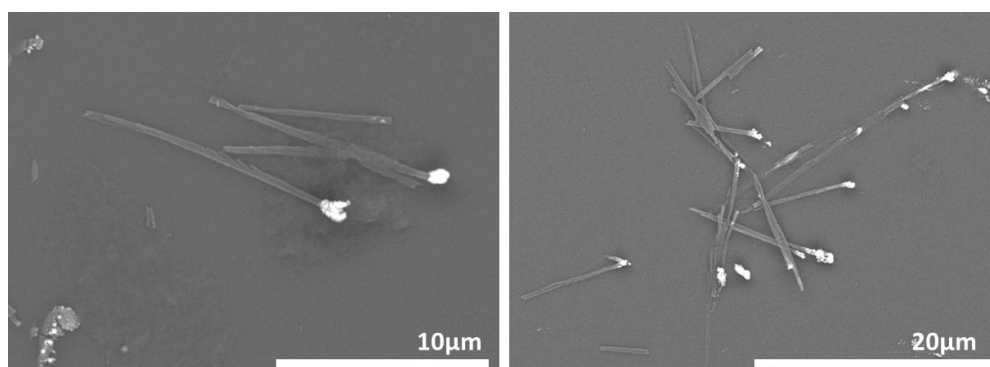


Fig. 3.18. SEM images of CMTs asymmetrically modified with copper deposit, using the new cell with a focused potential drop. 0.1 mM  $\text{CuSO}_4$ ,  $E = 0.3 \text{ kV cm}^{-1}$ ,  $t = 5 \text{ min}$ .

The same strategy then was used with DNA filaments deposited on mica coverslips, but unfortunately, modified filaments were not observed at this stage. Investigation of the resulting samples as well as a series of control experiments revealed sometimes the formation of samples with a large surface roughness and some deteriorations, making a clear visualization of DNA filaments quite difficult. In addition, the rare presence of DNA complicated the AFM characterization and generalization of the obtained results. This might be due to the

experimental setup, but also to the surface preparation that should be optimized in the future. Furthermore, the stretched DNA structures might also have different properties from that of the wild form and this factor could potentially influence the CT properties through DNA.

Even if these results are not fully conclusive, the idea of using BPE to study DNA CT looks promising. As we show at the beginning of this chapter, BPE modification of DNA with metal nanoparticles is possible, but seems to be very sensitive to the experimental conditions. Concerning the second approach, major difficulties arise from the characterization method imposing the detection of objects with a nanoscale dimension on perfectly clean and smooth surfaces. However, overall these results suggest that DNA can be modified by BPE, but this research is still at an early stage and more experiments are necessary in order to get the definite proof-of-principle and more accurate/reliable results.

### **3.3. Wireless DNA hybridization detection with BPE**

#### **3.3.1. Introduction**

Asymmetric particles synthesized by BPE can also be used as functionalized biosensing particles or it's possible to employ BPE-induced redox processes as a readout mechanism for biosensing purpose<sup>35–39</sup>.

As an example, we can use one side of an asymmetric particle where specific recognition reaction occurs and another as transduction side to read out the corresponding signal. In this study, we propose an original strategy to detect DNA hybridization with BPE.

There is an increasing interest in the detection of specific DNA sequences using various biosensor methods, which do not require the use of specific labels or fluorophores. The direct detection of DNA binding through base pairing has been reported based on electrochemical techniques<sup>40,41</sup>. The advantage of BPE compared to conventional electrochemistry relies on the sensing capability in a wireless way and without complicated devices.

The approach proposed in this this thesis is illustrated on fig. 3.19. Carbon beads (CB) are modified asymmetrically with a gold layer by using BPE. By controlling the electric field strength, it is possible to deposit a gold layer that covers almost half of the bead, resulting in a typical *Janus* particle. Then, thiol-modified oligonucleotides can be immobilized as a self-assembled monolayer (SAM) on the gold-coated part of the particles due to the well-known Au/S chemisorption process. For this, the CB/Au hybrid particles are immersed in a solution containing either a thiol-modified DNA-probe (P) or a hybridized mixture of thiol-modified DNA-probe (P) with a DNA-target (T) in order to obtain a SAM of ssDNA or dsDNA, respectively. These modified particles are then employed for BPE sensing, where the side covered by ssDNA or dsDNA is used as the site for the recognition event, whereas the unfunctionalized carbon part is used for the electrochemical readout. The concept of detection

is based on the increase of electronic conductivity associated with DNA hybridization. In the BPE configuration, the coupling of the electrochemical processes occurring at the two extremities of the BE allow detecting ET through the bipolar object. Successful DNA hybridization should be transduced by an increase in intensity of the redox reactions occurring at the edges of the BE (Fig. 3.19).

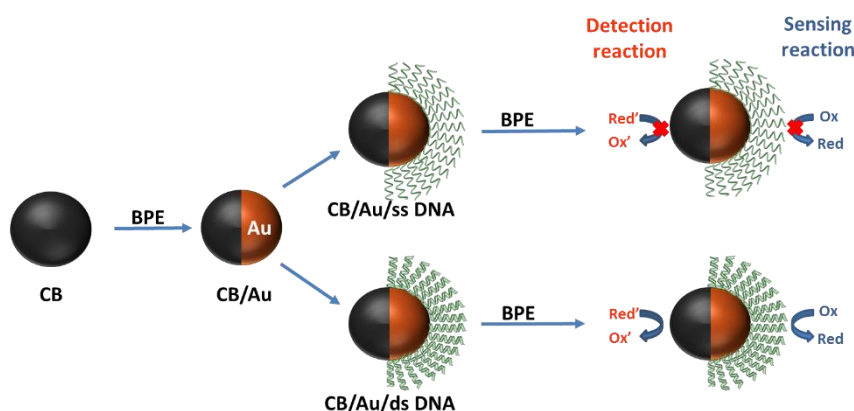


Fig. 3.19. Sequence of the (electro)chemical modification steps of the hemispheres of a CB by gold and either ssDNA or dsDNA monolayers and its impact on the corresponding BPE detection.

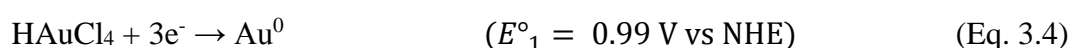
In order to propose a straight-forward read out of the hybridization process on the BE, simple redox couples were employed. Ferricyanide reduction into ferrocyanide ( $K_3[Fe^{III}(CN)_6]/K_4[Fe^{II}(CN)_6]$ ) was used as sensing reaction at the DNA modified side and water oxidation was used as the detection reaction based on the local change of proton concentration detected with a universal pH indicator (Fig. 3.21).

The ferricyanide/ferrocyanide redox couple has already been reported as a transducer of hybridization events based on the increase in electronic conductivity at the interface<sup>40</sup>. The use of such an anionic redox probes has the advantage that the diffusion of the redox species towards the surface of the electrode is blocked due to electrostatic repulsion with the negatively charged DNA layer. As a consequence the ss-DNA monolayer acts as an insulator, blocking ET and leading to the absence of redox reaction, while ET through ds-DNA monolayer is strongly enhanced by  $\pi$ -stacking (Fig. 3.21).

### 3.3.2. Experimental part

#### 3.3.2.1 Preparation of CB/Au Janus particles with BPE

A macroscopic CB with a diameter ranging between 0.8 and 1.0 mm was selected and fixed with an adhesive tape in the middle of the BPE cell (similar to the one shown in Figure 2.26). The distance between the two graphite electrodes was 3.5 cm and the cell was filled with 5 mM  $HAuCl_4$ . Gold deposition can be achieved at the cathodic pole of the CB beads by the following reaction:



Taking into account the water oxidation reaction with  $E^\circ_2 = 1.23 \text{ V}$  vs NHE, the minimum electric field for gold deposition can be calculated:

$$\varepsilon = \frac{\Delta V_{min}}{l_e} = \frac{E_2^\circ - E_1^\circ}{l_e} = \frac{(1.23 - 0.99) \text{ V}}{0.08 \text{ cm}} = 3 \frac{\text{V}}{\text{cm}} \quad (\text{Eq. 3.5})$$

However, since half of the surface of these beads needs to be covered with a gold deposit, a much larger electric field should be applied. For these reason, the applied electric field should be increased, but not too much in order to avoid the coupling with proton reduction, leading potentially to water splitting at the two faces of the CB:

$$\varepsilon = \frac{\Delta V_{min}}{l_e} = \frac{E_1^\circ - E_2^\circ}{l_e} = \frac{(1.23 - 0) \text{ V}}{0.08 \text{ cm}} = 15.4 \frac{\text{V}}{\text{cm}} \quad (\text{Eq. 3.6})$$

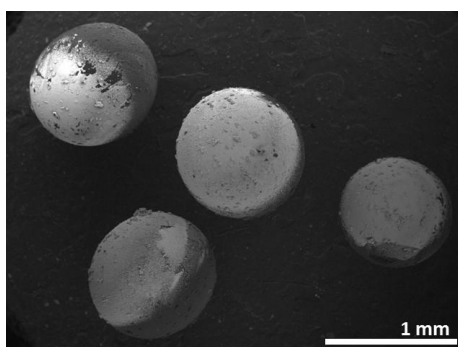


Fig. 3.20. SEM images of CB/Au Janus particles synthesized with BPE.

Thereby, an electric field of  $12 \text{ V cm}^{-1}$  was applied during 40 min, during which the electrochemical cell was refilled with 5 mM  $\text{HAuCl}_4$  solution every 10 minutes to ensure the presence of electrodeposable species all along the duration of these experiments. It was possible to observe the corresponding gold deposit by naked eyes and a representative SEM image of CB/Au particles is provided in fig. 3.20.

### 3.3.2.2. DNA probe immobilization and target hybridization on CB/Au particles

The DNA probe (P) immobilization was performed by incubating the CB/Au particles for 2 hours in 1 mL of  $10 \mu\text{g mL}^{-1}$  of P solution in 0.5 M NaCl. Then, the CB/Au particles were rinsed with deionized water. Target (T) hybridization was performed by incubating the CB/Au particles for 2 hours in 1 mL of solution that contains  $10 \mu\text{g mL}^{-1}$  of P and  $20 \mu\text{g mL}^{-1}$  of T in 0.5 M NaCl. Later on, these particles were gently rinsed with 0.5 M NaCl.

Table 3.1. Thiol-labeled DNA probe (P) target (T) and mismatch (M) sequences

Name	Sequence
DNA-probe (P)	5' C3 thiol GTC TGT CAA TTC ATA GGT CAT 3'
DNA-target (T)	5' ATG ACC TAT GAA TTG ACA GAC 3'
DNA-mismatch (M)	5' ATG ACC TAT GTA TTG ACA GAC 3'

This procedure allows the formation of SAMs of ssDNA and dsDNA on the gold hemisphere of the CB. Taking into account the surface of the gold hemisphere ( $r = 0.45\text{mm}$ ), which is:

$$\frac{1}{2}S = 2\pi r^2 = 1.27 \cdot 10^{12} \text{ nm}^2, \quad (\text{Eq. 3.7})$$

and considering that the surface occupied by one DNA single- or double- strand is  $2.2 \text{ nm}^2$ , the quantity of DNA to form a monolayer is roughly  $6 \cdot 10^{11}$  molecules.

### 3.3.2.3. BPE experiments for sensing DNA hybridization event

BPE experiments were performed in a similar cell than the one reported above (shown in Figure 2.26), and CB/Au, CB/Au/dsDNA or CB/Au/ssDNA particles were positioned in the middle in such a way that the gold side was facing the feeder anode whereas the carbon side faced the feeder cathode. In this manner, when an external electric field is applied across the cell, the two following reactions could proceed:

at the cathodic pole of the particles which is the side covered with the DNA monolayer:



and at the anodic pole, which is the unfunctionalized side of the CB:



A universal pH indicator (pH 4 - 10) was added to the solution in order to detect proton formation due to water oxidation. For BPE experiments, the cell was filled with a solution that contains 5 mM  $\text{K}_3[\text{Fe}(\text{CN})_6]$ , 5 mM  $\text{MgCl}_2$  and  $10^{-8}\text{M}$  of Methylene Blue (MB). The latter chemical was added as a redox intercalator to facilitate ET through the dsDNA monolayer.

In such a configuration, by applying the electric field, the ET on CB/Au/ssDNA particles is blocked due to the presence of the insulating ssDNA monolayer. On the other hand, on CB/Au/dsDNA particles the reduction of ferricyanide can take place by ET through the dsDNA monolayer. This shuttling of electrons from the other side of the beads where protons are formed due to water oxidation can be detected locally by changing the color of the pH indicator (Fig.3.21).

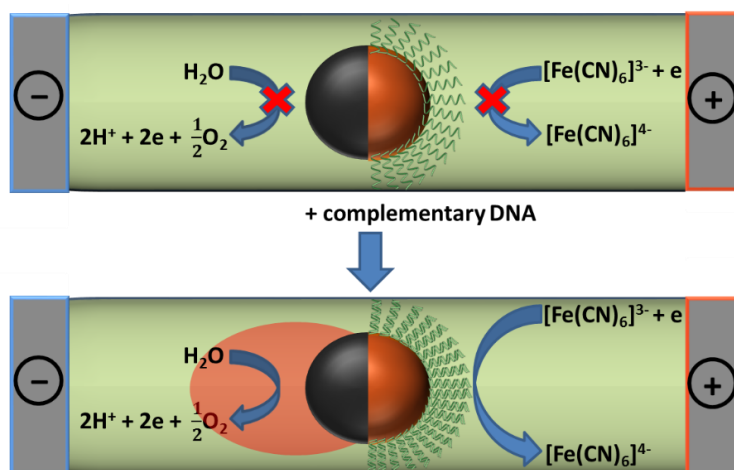


Fig. 3.21. Schematic illustration of BPE processes at the CB/Au particles modified with ssDNA and dsDNA monolayers.

Preliminary experiments were performed with 0.9 mm in diameter CB/Au particles in order to define the appropriate electric field range to avoid proton reduction reaction on the gold side of the particles. Suitable electric fields for this size of particles were found to be in the range from  $5.7 \text{ V cm}^{-1}$  to  $11.4 \text{ V cm}^{-1}$ . Therefore, at electric fields larger than  $11.4 \text{ V cm}^{-1}$ , proton reduction starts to take place at the gold side of the *Janus* particles. This process is undesirable for future experiments with DNA monolayers.

Subsequently, the DNA modified particles CB/Au/dsDNA or CB/Au/ssDNA as well as a control particle CB/Au used for comparison were placed in the BPE cell and electric fields of  $5.7 \text{ V cm}^{-1}$ ,  $7.1 \text{ V cm}^{-1}$  and  $8.6 \text{ V cm}^{-1}$  were applied. Pictures were taken directly after applying the potential (Fig. 3.22). One can see from fig. 3.22, that independently from the applied potential the same red color evolution is observed for CB/Au/dsDNA and CB/Au control particles. This red coloration visualizes the amount of protons formed locally at the anodic side of the particles. The comparable response for CB/Au/dsDNA and CB/Au means that roughly the same quantity of electrons is transferred through the beads and therefore the presence of the dsDNA monolayer apparently does not affect the heterogeneous ET.

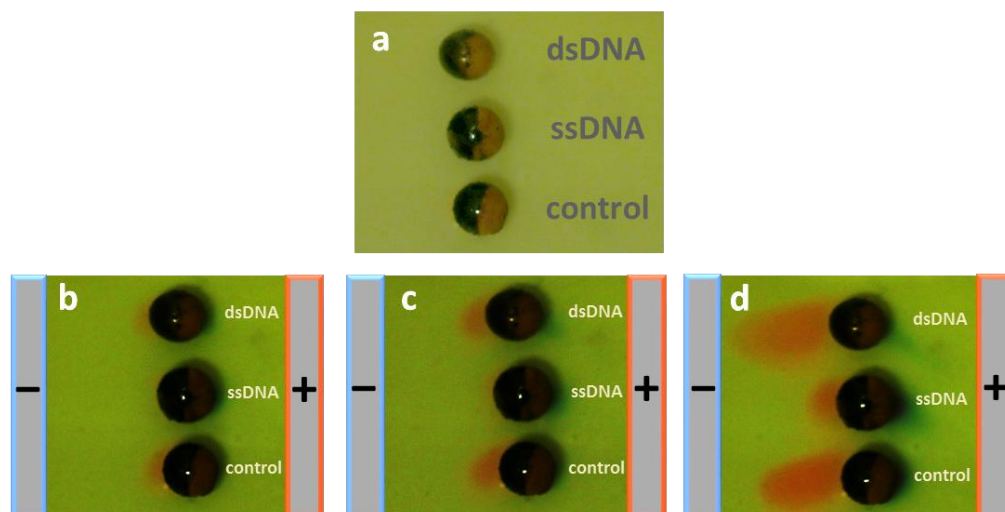


Fig. 3.22. Photographs of pH changes near the edges of 0.9 mm CB/Au particles, modified with dsDNA, ssDNA, and control particle in solution of 5 mM  $[\text{Fe}(\text{CN})_6]^{3-}$ , 5 mM  $\text{MgCl}_2$ ,  $10^{-8}$  MB, and universal pH indicator (a) prior to application of the electric field; and when applying an electric field of (b)  $5.7 \text{ V cm}^{-1}$ ; (c)  $7.1 \text{ V cm}^{-1}$ ; (d)  $8.6 \text{ V cm}^{-1}$ .

By comparison, on a CB/Au/ssDNA particle this response was not observed, meaning that the ET is fully blocked by the ssDNA monolayer (Fig. 3.22b,c). However, at larger electric fields, a small response is also observed on CB/Au/ssDNA particles (Fig. 3.22d) but can be explained by additional undesirable processes.

At the intermediate electric field value of  $7.1 \text{ V cm}^{-1}$ , a clear difference of response is observed between the particles modified with dsDNA and ssDNA monolayers. This original strategy based on BPE is very easy to perform and could be used for the detection of DNA hybridization event. Future experiments should be performed to study the hybridization with single mismatch complementary DNA.

## References

- (1) Dahm, R. *Hum. Genet.* **2008**, *122* (6), 565–581.
- (2) Levene P. A. *J. Biol. Chem.* **1919**, *40*, 415–424.
- (3) Chargaff, E.; Lipshitz, R.; Green, C. *J. Biol. Chem.* **1952**, *195* (1), 155–160.
- (4) Watson, J. D.; Crick, F. H. *Nature* **1953**, *171* (4356), 737–738.
- (5) Discovery of DNA Double Helix: Watson and Crick | Learn Science at Scitable  
<https://www.nature.com/scitable/topicpage/discovery-of-dna-structure-and-function-watson-397> (accessed May 24, 2018).
- (6) Treadway, C. R.; Hill, M. G.; Barton, J. K. *Chem. Phys.* **2002**, *281* (2–3), 409–428.
- (7) Dekker, C.; Ratner, M. *Phys. World* **2001**, *14* (8), 29–33.
- (8) Eric B. Brauns; Catherine J. Murphy, A.; Mark A. Berg. *J. Am. Chem. Soc.* **1998**, *120* (10), 2449–2456.
- (9) Georghiou, S.; Bradrick, T. D.; Philippetis, A.; Beechem, J. M. *Biophys. J.* **1996**, *70* (4), 1909–1922.
- (10) O'Neill, M. A.; Becker, H.-C.; Wan, C.; Barton, J. K.; Zewail, A. H. *Angew. Chem.* **2003**, *115* (47), 6076–6080.
- (11) Endres, R. G.; Cox, D. L.; Singh, R. R. P. *Rev. Mod. Phys.* **2004**, *76* (1), 195–214.
- (12) Kasumov, A. Y.; Klinov, D. V.; Roche, P.-E.; Guéron, S.; Bouchiat, H. *Appl. Phys. Lett.* **2004**, *84* (6), 1007–1009.
- (13) Rakitin, A.; Aich, P.; Papadopoulos, C.; Kobzar, Y.; Vedeneev, A. S.; Lee, J. S.; Xu, J. M. *Phys. Rev. Lett.* **2001**, *86* (16), 3670–3673.
- (14) Porath, D.; Bezryadin, A.; de Vries, S.; Dekker, C. *Nature* **2000**, *403* (6770), 635–638.
- (15) Storm, A. J.; van Noort, J.; de Vries, S.; Dekker, C. *Appl. Phys. Lett.* **2001**, *79* (23), 3881–3883.
- (16) Zhang, Y.; Austin, R. H.; Kraeft, J.; Cox, E. C.; Ong, N. P. *Phys. Rev. Lett.* **2002**, *89* (19), 198102.
- (17) Eley, D. D.; Spivey, D. I. *Trans. Faraday Soc.* **1962**, *58* (0), 411–415.
- (18) Cohen, H.; Nogues, C.; Naaman, R.; Porath, D. *Proc. Natl. Acad. Sci. U. S. A.* **2005**, *102* (33), 11589–11593.
- (19) Heim, T.; Deresmes, D.; Vuillaume, D. *J. Appl. Phys.* **2004**, *96* (5), 2927–2936.
- (20) Kratochvílová, I.; Král, K.; Bunčák, M.; Víšková, A.; Nešpůrek, S.; Kochalska, A.; Todorciuc, T.; Weiter, M.; Schneider, B. *Biophys. Chem.* **2008**, *138*, 3–10.
- (21) Xu, B.; Zhang, P.; Xiulan Li, A.; Tao, N. *Nano Lett.* **2004**, *4* (6), 1105–1108.
- (22) Guo, X.; Gorodetsky, A. A.; Hone, J.; Barton, J. K.; Nuckolls, C. *Nat. Nanotechnol.* **2008**, *3* (3), 163–167.
- (23) Muren, N. B.; Olmon, E. D.; Barton, J. K. *Phys. Chem. Chem. Phys.* **2012**, *14* (40), 13754.
- (24) Murphy, C. J.; Arkin, M. R.; Jenkins, Y.; Ghatlia, N. D.; Bossmann, S. H.; Turro, N. J.; Barton, J. K. *Science* **1993**, *262* (5136), 1025–1029.
- (25) Kelley, S. O.; Barton, J. K.; Jackson, N. M.; Hill, M. G. *Bioconjugate chem.* **1997**, *8* (1), 31–37.

- (26) Kelley, S. O.; Jackson, N. M.; Hill, M. G.; Barton, J. K. *Angew. Chem. Int. Ed.* **1999**, 38 (7), 941–945.
- (27) Boon, E. M.; Barton, J. K. *Curr. Opin. Struct. Biol.* **2002**, 12 (3), 320–329.
- (28) Fattah, Z.; Garrigue, P.; Lapeyre, V.; Kuhn, A.; Bouffier, L. *J. Phys. Chem. C* **2012**, 116 (41), 22021–22027.
- (29) Kaykov, A.; Taillefumier, T.; Bensimon, A.; Nurse, P. *Sci. Rep.* **2016**, 6 (1), 19636.
- (30) Nazari, E. Z.; Gurevich, L. *J. Self-Assembly Mol. Electron.* **2013**, 1 (1), 125–148.
- (31) Michalet, X.; Ekong, R.; Fougerousse, F.; Rousseaux, S.; Schurra, C.; Hornigold, N.; van Slegtenhorst, M.; Wolfe, J.; Povey, S.; Beckmann, J. S.; Bensimon, A. *Science* **1997**, 277 (5331), 1518–1523.
- (32) Benke, A.; Mertig, M.; Pompe, W. *Nanotechnology* **2011**, 22 (3), 35304.
- (33) Allemand, J. F.; Bensimon, D.; Jullien, L.; Bensimon, A.; Croquette, V. *Biophys. J.* **1997**, 73 (4), 2064–2070.
- (34) Shlyakhtenko, L. S.; Gall, A. A.; Lyubchenko, Y. L. *Methods Mol. Biol.* **2012**, 931, 295–312.
- (35) Eßmann, V.; Jambrec, D.; Kuhn, A.; Schuhmann, W. *Electrochem. commun.* **2015**, 50, 77–80.
- (36) de Poulpiquet, A.; Diez-buitrago, B.; Milutinovic, M. D.; Sentic, M.; Arbault, S.; Bouffier, L.; Kuhn, A.; Sojic, N. *Anal. Chem.* **2016**, 88, 6585–6592.
- (37) Poulpiquet, A. De; Diez-buitrago, B.; Milutinovic, M.; Goudeau, B.; Bouffier, L.; Arbault, S.; Kuhn, A.; Sojic, N. *ChemElectroChem* **2016**, 3, 404–409.
- (38) Sentic, M.; Arbault, S.; Goudeau, B.; Manojlovic, D.; Kuhn, A.; Bouffier, L.; Sojic, N.; Sojic, N.; Kan, C.; Wang, J. *Chem. Commun.* **2014**, 50 (71), 10202–10205.
- (39) Bouffier, L.; Doneux, T.; Goudeau, B.; Kuhn, A. *Anal. Chem.* **2014**, 86 (8), 3708–3711.
- (40) Nassi, A.; Guillon, F.-X.; Amar, A.; Hainque, B.; Amriche, S.; Maugé, D.; Markova, E.; Tsé, C.; Bigey, P.; Lazerges, M.; Bedioui, F. *Electrochim. Acta* **2016**, 209, 269–277.
- (41) Horny, M.-C.; Lazerges, M.; Siaugue, J.-M.; Pallandre, A.; Rose, D.; Bedioui, F.; Deslouis, C.; Haghiri-Gosnet, A.-M.; Gamby, J. *Lab Chip* **2016**, 16 (22), 4373–4381.



## Chapter IV. Conclusions and perspectives

### 4.1. Conclusions

This thesis presents the use of the concept of bipolar electrochemistry for several applications concerning the modification of different types of objects such as semiconducting organic or inorganic crystals and biomaterials such as DNA.

The first chapter gathers theoretical aspects of bipolar electrochemistry as well as a selection of some recent groundbreaking work that employed this method. Nowadays, asymmetric objects and/or asymmetric reactivity on particles is of great importance and could be useful at the fundamental level for an academic understanding but also in the context of industrial applications. Bipolar electrochemistry allows to provide this feature in a simple and easy way through an electrochemically-induced break of symmetry.

In the second part of the thesis, the example of generation of Janus-type hybrid organic-inorganic materials is exposed. Fulvalene-based charge transfer salts were successfully modified with site-selective copper deposits by BPE. Furthermore, it was shown that such an intrinsic break of symmetry enables anisotropic physico-chemical properties such as asymmetric photovoltage generation on this newly prepared hybrid organic/inorganic materials. In the same way, bipolar electrochemistry was also successfully applied to inorganic materials. Our findings demonstrate that bipolar electrochemistry is indeed a powerful technique for producing asymmetric reactivity on conductive particles. In this way, MoSe<sub>2</sub> transition metal dichalcogenides macro-crystals were addressed wirelessly to promote site-selective metal deposition or hydrogen gas production, respectively. Furthermore, bipolar electrochemistry could be applied simultaneously to a large ensemble of MoSe<sub>2</sub> microparticles. In such a configuration, the same redox reactions occur at the edges of all addressed microparticles and this could enable a bulk electrochemical transformation of chemical species by the suspension of these microscale bipolar particles. In this context, MoSe<sub>2</sub> microparticles were shown to drive effectively the quantitative oxidation of a model organic compound. To follow-up this proof-of-principle, it could be interesting to study selective oxidation of biorelevant compounds of interest from a mixture. Also by using this principle, it might be possible to develop a fluidic device with filters or membranes, which contains such micrometer-sized crystals in a stationary phase for selective electrochemical elimination of aqueous contaminants under the application of an electric field.

In the last part, bipolar electrochemistry was extended to biological material namely DNA molecules. DNA conductivity and DNA-mediated charge transport studies are of great importance in science but remain an ongoing controversial area. In our studies, we tried to explore indirectly the electronic properties of DNA substrates by means of bipolar electrochemistry. DNA-mediated metal deposition at one extremity of dsDNA is a direct prove

of DNA conductivity. Promising results were obtained for copper deposits attached to the extremity of DNA molecules, as observed by TEM microscopy. Also, an additional approach involving DNA combing was developed in combination with AFM imaging, but further experiments are required in order to definitely conclude on the successful use of a biopolymer as a bipolar electrode. Future experiments will allow to investigate metal deposition on DNA molecules by using intercalators positioned inside the DNA strands. Furthermore, in this thesis we also demonstrate that asymmetric Janus particles prepared by BPE can be used for DNA hybridization detection with a very simple optical read-out based on DNA-controlled generation of pH gradients.

In summary, this thesis demonstrates that bipolar electrochemical is extremely useful and can be advantageously used for many applications in the field of materials science and (bio)analytical sensing. Also, BPE can be applied to various objects of different chemical nature and size such as organic and/or inorganic substrates. In some cases BPE allows to design experiments which would simply not be possible with any other (electrochemical) approach.

## **4.2. Perspectives**

Among the presented examples, BPE does still offer many unexplored possibilities and can be applied to other interesting fields. The production of asymmetric particles of different sizes (from macro- to sub-microscale) and chemical nature with high yield is a very important contemporary demand in materials science, especially in the context of industrial technologies.

Various other materials can be considered for bipolar electrochemical addressing based on the proof-of-principle experiments reported in the present thesis. Asymmetric modification of particles with monolayers or covalently grafted organic molecules on nanoparticles are very relevant, since they could be used for self-assembly of smart functional particles. For example, gold nanorods (GNRs) are very important for biomedical applications. However, GNRs are stabilized by surfactants, such as cetyltrimethylammonium bromide (CTAB), which is known for its cytotoxicity. In this case, bipolar electrochemistry could be used for electrochemical grafting of a functional diazonium compound on gold nanorods (500-800 nm), replacing advantageously the use of the toxic surfactant. Such asymmetric monolayers of organic species could potentially lead to self-assembly of nanorods, enabling thus a change of their optical properties and accordingly, could exhibit tunable features in photothermal therapy applications.

BPE is also a promising technique for the generation of self-propelled objects. Some examples of motion generation are presented in part 1.3.4. Carbon microtubes modified with nickel could be directionally controlled and actuated in the presence of rotating magnetic fields. Also, carbon tube/platinum asymmetric particles could be propelled using oxygen bubble generation occurring at the platinum surface when exposed to hydrogen peroxide chemical fuel in solution.

In the same way, spiral- shaped particles could be modified with a Pt deposit at one extremity. In that case, the exposure to hydrogen peroxide will promote a rotation around its axis and causing therefore a linear propulsion of such objects like a helical propeller motor.

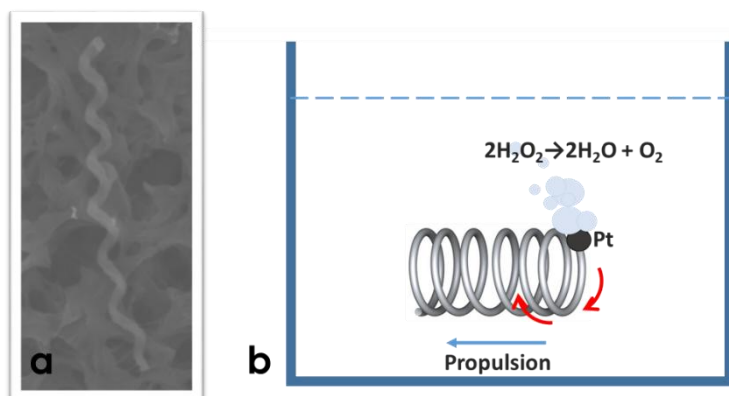


Fig. 4.1. (a) SEM micrographs of Polypyrrole (PPy)-based helix and (b) principle of propulsion of a Pt modified Ppy helix.

An interesting aspect will be the fabrication of micro- and nanoswimmers that are biocompatible for in vivo applications such as drug delivery. All in all, many exciting potential playgrounds still exist that have not been yet explored and which sometimes may open up perspectives that go far beyond our current expectations and imagination. It is therefore clear that the field of contemporary BPE is going to continue its exponential growth in scientific activity (see Figure 1 in chapter 1) for a couple of additional years.